



**UNIVERSITY OF TRENTO**

**International PhD Program in Biomolecular Sciences**

**Department of Cellular, Computational  
and Integrative Biology – CIBIO**

**31<sup>st</sup> Cycle**

**“Pro-Tumorigenic role of *ETS-related gene* (ERG)  
in precursor prostate cancer lesions”**

**Advisor**

Prof. Andrea Lunardi

The Armenise-Harvard Laboratory of Cancer Biology & Genetics  
Department of Cellular, Computational and Integrative Biology  
University of Trento

**Tutor**

Prof. Francesca Demichelis

Laboratory of Computational and Functional Oncology  
Department of Cellular, Computational and Integrative Biology  
University of Trento

**Ph.D. Thesis of**

Marco Lorenzoni

*The Armenise-Harvard Laboratory of Cancer Biology & Genetics  
Department of Cellular, Computational and Integrative Biology  
University of Trento*

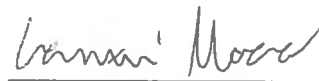
Academic Year 2018-2019

June 22<sup>nd</sup> 2019

Trento

**Declaration of Original authorship:**

"I, Marco Lorenzoni, confirm that this is my own work and the use of all material from other sources has been properly and fully acknowledged."

A handwritten signature in black ink, appearing to read "Lorenzoni Marco", written over a horizontal line.

Lorenzoni Marco

# INDEX

DECLARATION OF AUTHORSHIP .....	2
ABBREVIATIONS.....	6
INDEX OF FIGURES.....	8
1. ABSTRACT .....	9
2. INTRODUCTION.....	10
2.1. The Prostate .....	10
2.1.1. Biology and functions.....	10
2.1.2. Cell types and markers.....	10
2.2. Prostate Cancer (PCa).....	11
2.2.1. Natural history of PCa: clinical perspective.....	11
2.2.2. Natural history of PCa: molecular perspective.....	12
2.3. Biotechnology Innovations in Prostate Study .....	14
2.3.1. Organoid model .....	14
2.3.2. CLICK chemistry/Mass Spectrometry Approach.....	17
3. AIMS OF THE THESIS.....	21
4. RESULTS.....	22
4.1. Mouse Prostate Organoids (mPrOs).....	22
4.1.1. Establishing Mouse Prostate Organoids (mPrOs).....	22
4.1.2. Wild Type (WT) mPrOs characterization.....	22
4.2. Modeling ERG positive precursor prostate lesions .....	24
4.2.1. Generation of inducible ERG-overexpressing vector .....	24
4.2.2. ERG-overexpressing mPrOs.....	26
4.3. CLICK-MS approach .....	35
4.3.1. Combining CLICK-MS and WT mPrOs.....	35
4.3.2. CLICK-MS approach refinement .....	37
4.4. Studying ERG role(s) in precursor prostate lesions from an extracellular perspective.....	40
4.4.1. Profiling the secreted protein signature of ERG expressing mPrOs .....	40
4.4.2. Data mining from ERG-driven secretome .....	43

4.4.3.	RNA expression analysis of oversecreted proteins.....	45
5.	DISCUSSION .....	46
5.1.	Biotechnology driven PCa research.....	46
5.2.	Identification of ERG-induced alterations in mPrOs.....	48
5.2.1.	Lipocalin2 ( <i>Lcn2</i> ) .....	49
5.2.2.	Spondin2 ( <i>Spon2</i> ).....	49
5.2.3.	Serine Protease Inhibitor Kazal-type 5 ( <i>Spink5</i> ) .....	50
5.2.4.	Cytotoxic T Lymphocyte-Associated protein 2 alpha ( <i>Ctla2α</i> ) .....	50
6.	FUTURE PERSPECTIVES.....	52
6.1.	Understanding the effects of mPrOs secreted factors .....	52
6.2.	Potential clinical application of ERG-driven secreted factors .....	53
7.	CONCLUSIONS.....	54
8.	MATERIALS AND METHODS.....	55
8.1.	Mouse Prostate Organoids (mPrOs).....	55
8.1.1.	Reagents and solutions used for mPrOs culture .....	55
8.1.2.	mPrOs culture.....	56
8.1.3.	Sample preparation for IF and IHC.....	57
8.1.4.	EGF deprivation experiment.....	57
8.1.5.	EdU labeling and FACS analysis .....	58
8.1.6.	Engineering mPrOs .....	58
8.1.7.	RNA extraction from mPrOs .....	59
8.1.8.	Protein extraction from mPrOs .....	59
8.2.	RNA Reverse Transcription .....	59
8.3.	Quantitative Real Time PCR (RT-qPCR).....	60
8.4.	Immunofluorescence (IF) of Formalin-fixed Paraffin-embedded sections .....	61
8.5.	Hematoxylin & Eosin staining of Fomalin-fixed Paraffin-embedded sections .....	62
8.6.	AR Immunohistochemistry staining of Formalin-fixed Paraffin-embedded sections.....	63
8.7.	Immunoblot analysis.....	63
8.8.	CLICK-IT enrichment of secreted proteins .....	64
8.8.1.	AHA and Methionine labeling of newly synthesized proteins from CD1-derived mPros .....	64

8.8.2.	AHA labeling of newly synthesized proteins from C57B6/J-derived mPrOs .....	65
8.8.3.	CLICK-IT enrichment of secreted proteins from conditioned medium of CD1-derived mPrOs	65
8.8.4.	MS analysis and identification of enriched proteins.....	66
8.8.5.	Albumin Deprivation .....	67
8.8.6.	Refined CLICK-IT protocol for enrichment of secreted proteins from conditioned medium of C57B6/J-derived mPrOs.....	67
8.9.	Shared protein analysis.....	68
8.10.	Protein network and gene ontology analysis.....	68
8.11.	Statistical Analysis.....	69
9.	ACKNOWLEDGMENTS .....	70
10.	ACKNOWLEDGMENTS (part Two) .....	71
11.	REFERENCES .....	74

# ABBREVIATIONS

ADT: Androgen Deprivation Therapy	DOXY: Doxycycline
AHA: L-Azido-Homo-Alanine	ECM: Extra-Cellular Matrix
APC: APC regulator of WNT signaling pathway	EdU: 5-ethynyl-s'-deoxyuridine
AR: Androgen Receptor	EGF: Epithelial Growth Factor
ATM: ATM serine/threonine kinase	ERG: ETS-related gene
BPH: Benign Prostatic Hyperplasia	ETV#: ETS variant #
BRCA1/2: BRCA1/2 DNA repair associated	EWS: EWS RNA binding protein 1
BSA: Bovine Serum Albumin	FC: Fold Change
CAF: Cancer Associated Fibroblast	FLI1: Fli-1 proto-oncogene
CCND1: Cyclin D1	FoxA1: Forkhead box A1
CCNE1: Cyclin E1	FoxP3: Forkhead box P3
CDKN2A/B: Cyclin Dependent Kinase inhibitor 2A/B	FUS: FUS RNA binding protein
CHD1: Chromodomain Helicase DNA binding protein 1	GC: Gas Chromatography
CHGA: Chromogranin A	GEMM: Genetically Engineered Mouse Models
CK5: Cytokeratin 5	H&E: Hematoxylin and Eosin
CK8: Cytokeratin 8	HGPIN: High-Grade Prostatic Intra-epithelial Neoplasia
CK14: Cytokeratin 14	HoxB13: Homeobox B13
CK18: Cytokeratin 18	IDH1: Isocitrate dehydrogenase (NADP(+)) 1, cytosolic
CLICK-MS: CLICK-chemistry coupled Mass Spectrometry	IF: Immunofluorescence
CTLA2 $\alpha$ : Cytotoxic T Lymphocyte-associated protein 2 alpha	IHC: Immunohistochemistry
CTNNB1: Catenin beta 1	LC: Liquid Chromatography
CuAAC: Copper (I)-catalyzed Alkyne-Azide Cycloaddition	LCN2: Lipocalin 2
CUL3: Cullin 3	mCRPC: metastatic Castration-Resistant Prostate Cancer
DAVID: Database for Annotation, Visualization and Integrated Discovery	Met: Methionine
DHT: Di-Hydro-Testosterone	mPrOs: mouse Prostate Organoids
	MS: Mass Spectrometry
	m/z: mass-to-charge ratio

NDRG1: N-myc downstream regulated 1

O/N: Overnight

PCa: Prostate Cancer

PFA: Paraformaldehyde

PIN: Prostatic Intra-epithelial Neoplasia

PSA: Prostate Specific Antigen

#PSM: # Peptide-Spectra Matching

PTEN: Phosphatase and Tensin homolog

PURO: Puromycin resistance gene

PVDF: Polyvinylidene fluoride

RB: RB transcriptional corepressor 1

RT: Room Temperature

RT-qPCR: Real-Time quantitative Polymerase Chain  
Reaction

rtTA3: reverse tetracycline-controlled

Transactivator 3

RTU: Reverse Transcriptase Units

SBSN: Suprabasin

SDS-PAGE: Sodium-dodecyl-phosphate-poly-  
Acrylamide Gel Electrophoresis

SLC45A3: Solute carrier 45 member 3

SPINK1/5: Serine Protease Inhibitor Kazal-type 1/5

SPON2: Spondin 2

SPOP: Speckle type BTB/POZ protein

SU2C: Stand Up 2 Cancer Foundation

TCGA: The Cancer Genome Atlas

TMPRSS2: Transmembrane Serine Protease 2

TP53: Tumor Protein 53

$\Delta$ N-TP63: Delta-N Tumor Protein 63

TRE: Tetracycline Response Element

Tregs: CD4<sup>+</sup> T-regulatory lymphocytes

UGS: Uro-Genital Synus

WT: Wild Type

## INDEX OF FIGURES

<b>Fig. 4.1:</b> Establishing mouse Prostate Organoids Culture. ....	23
<b>Fig. 4.2:</b> Characterization of mouse Prostate Organoid model. ....	26
<b>Fig. 4.3:</b> TMPRSS2:ERG alteration in PCa and inducible ERG-expression vector system. ....	27
<b>Fig. 4.4:</b> Characterization of mPrOs-ERGM40. ....	27
<b>Fig. 4.5:</b> Analysis of Cytokeratins expression in mPrOs-ERGM40. ....	29
<b>Fig. 4.6:</b> Analysis of wild type and ERGM40 mPrOs proliferative state. ....	32
<b>Fig. 4.7:</b> Effects of long term ERG induction on mPrOs cultures. ....	33
<b>Fig. 4.8:</b> Effects of long term induction of ERG expression in growth factor restrictive mPrOs cultures conditions. ....	34
<b>Fig. 4.9:</b> Coupling CLICK-MS approach to mouse prostate organoids. ....	35
<b>Fig. 4.10:</b> CLICK-MS approach refinement. ....	38
<b>Fig. 4.11:</b> Analysis of secreted proteome from doxycycline-treated and untreated organoids. ....	41
<b>Fig. 4.12:</b> Analysis of ERG-induced alterations in secreted proteome. ....	42
<b>Fig. 4.13:</b> Protein-protein interactions analysis in secreted proteome under ERG influence. ....	43
<b>Fig. 4.14:</b> RNA expression analysis of oversecreted proteins. ....	45
<b>Fig. 5.1:</b> Analysis of predicted ETS-binding sites at <i>Ctla2<math>\alpha</math></i> , mouse <i>CtsL</i> and human <i>CTSL</i> promoters. ....	51



# 1. ABSTRACT

Prostate cancer (PCa) is the second most common cancer in men with more than 1 million new cases worldwide each year. While some of the genomic, genetic and molecular events characterizing PCa have been functionally associated with tumor onset, development and resistance to therapy, the meaning of many other molecular alterations remains poorly understood.

Recent development of organoids technology and prostate organoid cultures has established an innovative and valuable model for the study of adult tissue homeostasis, physiology and disease.

In this project we combined prostate organoids technology with genetic engineering and CLICK-chemistry coupled Mass Spectrometry approaches in order to better characterize molecular features of wild type and genetically engineered mouse prostate organoids modeling early steps of human prostate tumorigenesis.

In details, by manipulating mPrOs to proxy *ETS-related gene* (ERG) precursor PIN/HGPIN lesions of human prostate, we identified possible novel pro-tumorigenic roles of ERG which unleashes cells proliferation from the tight control of growth stimuli, and, even more interesting, corrupts immune system components to escape immune surveillance.

In conclusion, this project shows that coupling innovative biological systems and technological approaches can lead to significant improvements in the analysis and understanding of disease mechanisms.

## 2. INTRODUCTION

### 2.1. The Prostate

#### 2.1.1. Biology and functions

Prostate is a compound tubuloalveolar exocrine gland located beneath the bladder and surrounded by fibromuscular tissue. This male-specific gland originates from the urogenital sinus (UGS) through a process of continuous budding, branching and differentiation that starts during embryonic development, continues through birth and is completed during puberty (Prins and Putz, 2008).

Human prostate is usually subdivided into three different anatomical regions or “zones”: the peripheral zone that accounts for the majority of the gland; the central zone that is the region closer to the ejaculatory ducts, and, finally, the transition zone that surrounds the proximal urethra (Myers, 2000).

The main function of this gland is the production and secretion of molecules that contributes to the seminal fluids and help to nourish and protect the sperm.

#### 2.1.2. Cell types and markers

At the histological level human prostate is formed by a pseudo-monostriated epithelium composed by three cellular populations, basal and luminal epithelial cells and neuroendocrine cells, surrounded by the stroma (Shen and Abate-Shen, 2010).

Luminal epithelial cells are the most prominent cell population in the prostate epithelium and can be identified by their unique columnar polarized morphology. These are androgen-dependent cells that are responsible for the secretory functions and are characterized by the expression of genes such as *Androgen Receptor (AR)*, *Prostate-Specific Antigen (PSA)*, *Cytokeratin 8 and 18 (CK8 and CK18)*, *TRPM8*, *NKX3.1*, *HOXB13* and *FOXA1*.

Basal epithelial cells form a continuous layer of cells surrounding the luminal compartment. They express very low amount of AR, have minimal secretory capacities, and can be identified by the expression of  $\Delta N$ -*Tp63* isoform and *Cytokeratin 5 and 14 (CK5 and CK14)* genes.

Lastly, neuroendocrine cells are a very rare and sparse population in the prostate tissue and their origin and function is still controversial. These cells do not express AR and are characterized by the expression of *Chromogranin A (CHGA)*, *Serotonin* and other neuropeptides (Abate-Shen and Shen, 2000; Toivanen and Shen, 2017).

The basic unit of the prostate organ is the *duct* that is composed by a single layer of luminal epithelial cells surrounded by the basal epithelial compartment and the basal membrane. These ducts are highly branched and

folded in a way that creates a complex system of channels. The prostate ducts are supported by the stromal compartment where the fibromuscular tissue together with blood vessels, lymphatic vessels and immune cells create a structural and functional environment which plays essential roles in prostate organogenesis, homeostasis, and tumorigenesis (Toivanen and Shen, 2017).

Adult prostate is an extremely quiescent organ in the body, thus identification and characterization of prostate stem cells is quite challenging and debated since many years. Early studies have shown that adult prostate contains cells expressing both basal and luminal markers leading to the hypothesis of a population of progenitor “intermediate” cells (Wang *et al.*, 2001). Subsequent and more specific analyses have shown that both basal and luminal compartments contain multipotent progenitors able to give rise to both luminal and basal cell lineages (Chua *et al.*, 2014; Wuidart *et al.*, 2016).

## 2.2. Prostate Cancer (PCa)

### 2.2.1. Natural history of PCa: clinical perspective

Prostate Cancer is one of the most commonly diagnosed cancer in men (Ferlay *et al.*, 2015). PCa is generally a slow growing tumor that affects people starting from their 50 with a peak of incidence around 65-69 years of age. In addition to aging, other risk factors for PCa are ethnicity (African American > Caucasian > Asian), family history (hereditary gene mutations, e.g. *Brca1*), and lifestyle (Shen and Abate-Shen, 2010; Hodson, 2015; Attard *et al.*, 2016).

PCa is commonly considered the natural progression of so-called precursor prostatic lesions (Benign Prostatic Hyperplasia (BPH); Prostatic Intra-epithelial Neoplasia (PIN); High-Grade PIN (HGPIN)). While BPH is an hyperplastic status of prostatic cells, PIN and HGPIN identify sites of hyperproliferative epithelium with clusters of cells invading the lumen of the prostatic ducts, condition which is frequently accompanied by a reduced integrity of the basal epithelial compartment (Bostwick and Qian, 2004; Montironi *et al.*, 2007; Klezovitch *et al.*, 2008).

Exploiting the PSA test, 90% of PCa are identified early when they are still localized tumors at the time of diagnosis (Abeshouse *et al.*, 2015), yet, with almost 75% false positive and 12% false negative rates, PSA is a poor biomarker for PCa diagnosis (Thompson *et al.*, 2004; Sohn, 2015; Attard *et al.*, 2016).

Once diagnosed, medium- and high-risk PCa are usually treated by either Surgery or Radiotherapy. Adjuvant chemo and/or hormonal therapy, depending on the risk level, is administered in order to reduce the probability of relapse. Low-risk PCa patients can be enrolled in an Active Surveillance protocol, which implies a frequent monitoring of the tumor and clinical intervention just in case of tumor progression (Wadman, 2015).

Despite the initial success, a large number of patients experiences tumor recurrence, frequently associated with metastatic disease progression. Main systemic treatment for metastatic PCa is Androgen Deprivation Therapy (ADT) that aims at reducing testosterone levels from the body and AR activity. This is achieved through either surgical or chemical castration (Tran *et al.*, 2009; Ryan *et al.*, 2013; Beer *et al.*, 2014), however sooner or later tumor cells develop resistance to hormonal therapy leading to an incurable condition identified as metastatic Castration-Resistant PCa (mCRPC) (Shen and Abate-Shen, 2010; Carreira *et al.*, 2014; Watson, Arora and Sawyers, 2015).

### 2.2.2. Natural history of PCa: molecular perspective

In an attempt to identify specific molecular classes of PCa, the Cancer Genome Atlas Research Network (TCGA) and the SU2C-Prostate Cancer Foundation have analyzed almost 700 primary PCa in the last few years (Abeshouse *et al.*, 2015; Armenia *et al.*, 2018). These studies highlighted the presence of different classes of PCa, characterized by specific molecular alterations. As expected, the first four classes grouped almost 50% of total PCa and were characterized by a mutually exclusive genomic recombination event between a member of the ETS transcription factor family (*ERG*, *ETV1*, *ETV4* or *FLI1*) and a specific androgen-responsive gene (e.g. *TMPRSS2*, *SLC45A3* and *NDRG1*). The remaining classes were instead characterized by mutations affecting *SPOP*, *FOXA1*, *Cul3* and *IDH1* genes. Other genes such as *TP53*, *PTEN*, *ATM*, *BRCA2*, *CHD1*, and *SPINK1* resulted affected in primary PCa, even though they did not segregate with a specific class of PCa (Abeshouse *et al.*, 2015; Armenia *et al.*, 2018).

In addition, genes and pathways that had never been associated with this type of tumor were identified as recurrently altered in PCa. Among them, epigenetic and chromatin modifiers (mutated in up to 20% of PCa cases); DNA repair genes (16%) and members of WNT signaling (10%) resulted the most common. Finally, a high number of low-frequency mutated genes was also characterized, thus strengthening once again the remarkable molecular heterogeneity characterizing PCa (Taylor *et al.*, 2010; Abeshouse *et al.*, 2015; Armenia *et al.*, 2018).

Due to the high rate of metastatic progression and hormone therapy resistance, characterization of the molecular mechanisms leading to tumor evolution to aggressive stages of the disease is a primary goal.

A first attempt came from the work of Taylor and colleagues (Taylor *et al.*, 2010) where more than 200 cases (181 primary and 37 metastatic PCa samples) were studied. Copy number variations, genomic rearrangements and transcriptome profiling studies highlight AR, PI3K/PTEN, RAS/RAF and RB pathways deregulation frequencies as significantly increased in the metastatic disease compared to primary PCa (34% to 43% in primary PCa versus 74% to 100% in metastases).

More recently, Robinson and colleagues published their genomic studies on a smaller but more homogeneous set of samples (150 biopsies from mCRPC cases) (Robinson *et al.*, 2015). Again, *AR*, *TP53* and *PTEN* (63%, 53% and 40% respectively) resulted the genes showing the most significant increase in the frequency of alteration in metastatic PCa compared to primary tumors. Other genes whose deregulation resulted to be enriched in metastatic PCa belonged to WNT signaling (e.g. *APC*, *CTNNB1*, *R-Spondin2*), G1/S cell cycle check point (e.g. *RB1*, *CCND1*, *CDKN2A*, *CDKN2B*) and DNA repair (e.g. *BRCA1/2*, *ATM*) (Robinson *et al.*, 2015).

Finally, whole genome duplication has also been described by Bielski and colleagues as a hallmark of PCa aggressiveness (Bielski *et al.*, 2018). This phenotype is associated with deregulation of key factors controlling the G1/S cell cycle check point, in particular, highly significant is the correlation with *CNNE1* gene amplification. Interestingly, whole genome duplication is independent by the p53 status.

Overall, even though our knowledge of the molecular mechanisms driving PCa, metastatic disease progression and resistance to hormonal therapy is considerably improved in the past 10 years, clinical management of PCa patients has been minimally influenced by these findings.

#### 2.2.2.1. *ERG* function in normal tissue and PCa

Among the molecular alterations described in PCa, unquestionably *ERG* rearrangement is the one with the highest incidence (Demichelis *et al.*, 2007; Kumar-Sinha, Tomlins and Chinnaiyan, 2008; Yu *et al.*, 2010). The most common event is the internal rearrangement of chromosome 21 where a microdeletion in the q22 region determines the fusion between exon 1 of the AR-responsive *Transmembrane Serine Protease 2 (TMPRSS2)* gene and exon 4 of *ERG* gene (Tomlins *et al.*, 2005).

TMPRSS2 is a transmembrane protease that may release in the extracellular compartment its catalytic domain after self-cleavage (Paoloni-Giacobino *et al.*, 1997). This enzyme is mainly expressed by luminal epithelial cells in the prostate since it is strongly regulated by AR activity, yet its function is still debated (Lin *et al.*, 1999). ERG is a transcription factor that is expressed by several tissues and that is involved in many different processes: from cell proliferation and angiogenesis to cell differentiation and apoptosis (Loughran *et al.*, 2008; Taoudi *et al.*, 2011). ERG protein is characterized by an ETS-DNA binding domain and a PNT/SAM domain that is involved in protein-protein interactions. Genomic rearrangements of *ERG* have been described in Ewing's sarcoma, where *ERG* is fused with *EWS* gene, and acute myeloid leukemia, where *ERG* is fused with *TLS/FUS* gene (Ichikawa *et al.*, 1994; Sorensen *et al.*, 1994). The result of these events is the formation of a chimeric protein leading to significant alterations in targeted gene expression and, finally, to malignant cell transformation (Yi *et al.*, 1997; Arvand and Denny, 2001; Gorthi and Bishop, 2018; Grünwald *et al.*, 2018).

In prostate, since *TMRPSS2* Ex1 covers the promoter and 5'UTR region of the gene, the outcome of *TMRPSS2:ERG* fusion is not a chimeric protein but the *de-novo* AR-driven expression of a delta-40 amino-terminal truncated isoform of ERG in prostate epithelium (Demichelis *et al.*, 2007; Perner *et al.*, 2007; Tomlins *et al.*, 2008; King *et al.*, 2009).

*TMRPSS2:ERG* rearrangement is considered a very early event during prostate tumorigenesis and it is commonly identified in 5-30% of precursor PIN and HGPIN prostate lesions (Perner *et al.*, 2007; Mosquera *et al.*, 2008; He *et al.*, 2012; Teng *et al.*, 2013; Park *et al.*, 2014; Lee *et al.*, 2015; Morais *et al.*, 2016). Interestingly, however, several *in vivo* studies exploiting Genetically Engineered Mouse Models (GEMM) showed that the expression of ERG in mouse prostate can, at most, induces benign lesions in the prostatic epithelium, but never malignant cell transformation and PCa (Klezovitch *et al.*, 2008; Tomlins *et al.*, 2008; Carver *et al.*, 2009; King *et al.*, 2009; Chen *et al.*, 2013). Accordingly, these findings were further proved by a plethora of studies that confirmed the inability of ERG to trigger cell transformation also *in vitro*, in immortalized human prostate cell lines. Yet, all these works reproducibly describe the acquisition of migratory and invasive capabilities of prostate cancer cells as a direct consequence of exogenous ERG overexpression (Tomlins *et al.*, 2008; Carver *et al.*, 2009; Chen *et al.*, 2013).

Even if the oncogenic role(s) of ERG in PCa have been functionally associated with invasive and metastatic tumor progression, the presence of genomic rearrangements driving ERG expression in 5-30% of precursor PIN and HGPIN prostate lesions is at least counterintuitive and suggests possible critical role(s) of ERG in the very early stages of prostate tumorigenesis that remain unexplored.

## 2.3. Biotechnology Innovations in Prostate Study

### 2.3.1. Organoid model

#### 2.3.1.1. *In vitro* Tissue Avatars

The development of the organoid technology has been a pioneering milestone in our ability to model and study organ development, differentiation processes and disease onset, progression and response to therapy.

An organoid is defined as a precise set of cells that are derived from the proliferation of embryonic or adult organ resident stem/progenitor cells and are able to differentiate in the correct cellular lineages and to self-organize themselves in a 3D architecture that closely recapitulates the anatomy of the organ of origin (Lancaster and Knoblich, 2014; Clevers, 2016; Drost and Clevers, 2018).

The first attempt to recapitulate *in vitro* the differentiation and organization of the organ was done by Yoshiki Sasai and colleagues. Starting from Embryonic Stem Cells (ESCs) they were able to obtain cortical neurons

organized in 3D structures and showing neural connections upon the induction of differentiation through a specific cocktail of factors mixed to the culture medium (Eiraku *et al.*, 2008). One year later the laboratory of Hans Clevers published the protocol to establish organoids from adult intestinal stem cells (Sato *et al.*, 2009). Importantly, intestinal organoids can be maintained in culture for a very long period of time, expanded and stored in liquid nitrogen. Moreover, the feasibility to derive organoids from both healthy and diseased human intestine is paving the way towards translational studies of personalized medicine (Chua *et al.*, 2014; Karthaus *et al.*, 2014; Lancaster and Knoblich, 2014).

Since then, many different groups were able to derive organoids cultures from different tissues: retina (Eiraku *et al.*, 2011), cerebellum (Muguruma *et al.*, 2015), stomach (McCracken *et al.*, 2014), lung (Jain *et al.*, 2015), thyroid (Antonica *et al.*, 2012), liver (Huch *et al.*, 2015), pancreas (Boj *et al.*, 2015), prostate (Chua *et al.*, 2014; Drost *et al.*, 2016), and many more.

Organoids culture represent a great improvement in the researcher's toolbox since:

- They derive from embryonic or adult primary cells
- They are genomically stable
- Cultured in a selective 3D environment they self-assemble to recap tissue architecture, cell polarity, molecular signaling and homeostasis of the tissue of origin
- They can be used to better understand those processes responsible for the development, maintenance and repair of organs
- They can be genetically modified and used as platform for genetic and molecular *in vitro* studies
- They can be xeno- or orthotopic transplanted for the generation of *in vivo* models of human disease

Despite their enormous advantages and potential, organoids still have some drawbacks that are mainly linked to their poor degree of differentiation (the majority of organoid models are highly proliferative minimally differentiated progenitor-like cells) and to the absence of key cellular components of the tissue microenvironment (like vasculature, fibroblasts and immune cells) (Lancaster and Knoblich, 2014; Clevers, 2016).

In addition, organoid cultures are more demanding in terms of time and resources respect to cell line models and this may represent a relevant point when writing or evaluating projects. Another limitation affecting this system is the necessity to use, in almost all cases, extra-cellular matrix (ECM)-like scaffolds or not-completely defined medium, for the 3D growth of these cultures, that can have an impact on culture itself or experimental results. Finally, it is interesting to note that most of the 3D organoid systems are derived from epithelial tissues or tumors of epithelial origin pointing out that our knowledge is still far from complete and there is room for the improvement of organoid cultures and for derivation of non-epithelial organoid lines (Drost and Clevers, 2018).

### 2.3.1.2. Prostate Organoids

The generation of Prostate Organoids started in 2014 when the groups of Hans Clevers, at Utrecht University in the Netherlands, and Charles Sawyers, at Memorial Sloan Kettering Cancer Center in New York, published their research showing the generation of organoids from both mouse and human adult normal prostate (Karthaus *et al.*, 2014). Exploiting Matrigel® as 3D scaffold and a defined medium supplemented with specific soluble factors, they were able to establish prostate organoids from adult normal tissue while a companion publication described the generation of organoids cultures from advanced metastatic PCa (Gao *et al.*, 2014). Curiously, despite a massive effort, a reproducible protocol to establish prostate organoids from primary prostate tumors has not yet been established.

Prostate organoids are spherical in shape and characterized by a pseudo-monostratified epithelium composed by self-organizing luminal (AR<sup>+</sup>; CK8/18<sup>+</sup>) and basal epithelial cells (p63<sup>+</sup>; CK5<sup>+</sup>). Importantly, prostate organoids can be maintained in culture for many months without affecting their genome stability, lineage and spatial organization capacity, and the androgen pathway (Karthaus *et al.*, 2014). Finally, reconstitution experiments show that organoids injection with UGS mesenchyme under the kidney capsule of recipient mice give rise to mature prostate structures closely resembling normal prostate gland (Chua *et al.*, 2014; Karthaus *et al.*, 2014).

Organoid technology is a novel powerful tool to study development, homeostasis, physiology and, overall, tumorigenesis of different tissues and organs (Drost and Clevers, 2018; Barbosa *et al.*, 2019; Wei *et al.*, 2019).

Particularly in PCa, mouse and human organoids have substantially changed the research landscape. Limitations dictated by the minimal number of immortalized cell lines, all characterized by dysfunctional androgen pathway; lack of cell lines derived from primary human PCa lesions; paucity of metastatic prostate cell lines combined with a substantial intra-line heterogeneity dependent by a high level of genomic instability, will be overcome by the use of wild type and genetically engineered prostate organoids. Furthermore, 3D-*in vitro* analysis can be integrated through xeno- and orthotopic organoids transplants under the kidney capsule or into the prostate of recipient mice. Compared to GEMMs, the *ex vivo-in vitro-in vivo* approach based on organoids will give us the opportunity to accelerate *in vivo* pre-clinical studies and make them more consistent with a scenario of 'precision oncology', thanks to organoids cultures derived from PCa patients and the possibility to concomitantly enroll higher numbers of age-matched transplanted mice in preclinical studies (Gao *et al.*, 2014; Park *et al.*, 2016; Barros-Silva *et al.*, 2018; Chua *et al.*, 2018; Drost and Clevers, 2018; Puca *et al.*, 2018; Shoag *et al.*, 2018; Njoroge, Vatapalli and Abdulkadir, 2019).

Although very promising, further studies and deeper analyses will be necessary to fully understand pros and cons of this model. Accurate characterization of the function of each single supplement necessary for establishing and culturing prostate organoids is still missing. This knowledge could help us to define a protocol promoting a



better differentiation of the luminal lineage or maybe, finally, the conditions that favors the growth of organoids derived from primary PCa.

## 2.3.2. CLICK chemistry/Mass Spectrometry Approach

### 2.3.2.1. *CLICK chemistry and Mass Spectrometry*

The term “CLICK” chemistry identifies a set of chemical processes characterized by simple reaction conditions that may not require solvents, they have high yield and specificity for a define reaction product mainly due to high thermodynamic driving force present in the system (Kolb, Finn and Sharpless, 2001). CLICK processes mimic natural reactions starting from small molecules and linking them together in a specific way to build bigger elements, the interest on this topic and its uses arise in the early years of the new century mainly due to their potential application with polymers, biomaterials or pharmacological studies.

The features that define “CLICK” reactions make them available also for complex systems since they can react with no or very low influence on surrounding processes. This approach was progressively adapted and evolved for the use within living cells or *in vivo*, meeting the definition of bio-orthogonal chemistry (Sletten and Bertozzi, 2011), up to the development of new tools for better and more efficient analysis and tracking of biological events. Of particular interest is the development, in the last years, of methods for the use or incorporation of unnatural modified amino acids and nucleotides bearing reactive elements that can be used as “CLICK” reaction partners.

Thanks to the almost unlimited applications, CLICK reactions are widely used in many different fields of research with relevant benefits in term of both analytical power and quality of the results. At the moment, limitations affecting this field regard mainly the substrates and the mechanism underlying specific reactions; this translates into efforts aiming at a better understanding of CLICK chemistry, repositioning of known reactions and development of better/novel substrates and applications

Among the many different reactions that can be associated to CLICK chemistry, one of the most known is the Copper(I)-catalyzed Azide-Alkyne Cycloaddition (CuAAC), a reaction that links together a molecule with an azide group and one with an alkyne group in presence of copper to form a cyclic and selective product. This strategy may be exploited to covalently bind fluorophores or reporters like biotin to labeled molecules and track their production or the post-translational modifications of proteins or the localization of RNAs in presence of specific stimuli (Prescher and Bertozzi, 2005; Dieterich *et al.*, 2006; Eichelbaum *et al.*, 2012).

The term “Mass Spectrometry” (MS) identifies an analytical method that measures the mass-to-charge ratio of charged molecules. This instrument exploits the interaction between perpendicular electric and magnetic fields that can deflect the trajectory of a charged molecule (ion) that is moving through that field, the dynamic of this particle can be described combining the electromagnetic force and the Newton’s second law, respectively:

$$F = Q(E + v \times B) \quad F = m a$$

$$\left(\frac{m}{Q}\right) a = E + v \times B$$

[*F*: force applied to the ion, *Q*: charge of the ion, *E*: Electric field, *v* × *B*: vector-cross-product of ion velocity and magnetic field, *m*: ion mass, *a*: acceleration]

While *m/Q* represents the mass-to-charge ratio, data are usually presented as “*m/z*” where *z* indicates the number of elementary charges (*e*) of the ion ( $z = Q/e$ ).

The result of the analysis is the so called “MS-spectrum” that displays the intensity of recorded ions as a function of *m/z*, each spectrum is specific for a particular ion or set of ions and it may allow to identify the atom or molecule from which it derives through its fragmentation pattern or exploiting previous knowledge (e.g. databases of spectra).

There are three basic units of an MS machine:

- I. The ion source is the part of the machine responsible for sample fragmentation and ionization, it is possible to distinguish between hard and soft ionization depending on the technique used and the type of molecule/sample to be analyzed (e.g. Electronic Impact, Electrospray Ionization, MALDI, etc.)
- II. The mass analyzer is the core of the machine and it is the part responsible for the separation of the charged molecules moving within it; many different analyzers are available depending on the type of molecule to be analyzed and the ion source (the most common are: quadrupole, time-of-flight, ion trap and Orbitrap)
- III. The detector is the third element of an MS and it is the part of the instrument that measures the incoming ions, it is coupled to the data system software that integrates this signal with the parameters of the machine allowing the identification of the *m/z* value of each specific ion

The MS-spectrum obtained from the measurement is specific for the molecule and the instrumentation that is used, the resulting set of spectra are then used for the subsequent step of data analysis and molecule identification that is usually performed exploiting already available databases

The MS analysis is widely applied in biology and in this field one of the most used approaches is the “tandem” Mass Spectrometry, also known as MS/MS or MS<sup>2</sup>; this technique is based on a second pair of fragmentation chamber and mass analyzer, added to the output of the first one, allowing a deeper analysis of the sample. Exploiting this method it is possible to identify the peptide sequence of specific ions and reconstruct the entire protein sequence or localize specific modifications; moreover, the tandem MS is one of the possible strategies for quantitative proteomics especially when using Tandem Mass Tags (Maher, Jjunju and Taylor, 2015).

A pivotal improvement in the evolution of mass spectrometry was the use of separation techniques in line with the mass spectrometer, this modification significantly increased the resolution of the mass analysis and the

identification power of the instrument. The most common method is the chromatographic technique, mainly gas- or liquid-chromatography (GC or LC, respectively), that allows sample fractionation based on specific characteristics of the substrate (e.g. polarity, ionic strength, temperature, etc.), this reduces the overall complexity of the sample resulting in more efficient ionization and clearer fragmentation spectra. This step is very important especially for high-resolution MS or MS<sup>2</sup> since its absence may cause ions from different molecule to overlap on the same spectrum making more difficult, or impossible, to identify the specific compounds.

#### 2.3.2.2. *Coupling CLICK chemistry and Mass Spectrometry for secretome analysis*

The set of all proteins secreted from a cell, tissue or organism is known as the “secretome”, these molecules are involved in important cellular functions and they represent a novel source of relevant knowledge for various biological processes, both physiological and pathogenic.

Regarding the cancer field, during the past 10-20 years it was observed an increasing interest in the cancer secretome especially related to a better understanding of tumorigenic mechanisms or the potential identification of novel biomarkers (Pavlou and Diamandis, 2010). Despite all the efforts and improvements in the proteomic field, the discovery of new or more efficient markers is still challenging and only a small number was able to reach the clinical stage. The poor results can be related to intrinsic limitations of the secretome analysis that can be observed in both *in vivo* and *in vitro* approaches, these are mainly the dynamic range of the molecules present in the sample (usually the proteins of interest are present at very low concentration) and the presence of contaminants (e.g. serum in blood samples, medium supplements in cell culture, etc.).

A way developed to improve proteomic analysis is based on coupling CLICK chemistry and Mass Spectrometry (CLICK-MS) to better separate and identify those proteins that are regulated upon a specific stimulus (Eichelbaum *et al.*, 2012). The process is based on metabolic labeling of molecules within living cells and it allows to “fish out” these elements from the rest of the sample, thanks to CLICK reaction, reducing the presence of contaminants or unwanted molecules and increasing the quality of the MS analysis.

Regarding secreted proteins, this approach potentially represents the most efficient way to overcome the problem of the very low concentration of the molecules of interest within the mix of highly abundant components of bodily fluids or culture medium, these are usually maintained throughout the analysis increasing the signal-to-noise ratio and reducing both resolution and power of the analysis.

One of the possible *in vitro* applications exploits the uncommon amino acids L-Azido-Homo-Alanine (AHA), a methionine analogue that is characterized by the presence of an azide group and that labels all cellular proteins being naturally incorporated during protein synthesis (Dieterich *et al.*, 2006). By using this molecule only newly

synthesized cellular proteins will carry the functional group and it will be possible to separate them from the pool of contaminants/unwanted proteins (e.g. FBS, medium components, etc.)

After supplementing the medium with AHA and labeling proteins with the azide reactive moiety, CLICK reaction will covalently and exclusively bind the AHA-labeled proteins present in the sample to a resin bearing alkyne groups through a CuAAC reaction. Several washes of the resin with denaturing buffers will enrich the AHA-labeled cellular proteins by eliminating the vast majority of the AHA-negative molecules. The enriched proteins can then be detached from the resin by tryptic digestion and the resulting peptides analyzed by MS.

This approach requires minimal variations in the culture conditions (e.g. methionine-free regular medium to be completed with methionine as control or AHA) and 30 min-1 hour of AHA treatment is already sufficient for protein labeling, thus making this approach valuable for the analysis of highly dynamic cellular variations (Eichelbaum *et al.*, 2012; Bagert *et al.*, 2014).

The application of CLICK-MS for the analysis of cellular secretome was suggested for the first time by Eichelbaum and colleagues in 2012, when they clearly demonstrated that CLICK chemistry enrichment of AHA-labeled secreted proteins significantly improved both the resolution and identification power of MS analysis (Eichelbaum *et al.*, 2012; Eichelbaum and Krijgsveld, 2014).

### 3. AIMS OF THE THESIS

Tumorigenesis is considered an unfavorable event. Nutrients unbalance, changes in the activity of specific cellular pathways, enhanced proliferation rate, dedifferentiation, aberrations in apico-basal polarity, loss of lateral inhibition and extracellular matrix contact, are all crucial stress factors that trigger immediate cell autonomous and non-cell autonomous responses. Many tumor suppressive cellular mechanisms (e.g. TP53, RB, PTEN, TGF $\beta$ ) are commonly induced by different type of stress conditions. Primary functions of these '*guardians*' include cell cycle inhibition in order to allow the cell to rescue a normal condition, or cell death when resolution is impossible. Growth barriers overcome is mandatory for tumorigenesis, yet not sufficient (Ding *et al.*, 2011; Hanahan and Weinberg, 2011; Massagué, 2012; Fessler *et al.*, 2016). A further roadblock to tumorigenesis is immune surveillance. Innate and adaptive immune systems are rapidly recruited in areas of tissue abnormalities, attracted by inflammatory signals, thus taking care of the eradication of atypical cells.

In this scenario, we hypothesize that ERG expression in precursor prostate lesions can be functional to generate permissive conditions supporting the malignant progression of PIN/HGPIN lesions.

In order to test our hypothesis, we combined organoids technology and genetic engineering approaches to model ERG expression in non-malignant prostate epithelium. Then, we set up a CLICK chemistry approach coupled to Mass Spectrometry analyses to identify, and functionally study, ERG associated autocrine and paracrine secreted signals with potential roles in facilitating the initial steps of prostate carcinogenesis.

## 4. RESULTS

### 4.1. Mouse Prostate Organoids (mPrOs)

#### 4.1.1. Establishing Mouse Prostate Organoids (mPrOs)

The recent development of 3D prostate organoids cultures from mouse and human adult prostate tissue (Chua *et al.*, 2014; Gao *et al.*, 2014; Karthaus *et al.*, 2014; Drost *et al.*, 2016) has opened a new window of opportunity for the study of prostate physiology, tissue homeostasis and tumorigenesis.

Taking advantage of this new knowledge and thanks to the effort of present and past members of “The Armenise-Harvard Laboratory of Cancer Biology & Genetics”, we established a biobank of mouse prostate organoid lines derived from wild type and genetically engineered mice of different strains, by pooling the different lobes (ventral, dorsolateral and anterior) or taking them separately (Cambuli *et al.*, *in preparation*).

Following euthanasia, mouse prostate is resected, either as a whole organ or single lobes, mechanically dissociated and enzymatically digested with trypsin to obtain small clumps of cells. Finally, they are cultured in 3D ECM-like domes (Matrigel®) with a defined medium supplemented with: 50 ng/ml EGF, 100 ng/ml Noggin, 10% of R-spondin1 conditioned medium, 0.2 µM A83-01 and 10 nM DHT (**Fig. 4.1A**). Three days after seeding, multicellular aggregates are observable inside the Matrigel® (**Fig. 4.1B**); two days later, aggregates are replaced by fast growing round hollow spheres (**Fig. 4.1B-C**). Finally, after 6 to 8 days of culture, the Matrigel® drops start to lose their physicochemical properties thus making it necessary to recover the spheres from the Matrigel® through an enzymatic digestion with Dispase, mechanically disaggregate the spheres and seed fragments in fresh Matrigel® and defined medium in order to maintain the culture.

#### 4.1.2. Wild Type (WT) mPrOs characterization

By definition, organoids are “A collection of organ-specific cell types that develops from stem cells or organ progenitors and self-organizes through cell sorting and spatially restricted lineage commitment in a manner similar to *in vivo*” (Lancaster and Knoblich, 2014).

Accordingly, cellular and molecular hallmarks of adult mouse prostate were then analyzed in the prostate spheres to compare the status of these 3D structures with the tissue of origin (Cambuli *et al.* *in preparation*).

Microscope analysis of hematoxylin and eosin stained sections of paraffin embedded spheres defines these 3D cellular structures as formed by a pseudo-monost stratified epithelium, while immunohistochemistry (IHC) and

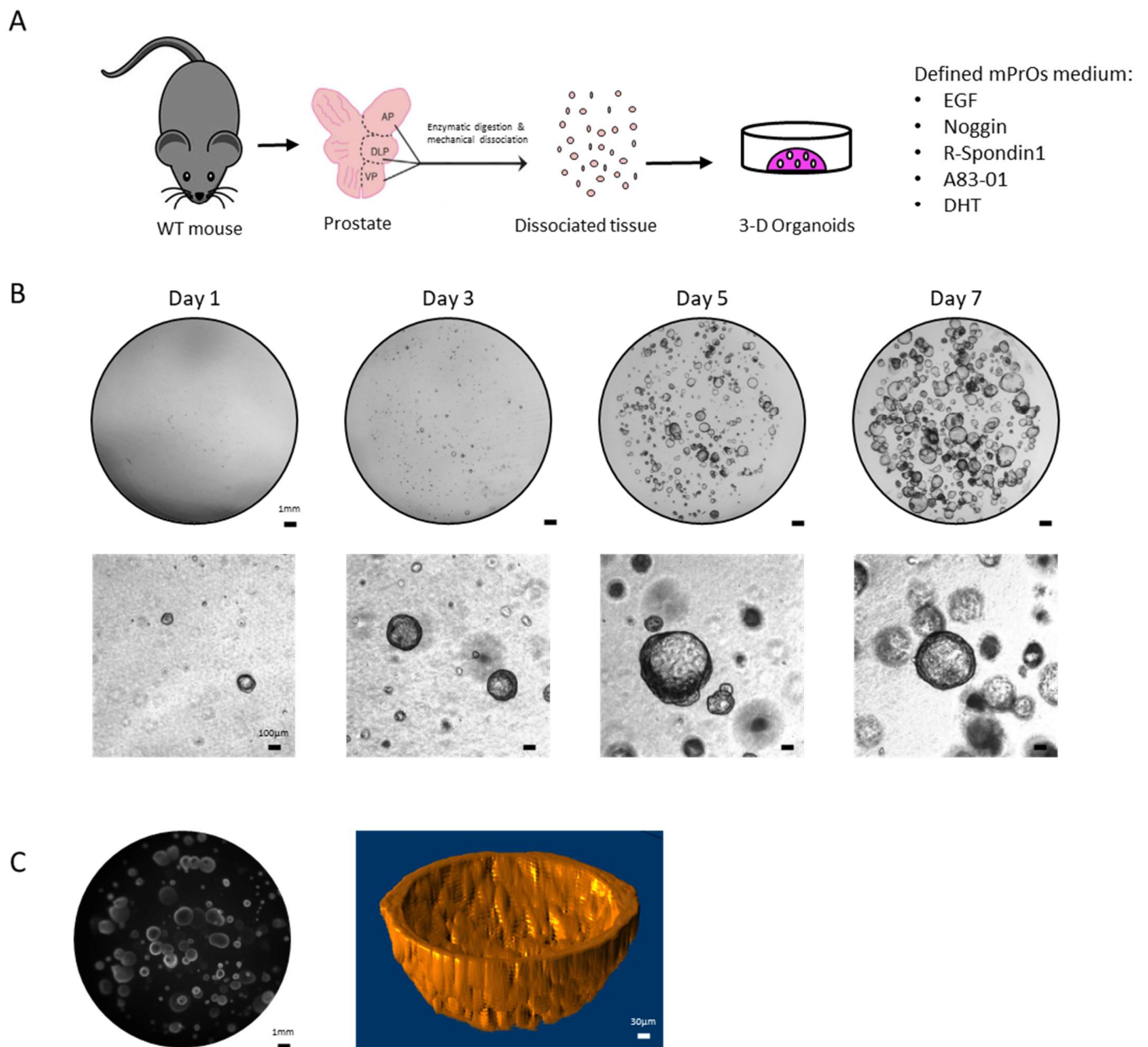


**Fig. 4.1:** Establishing mouse Prostate Organoids Culture. A) Scheme showing prostate organoids derivation from wild type mouse tissue. Resected prostate is dissociated as either whole organ or separated lobes through enzymatic and mechanical processing, then organoids are cultured in ECM-like domes with defined medium and 80% ECM-like matrix. B) Organoid culture growth within a single ECM-like dome. Upper images are taken with a stereomicroscope equipped with 1.6x objective, lower images are obtained with an inverted microscope equipped with 5x objective (scale bars: 1 mm for 1.6x images, 100µm for 5x images). C) Left image, taken with a stereomicroscope equipped with 1.6x objective, shows calcein viability dye staining (5 µM calcein incubated for 1 hour) of organoids culture highlighting the 3D organization within a single ECM-like dome. Right image represents a 3D reconstruction (ImageJ software with Volume Viewer plug-in) of a single calcein labeled organoid, generated from a series of images obtained through optical sectioning of an intact organoid (scale bars: 1 mm for fluorescent image, 30 µm for 3D reconstructed image).

epithelial cell lineages demonstrate the presence of both cellular populations. Importantly, the architecture of the spheres epithelium nicely resembles those of adult prostate tissue where basal cells surrounds luminal cells that face the lumen (**Fig. 4.2A-C**).

In addition to the assessment of the populations of cells forming the prostate spheres, we analyzed the dependency on testosterone, another key molecular aspect characterizing adult prostate tissue. Spheres were cultured in presence or absence of dihydrotestosterone (DHT) and levels and activity of AR was analyzed via Western blotting and AR-targets gene expression. These analyses show that AR is robustly expressed when DHT is added to the culture medium while protein level is substantially reduced following testosterone withdrawal (**Fig. 4.2D**). As expected, this is also evident from the analysis of AR-target genes whose expression is strongly influenced by DHT (**Fig. 4.2E**).

As a final confirmation of testosterone dependency, we performed a DHT cycling experiment (**Fig. 4.2F**). Spheres regularly cultured in complete medium for several passages were disaggregated and derived fragments seeded in medium depleted of DHT. After few days cellular aggregates were evident into the Matrigel® but they grew as such without forming round hollow spheres (**Fig. 4.2F**, central). Cell aggregates grow well in DHT-free medium and can be maintained indefinitely, but they lose the ability to self-assemble a prostate-like 3D architecture. However, administration of DHT to the medium is sufficient to rescue their ability to form round hollow prostate spheres (Cambuli *et al.*, *in preparation*).

To conclude our characterization, we decided to investigate the status of differentiation of basal and luminal cells in the spheres. The minimal expression of differentiation markers (Cambuli *et al.*, *in preparation*) combined with the high proliferation rate suggest that spheres are mainly composed by luminal and basal progenitor cells.

Overall, based on the data presented, we retain that mouse prostate spheres can be considered mouse prostate organoids (mPrOs) since they match the essential requisites defined by the scientific community (Lancaster and Knoblich, 2014).

## 4.2. Modeling ERG positive precursor prostate lesions

### 4.2.1. Generation of inducible ERG-overexpressing vector

In order to genetically engineer wild type mPrOs with a doxycycline inducible ERG expression vector system, we cloned *ERG* cDNA from VCaP cells, a human PCa cell line derived from a vertebral metastasis bearing the *TMPRSS2:ERG* translocation. In details, *ERG* cDNA starting from the methionine 40 within exon4 (*ERG*-isoform2, NM\_004449.4), that is considered the starting methionine in *TMPRSS2:ERG* mRNA (**Fig. 4.3A**) (Tomlins *et al.*, 2005; King *et al.*, 2009), was amplified by PCR with a specific set of primers and inserted following enzymatic



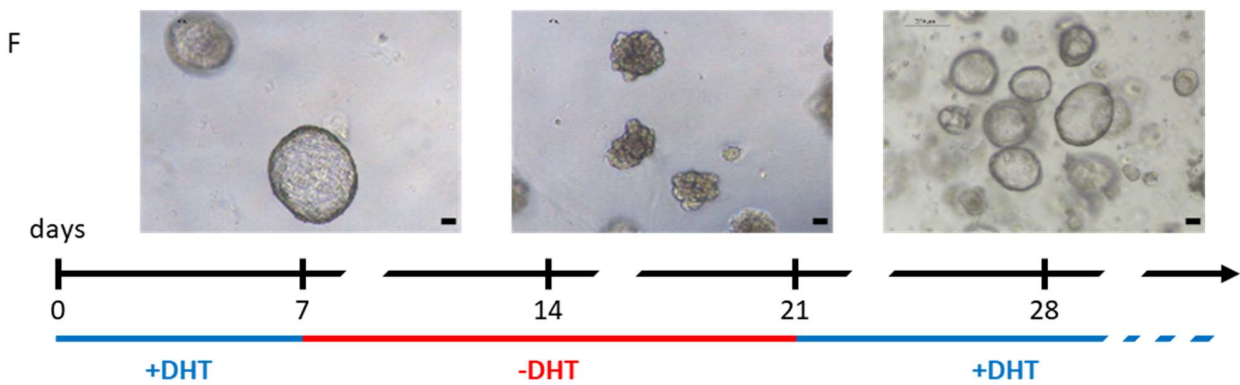
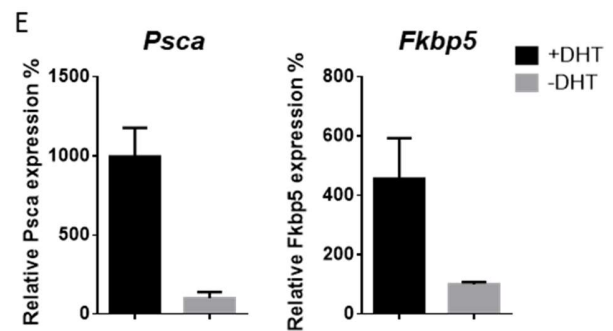
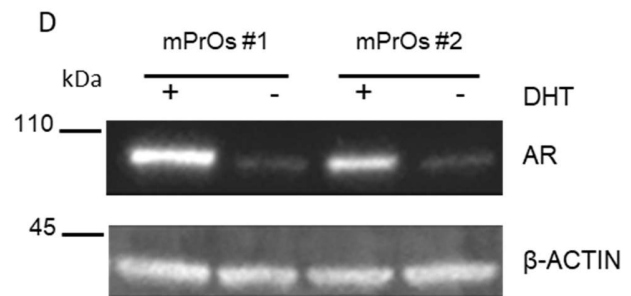
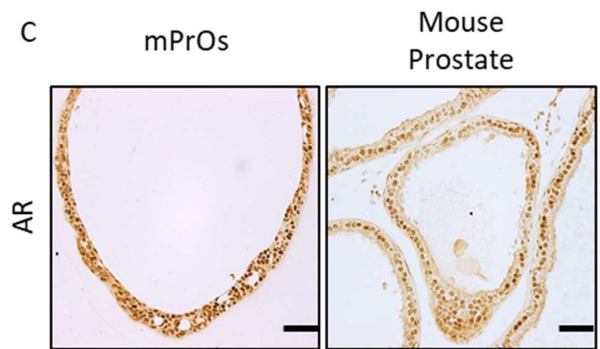
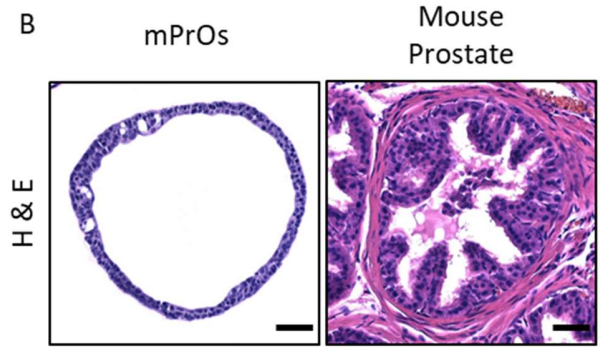
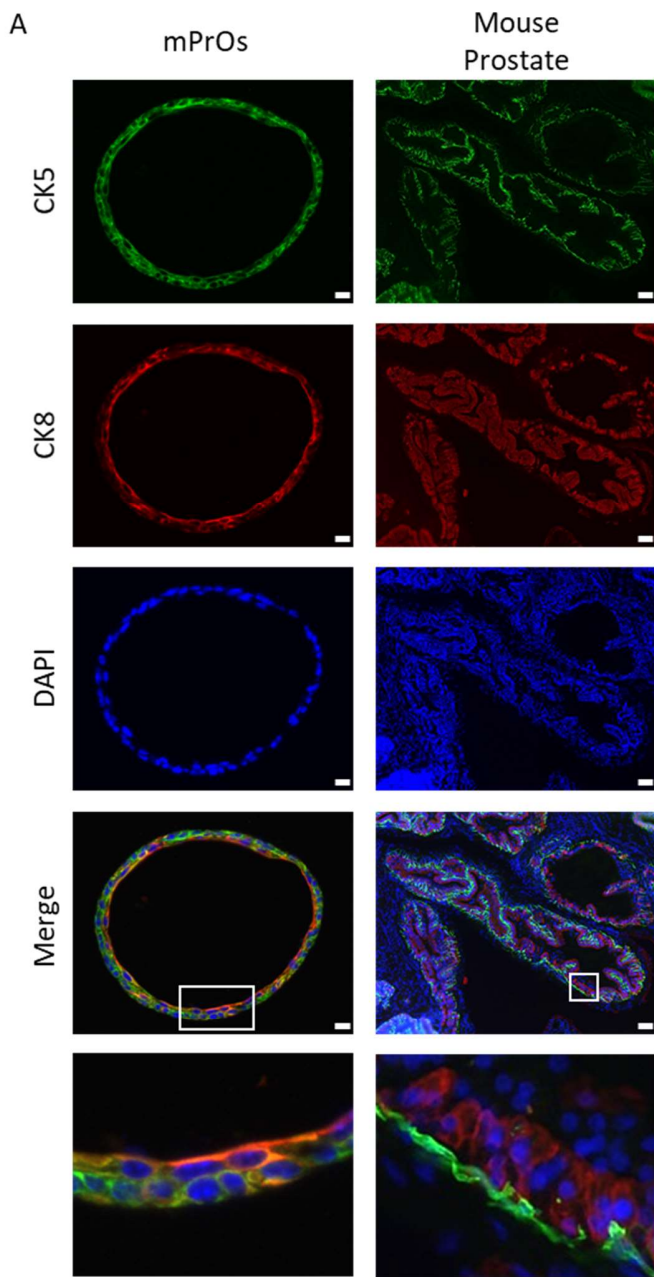


**Fig. 4.2:** Characterization of mouse Prostate Organoid model. A) Immunofluorescence analysis of luminal (CK8) and basal (CK5) cytokeratin localization in wild type mPrOs and mouse prostate tissue. Both series of images are taken with upright microscope equipped with 20x objective for mPrOs and 10x objective for prostate tissue, DAPI is used for nuclear staining (scale bars: 50  $\mu$ m for mPrOs, 500  $\mu$ m for mouse prostate; lowest row shows inset magnification of specified area within Merge images). B) Hematoxylin & Eosin stain of mPrOs-WT and mouse Prostate tissue. Both images are obtained with upright microscope equipped with 20x objective (scale bars: 50  $\mu$ m). C) Immunohistochemistry staining for AR comparing wild type mPrOs and prostate tissue. Both images are obtained with upright microscope equipped with 20x objective (scale bars: 50  $\mu$ m). D) Western immunoblot analysis of AR expression in organoid cultures in presence or absence of DHT.  $\beta$ -ACTIN used as loading control (n=2 biological replicates). E) RT-qPCR analysis of mouse AR-target genes in mPrOs-WT cultured in presence or absence of DHT. Sample cultured without DHT is used as reference. F) DHT cycling experiment showing the morphology of organoids culture in presence or absence of DHT, organoids are disaggregated and reseeded every 7 days, DHT is removed from culture medium at day 7 and administered again at day 21. Images are taken with inverted microscope equipped with 5x objective (scale bars: 100  $\mu$ m) at day 7, 21 and 28, respectively.

digestion into the retroviral pTGM-rtTA3-PURO plasmid downstream the TRE-CMV promoter element (**Fig. 4.3B**, pTGMP-ERG<sub>M40</sub>). The correct insertion of ERG<sub>M40</sub> cDNA was confirmed by sequencing.

The plasmid was then transfected into packaging (HEK293T) cells together with the packaging (pRetro-Gag-Pol) and the envelope (pHDM-VSVG) plasmids. 48 hours post transfection, retroviral particles were collected from the HEK293T cell supernatant and used for mPrOs transduction.

#### 4.2.2. ERG-overexpressing mPrOs

pTGMP-ERG<sub>M40</sub> allows the constitutive expression of rtTA3 and puromycin resistance while ERG transcription is inducible through doxycycline administration. pTGMP-ERG<sub>M40</sub> bearing viral particles were used to transduce wild type mPrOs generated by our group from the whole prostate of C57B6/J mice (Cambuli *et al.*, *in preparation*). Two days after transduction puromycin was added to the medium in order to obtain a homogeneous population of pTGMP-ERG<sub>M40</sub> transduced mPrOs (mPrOs-ERG<sub>M40</sub>).

mPrOs-ERG<sub>M40</sub> were grown for 4 passages (one month) in presence of puromycin to stabilize the line, then RT-qPCR and Western blot analyses were run on wild type mPrOs and mPrOs-ERG<sub>M40</sub> treated or not with 1  $\mu$ g/ml doxycycline for 96 hours (**Fig. 4.4A**). At mRNA level, ERG<sub>M40</sub> was robustly expressed in the mPrOs-ERG<sub>M40</sub> treated with doxycycline while a minimal expression was also noted in the non-induced mPrOs-ERG<sub>M40</sub> (**Fig. 4.4B, D**). These results highlight the fact that the system used for ERG<sub>M40</sub> overexpression has some leakage causing the production of few, but detectable, mRNA molecules in absence of doxycycline. At protein level, immunoblot analysis with a specific antibody showed ERG<sub>M40</sub> exclusively in the mPrOs-ERG<sub>M40</sub> treated with doxycycline (**Fig. 4.4C**).

Being ERG a transcription factor, we performed gene expression analysis on specific ERG-target genes in wild

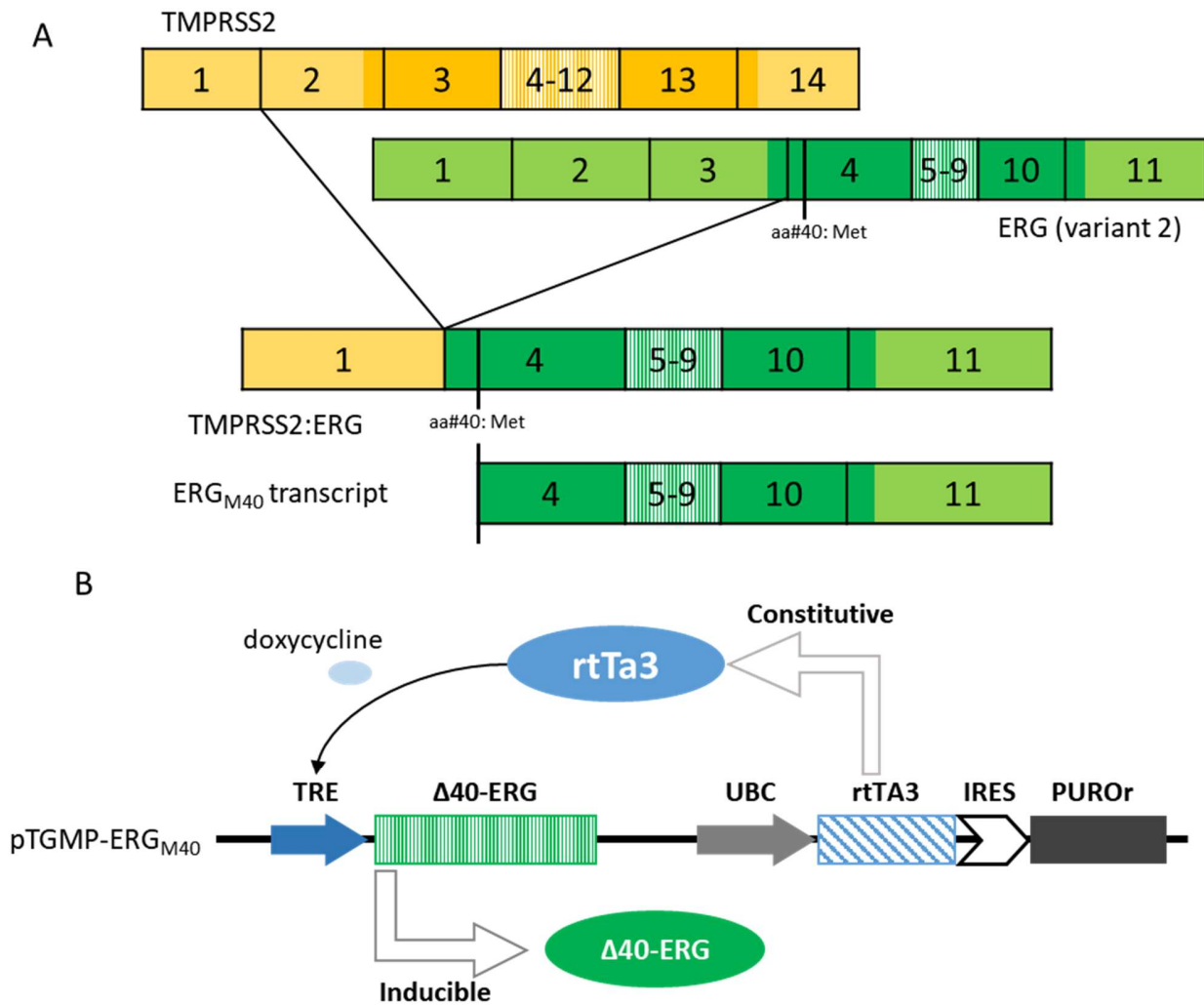
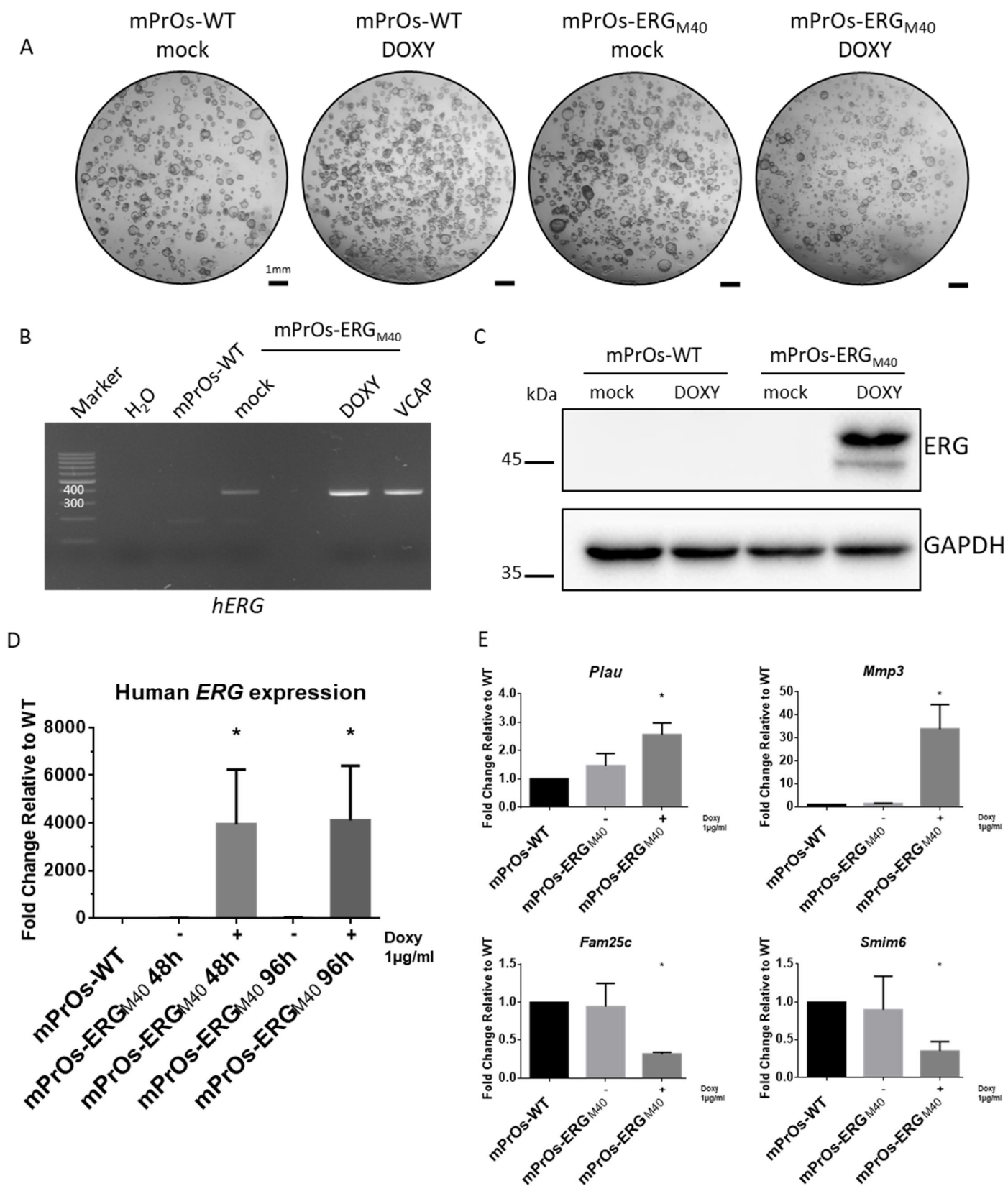


**Fig. 4.3:** TMPRSS2:ERG alteration in PCa and inducible ERG-expression vector system. A) Scheme of the most common TMPRSS2:ERG translocation identified in PCa; light colors: untranslated regions; darker color: coding region; vertical line in the ERG coding region identifies the Methionine at position 40, considered the starting methionine for the translation of the ERG fusion construct (Tomlins *et al.*, 2005; King *et al.*, 2009). B) Scheme of the retroviral system used for transduction and controlled expression of ERG<sub>M40</sub> sequence; vector contains a constitutive expressed rtTA3 coupled with puromycin resistance gene for selection of positive cells; ERG<sub>M40</sub> expression is induced upon rtTA3 binding to TRE after interaction with doxycycline molecule.

**Fig. 4.4:** Characterization of mPrOs-ERG<sub>M40</sub>. A) Phenotypic analysis of fully grown wild type and engineered mPrOs. Cultures were treated for 96h with or without doxycycline; images obtained with stereomicroscope equipped with 1.6x objective (scale bars: 1 mm). B) PCR analysis of human ERG expression in mPrOs; expected product length 368 bp, water used as negative control, cDNA from VCAP cell line used as positive control. C) Western immunoblot with ERG-specific antibody of protein extracts from mPrOs-WT and mPrOs-ERGM40 treated with or without doxycycline for 96 hours; GAPDH used as loading control. D) RT-qPCR analysis of human ERG expression on engineered mPrOs-ERG<sub>M40</sub> with or without doxycycline treatment for either 48 or 96 hours; mPrOs-WT used as reference; n=4. E) Gene expression analysis of known ERG-target genes; RNA was extracted and retrotranscribed from mPrOs-ERG<sub>M40</sub> after treatment with or without doxycycline for 96 hours; mPrOs-WT used as reference, n=3. Statistical analyses performed with GraphPad PRISM V. 6.01; \* = p value <0,05; \*\*\* = p-value <0,001



type mPrOs and mPrOs-ERG<sub>M40</sub> cultured for 96 hours either in presence or absence of 1 µg/ml doxycycline. RT-qPCR analysis on *Plau*, *Mmp3*, *Fam25c* and *Smim6* suggests a transcriptionally active ERG<sub>M40</sub> (Fig. 4.4E) since all four genes behave as expected from literature (Tomlins *et al.*, 2008; Chen *et al.*, 2013).

In addition to gene expression, immunofluorescence analysis performed on paraffin embedded sections of both wild type mPrOs and mPrOs-ERG<sub>M40</sub> either treated or not with doxycycline for 96 hours showed nuclear ERG staining only in doxycycline treated mPrOs-ERG<sub>M40</sub> (Fig. 4.5A). Unexpectedly, immunofluorescence staining for the basal lineage marker cytokeratin 5 (CK5) and for the luminal lineage marker cytokeratin 8 (CK8) pointed out the diffusion of CK8 signal towards the basal layer that appeared thinner in doxycycline treated mPrOs-ERG<sub>M40</sub> (Fig. 4.5A, 3<sup>rd</sup> and 4<sup>th</sup> rows). To verify the qualitative data coming from the IF studies, both RT-qPCR and immunoblot were performed on wild type mPrOs and mPrOs-ERG<sub>M40</sub> either treated or not for 96 hours with doxycycline (Fig. 4.5B-C). In line with immunofluorescence analysis, these additional experiments showed a marked and significant reduction in the expression of the basal cell marker *Ck5* with a concomitant increase of the luminal marker *Ck8* at both mRNA and protein level.

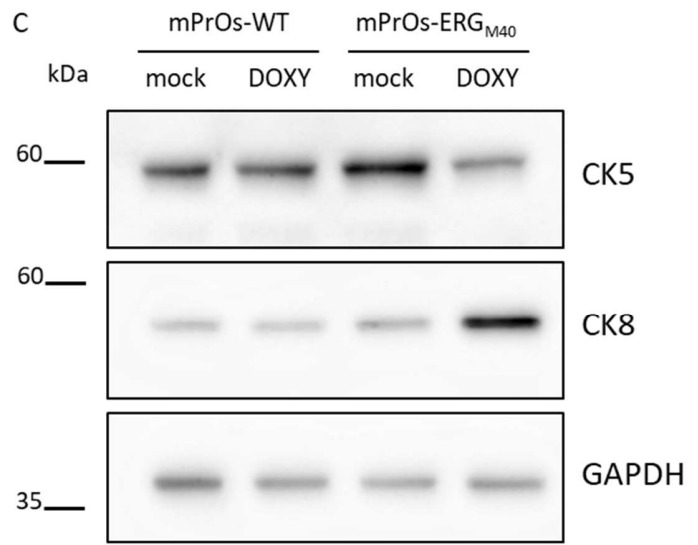
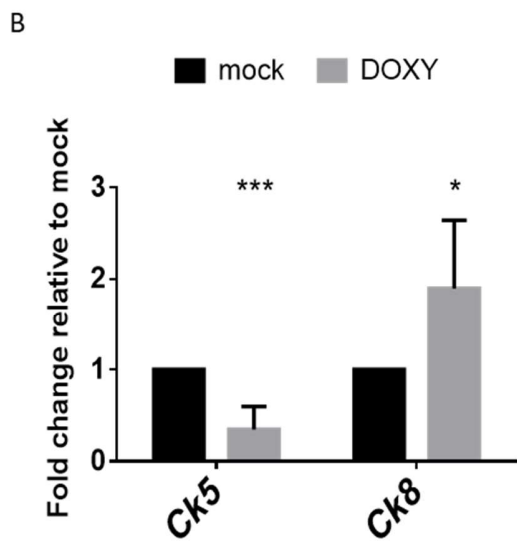
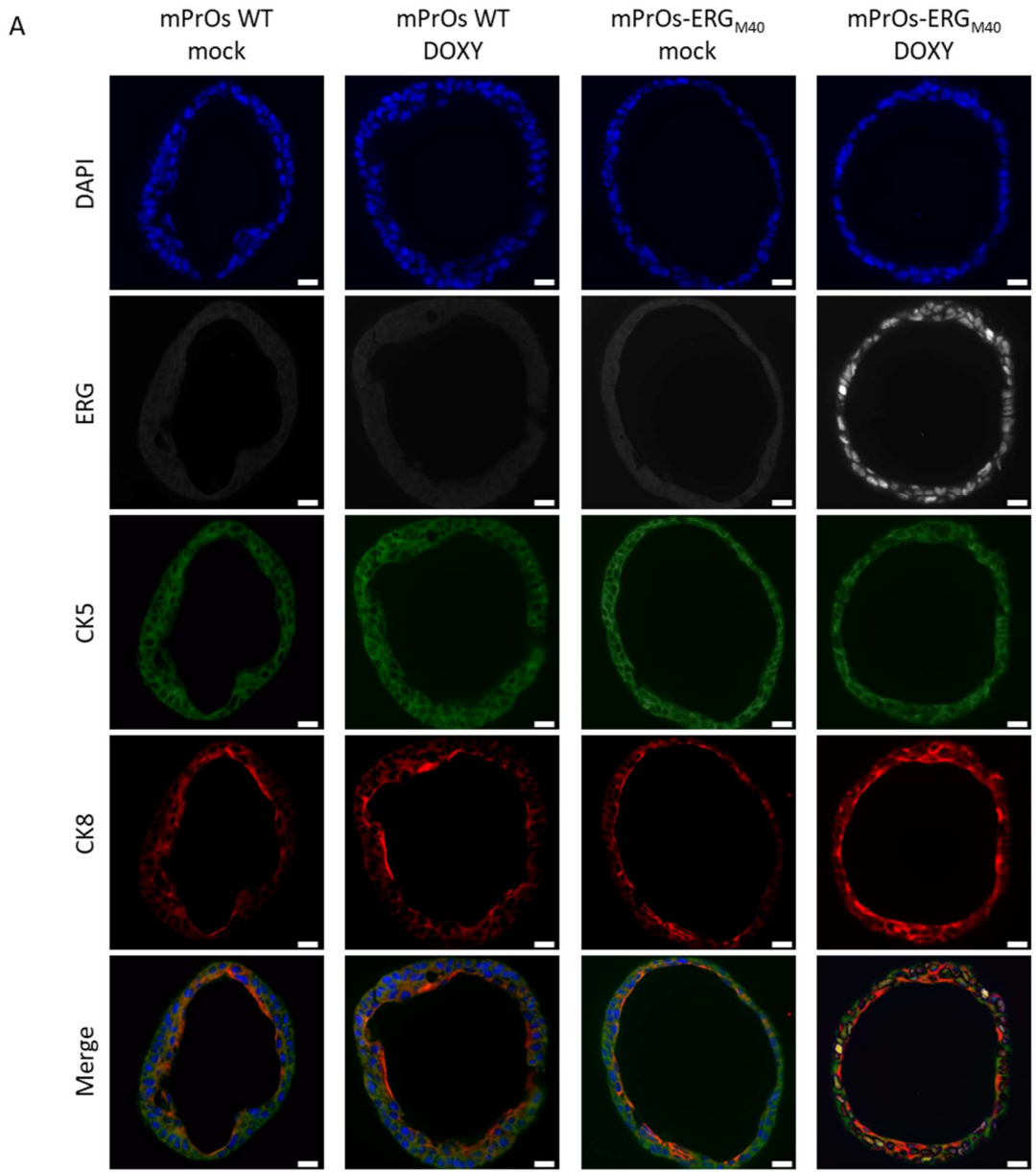
Interestingly, the increase in the luminal epithelial compartment in PIN and HGPIN prostate lesion is frequently associated with a reduction of the basal cell layer (Klezovitch *et al.*, 2008).

In addition to the expression and localization of luminal and basal epithelial markers, we analyzed the proliferation rate of wild type mPrOs and mPrOs-ERG<sub>M40</sub> either with or without doxycycline administration. Immunofluorescence staining of the proliferation marker Ki67 was performed on paraffin embedded sections following 96 hours of doxycycline treatment (Fig. 4.6A). Quantification of Ki67<sup>+</sup> cells in the four different conditions shows a significant reduction in the number of proliferating cells in ERG<sub>M40</sub> expressing mPrOs (Fig. 4.6B-C). Even though the context is different, ERG expression was recently described to reduce tumor aggressiveness in the *Pten/Trp53* double null genetic engineered mouse model of PCa by decreasing cell proliferation and promoting luminal differentiation in mouse prostate tumors (Blee *et al.*, 2018).

In order to further investigate this phenotype, wild type mPrOs and mPrOs-ERG<sub>M40</sub> were either treated or not with doxycycline for 96 hours, of which the last 3 hours with 5-ethynyl-2'-deoxyuridine (EdU). Then, organoids were dissociated to single cells and EdU incorporation analyzed by flow cytometry to identify and quantify cells

**Fig. 4.5:** Analysis of Cytokeratins expression in mPrOs-ERG<sub>M40</sub>. A) Immunofluorescence analysis of ERG, CK8 and CK5 expression and localization in wild type and engineered organoids after treatment with or without doxycycline for 96 hours, DAPI used for nuclear staining; all images are obtained with an upright microscope equipped with 20x objective (scale bars: 100 µm). B) Results from RT-qPCR analysis of *Ck5* and *Ck8* expression in mPrOs-ERG<sub>M40</sub> with or without doxycycline treatment for 96 hours, untreated mock condition used as reference, n=3. C) Western immunoblot analysis of CK8 and CK5 expression in wild type and engineered mPrOs after either mock or doxycycline treatment for 96 hours; GAPDH is used as normalization and loading control.

Statistical analyses performed with GraphPad PRISM V. 6.01; \* = p value <0,05; \*\*\* = p-value <0,001



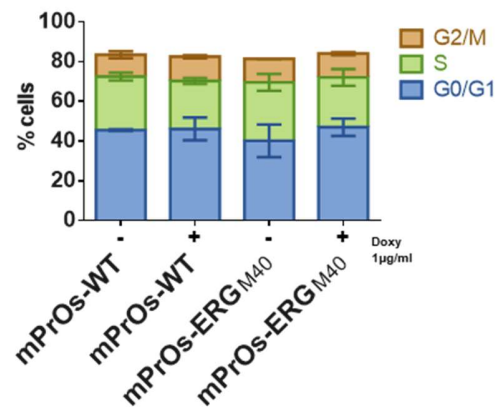
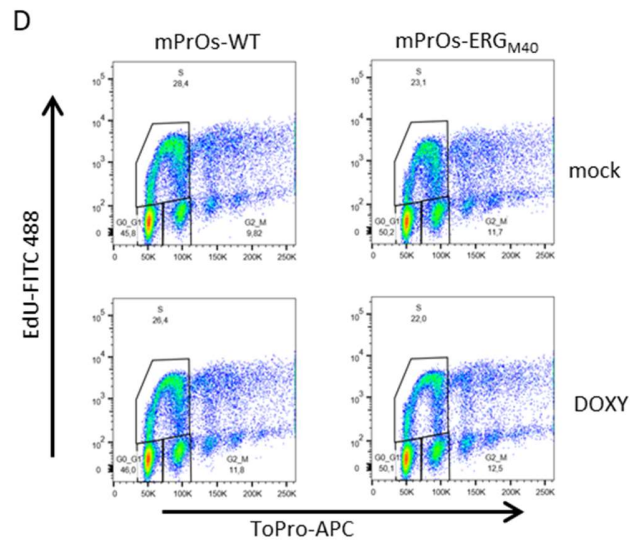
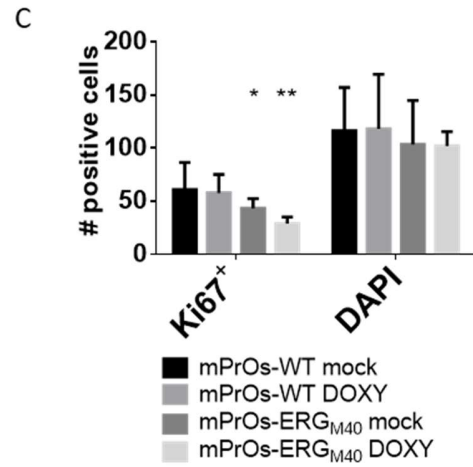
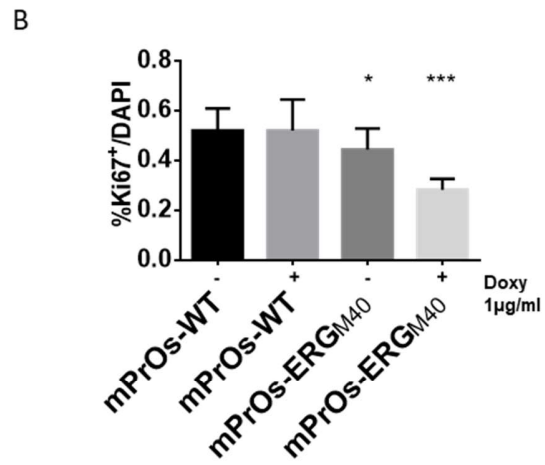
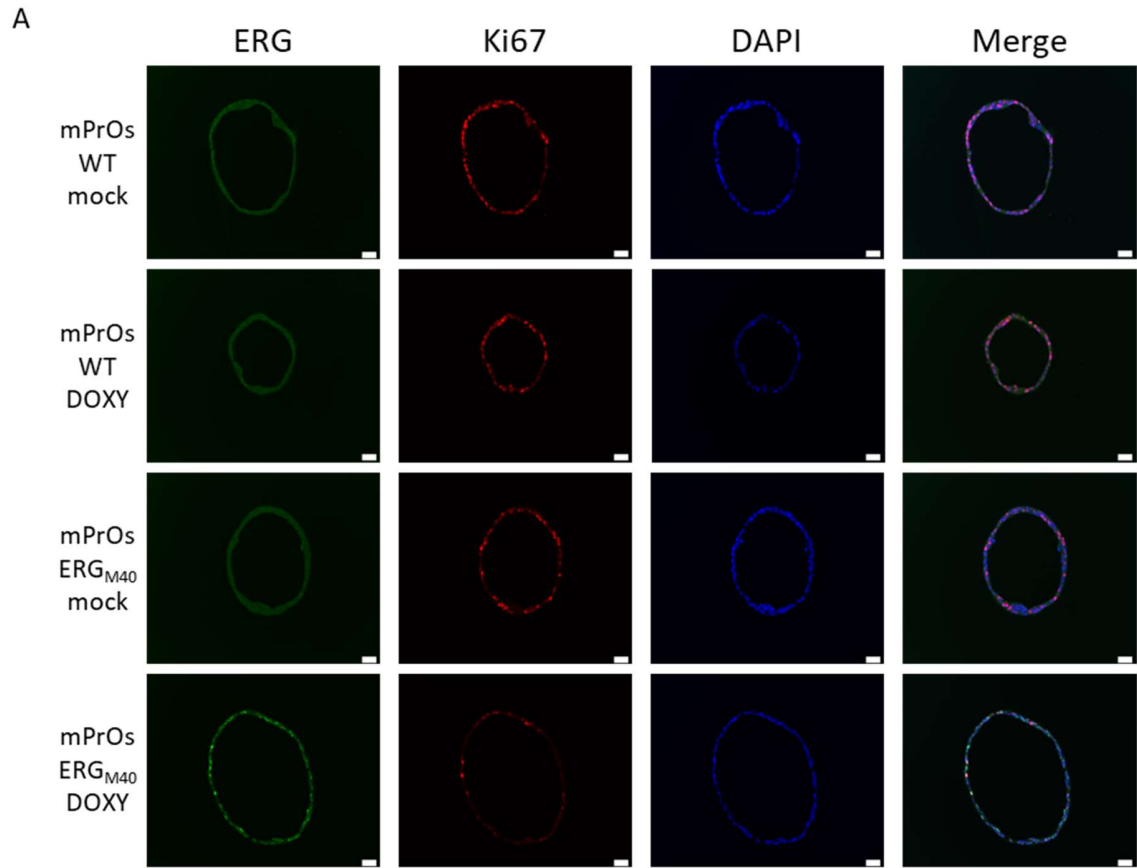


**Fig. 4.6:** Analysis of wild type and ERG<sub>M40</sub> mPrOs proliferative state. A) Immunofluorescence analysis of ERG and Ki67 expression in wild type and engineered organoids treated with or without doxycycline for 96h, DAPI is used for nuclear staining; images are acquired with an upright microscope equipped with 20x objective (scale bars: 50  $\mu$ m). B) Quantification of Ki67<sup>+</sup> cell fraction from immunofluorescent staining of wild type mPrOs and mPrOs-ERG<sub>M40</sub> treated for 96 hours with or without doxycycline; n=11. C) Quantification of the number of Ki67<sup>+</sup> cells and total number of cells from immunofluorescent staining of wild type mPrOs and mPrOs-ERG<sub>M40</sub> treated for 96 hours with or without doxycycline; data used to calculate fraction of Ki67<sup>+</sup> cells in B, n=11. D) Analysis of cell cycle progression of wild type and engineered organoids treated for 96 hours with or without doxycycline, the FACS plots show the gates identifying the different cell cycle phases. The histogram on the left shows the quantification of the FACS analysis; blue: G0/G1 phase cells, green: S phase cells, red: G2/M phase cells; n=3. Statistical analyses performed with GraphPad PRISM V. 6.01; \*= p-value <0,05; \*\*= p-value <0,01; \*\*\*= p-value <0,001

in S-phase (active DNA replication). Unexpectedly, EdU incorporation did not show any significant alteration in the fraction of cells in active DNA replication in the four different conditions (**Fig. 4.6D**). To disentangle this apparent paradox, we decided to maintain ERG expression in mPrOs for two weeks and evaluate phenotypically the possible effect of ERG on mPrOs. At the end of the first week a barely detectable reduction of organoids size and number characterized doxycycline treated mPrOs-ERG<sub>M40</sub> (**Fig. 4.7**). Such differences became much more pronounced in doxycycline treated mPrOs-ERG<sub>M40</sub> at the end of the second week, thus confirming a mild but consistent role of ERG in decreasing the proliferative potential of mPrOs.

Overall, since Ki67 expression characterizes the G1, S, G2 and M phases of the cell cycle with the exclusion of G0, while EdU incorporation labels cells in the S-phase, these results could suggest a role of ERG in favoring the transition of proliferating prostate cells to a more quiescent status, more than the inhibition of the G1-S progression of the cell cycle.

Cell cycle exit and luminal commitment hardly match the thesis of a pro-tumorigenic role of ERG expression in PIN and HGPIN prostate lesions. However, besides proliferation and poor differentiation, an essential requisite that increases the risk of a malignant transformation is the ability of pre-malignant cells to grow in conditions of nutrients and growth factors restrictions.

To address this point, wild type and ERG<sub>M40</sub> mPrOs were cultured with or without doxycycline, and with or without Epithelial Growth Factor (EGF) for up to two weeks. Compared to normal conditions (EGF 50 ng/ml), EGF withdrawal drastically affects the growth of doxycycline treated and untreated wild type mPrOs and doxycycline untreated mPrOs-ERG<sub>M40</sub>. Contrarily, doxycycline treated mPrOs-ERG<sub>M40</sub> could still form 3D organoids composed of vital cells, as observed with calcein labeling, in the absence of EGF (**Fig. 4.8**).

Overall, these findings demonstrate that ERG expressing organoids can be less influenced by restrictive growth conditions than wild type mPrOs, even though ERG may reduce cell proliferation and increase luminal commitment in normal culture settings.



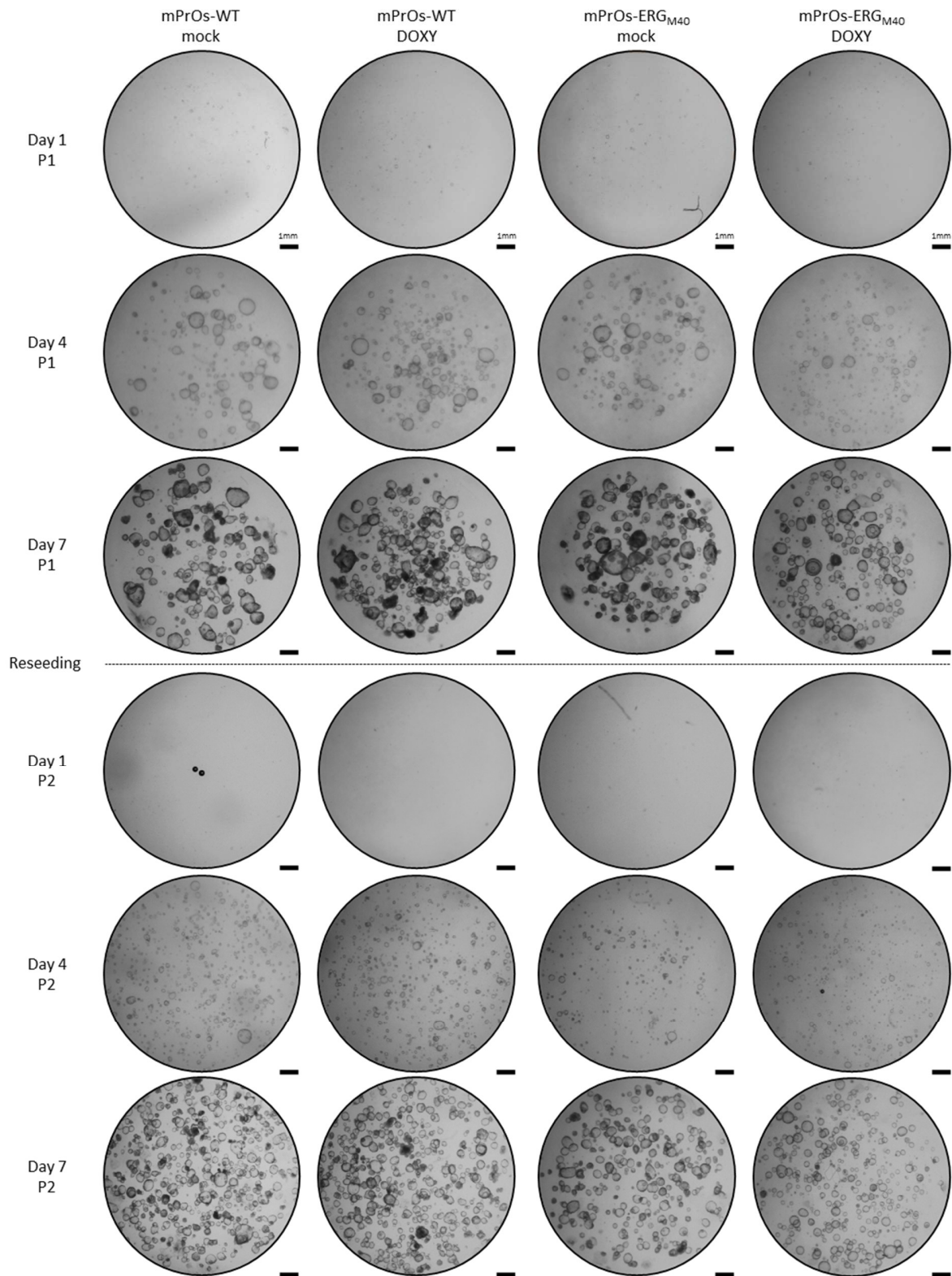


**Fig. 4.7:** Effects of long term ERG induction on mPrOs cultures, phenotypic analysis of mPrOs growth with defined culture medium. Both wild type or engineered organoids treated with or without doxycycline were cultured for up to two weeks, on the eighth day organoids were mechanically disaggregated and reseeded to maintain them for additional 7 days, doxycycline treatment was maintained for the whole duration of the experiment. Images obtained with stereomicroscope equipped with a 1.6x objective (scale bars: 1 mm).

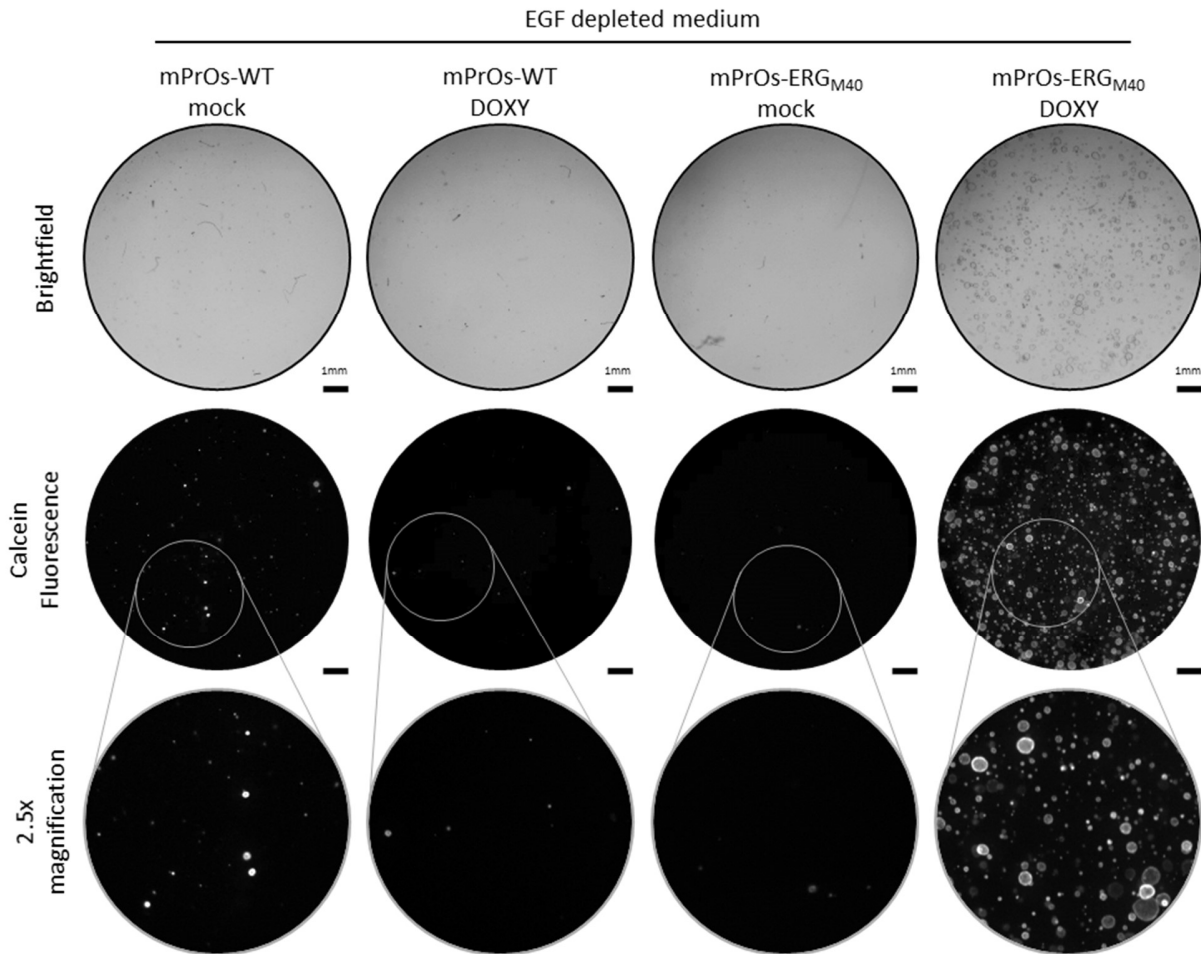


**Fig. 4.8:** Effects of long term induction of ERG expression in growth factor restrictive mPrOs cultures conditions, phenotypic analysis of organoids growth in absence of EGF. Both wild type and engineered mPrOs with or without doxycycline treatment were cultured with EGF-free medium for up to two weeks, doxycycline was maintained throughout the duration of the experiment, on the eighth day cultures were disaggregated and entirely reseeded. Images are acquired with stereomicroscope equipped with 1.6x objective (scale bars: 1 mm), fluorescent images obtained incubating the culture for 1 hour with 5  $\mu$ M calcein viability dye. Lowest series shows 2.5x magnification of specified area within fluorescent images.

Based on the results obtained so far, we can conclude that: **i)** mPrOs are an innovative and valuable tool to model and study *in vitro* prostate physiology and tumorigenesis, a better characterization of this model will further improve its reliability and applicability in PCa research; **ii)** viral vector transduction can be used to model common PCa alterations in mPrOs; **iii)** the system that we developed is functional and can be efficiently controlled; **iv)** human ERG can interact and regulate the expression of known ERG-target genes in the mouse genome; **v)** ERG activity may influence prostate epithelial cell by favoring a quiescent status and the commitment toward the luminal lineage; and, finally, **vi)** the analyses performed so far suggest a potential role of ERG as pro-survival factor in restrictive growth conditions.

### 4.3. CLICK-MS approach

#### 4.3.1. Combining CLICK-MS and WT mPrOs

Besides the acquisition of critical characteristics such as a deregulated proliferation, the ability to survive under restrictive growth conditions, the loss of a tight and precise cell-cell and cell-extracellular matrix architecture, pre-malignant cells have to succeed in modeling the tissue microenvironment in order to create a supportive and immune lenient niche. It is well known that, in such scenario, extracellular signals play pivotal functions.

CLICK chemistry coupled with Mass Spectrometry (CLICK-MS) is a novel and very efficient method for the study of secreted proteins (Eichelbaum *et al.*, 2012; Eichelbaum and Krijgsveld, 2014). CLICK-MS is based on the labeling

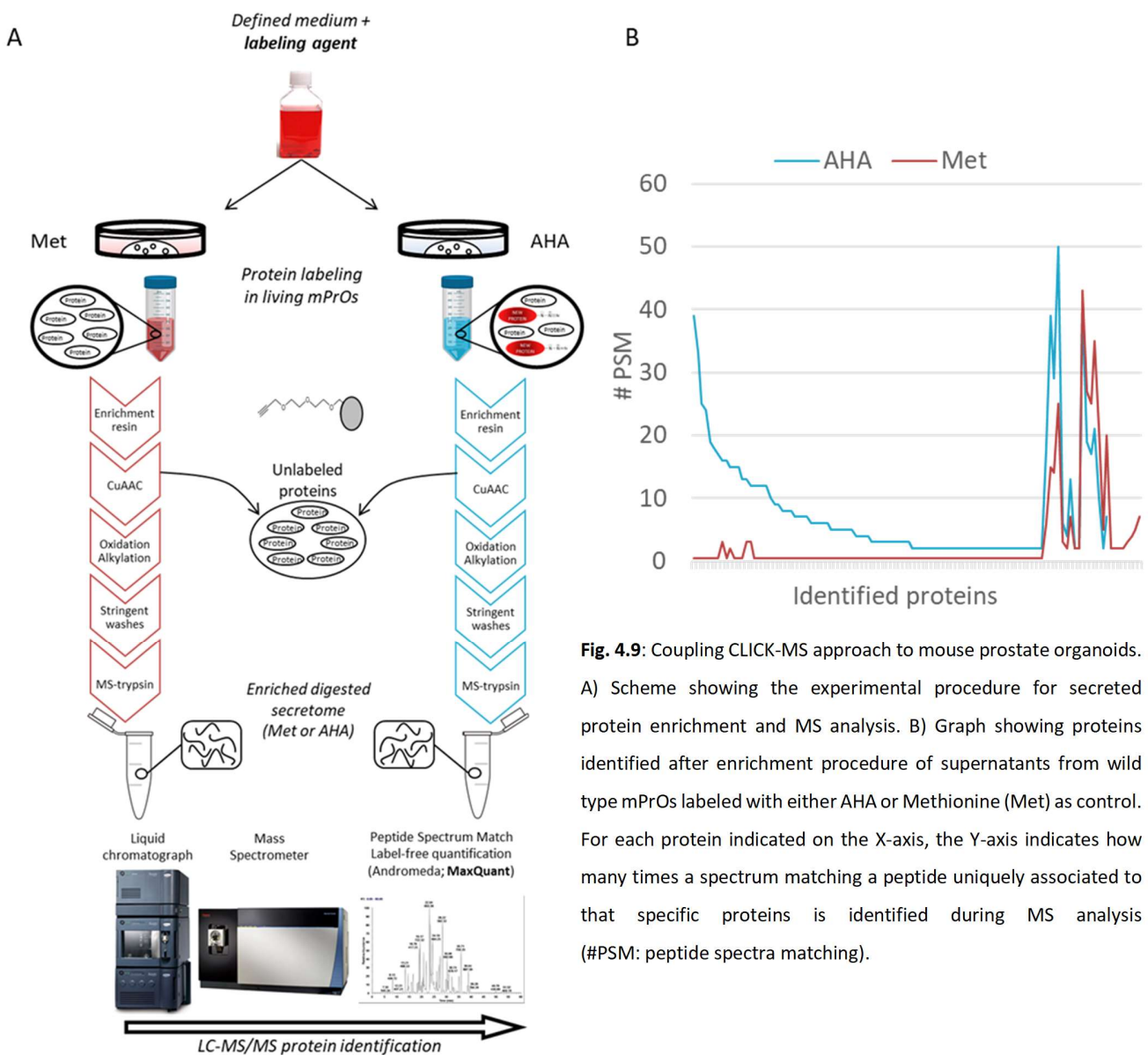


**Fig. 4.9:** Coupling CLICK-MS approach to mouse prostate organoids. A) Scheme showing the experimental procedure for secreted protein enrichment and MS analysis. B) Graph showing proteins identified after enrichment procedure of supernatants from wild type mPrOs labeled with either AHA or Methionine (Met) as control. For each protein indicated on the X-axis, the Y-axis indicates how many times a spectrum matching a peptide uniquely associated to that specific proteins is identified during MS analysis (#PSM: peptide spectra matching).

of newly synthesized proteins with AHA (L-Azido-homo-alanine, a methionine mimetic), which is internalized by living cells from the medium and utilized as methionine during protein synthesis. Incubation of cell supernatant with a specific matrix, followed by the addition of copper (CuII), promotes the covalent binding of AHA-labeled proteins to the resin. After several washes with denaturing buffers, enriched AHA-proteins are then digested with trypsin and peptides analyzed by mass spectrometry.

Secretome is an unexplored area in the biology of prostate organoids whose characterization, however, will be functional to deepen our knowledge about this new biological system and, potentially, to unravel important new aspects of prostate tissue homeostasis and tumorigenesis.

To fill this gap, we performed an initial set of experiments to test the applicability of CLICK-MS to profile the protein secretome of wild type mPrOs. Scheme in **Fig. 4.9A** shows the experimental protocol used for secretome labeling, enrichment and analysis. Due to the fact that Advanced DMEM/F12 (organoid basal medium) methionine-free is not commercially available, wild type mPrOs derived from the prostate of outbred CD1 mice grew over night in homemade methionine-free mPrOs medium (methionine-free cysteine-free DMEM, AlbuMAX™, Non-Essential amino acids, L-Cysteine, Ascorbic acid, holo-transferrin, insulin, ethanolamine, L-glutathione, sodium pyruvate, HEPES, Glutamax™, B27, N-acetyl-L-cysteine, EGF, Noggin, R-Spondin, A83-01, DHT), supplemented with either the labeling agent (AHA) or regular methionine (Met) as control. mPrOs cultures treated with AHA did not show any signs of stress or phenotypic differences due to the overnight (O/N) labeling when compared with control (Met) mPrOs (*data not shown*). Supernatants were collected and processed as accurately described in the methodological section of this thesis (Material and Methods chapter 8.8.1; Eichelbaum and Krijgsveld, 2014). The results of the MS-analysis of both Met- and AHA-labeled samples are presented in **Fig. 4.9B**, while the list of all the proteins identified is reported in Table-S1. The Y-axis in **Fig. 4.9B** describes how many times a peptide uniquely associated to a protein was identified respectively in AHA or Met samples (#PSM), while on the X-axis are reported the specific mouse proteins identified in this analysis.

Overall, this analysis demonstrates that CLICK-MS is a suitable approach to study mPrOs protein secretome. The minimal fraction of proteins actively secreted by mPrOs in the culture medium is efficaciously sequestered and enriched by the CLICK system. Furthermore, the majority of the proteins identified in the AHA-labeled samples results almost undetectable in the Met-labeled samples, thus proving the very high selectivity of the system for AHA-labeled neo-synthesized proteins. Finally, the prevalence of secreted and membrane associated extracellular proteins (validated or predicted) in the MS analysis highlights the effectiveness of our approach.

Even though the results obtained were encouraging, our MS analysis identified several abundant peptides derived from bovine albumin (AlbuMAX™) in both AHA- and Met-labeled samples. This contamination consistently reduces the protein identification power of MS (**Fig. 4.9B**, right side of the graph), but, being albumin an essential component of the medium, it could not be simply removed.

Therefore, before moving on with the analysis of the protein secretome from genetically modified mPrOs, we decided to test potential strategies to improve the CLICK-MS protocol by reducing albumin peptides contamination.

#### 4.3.2. CLICK-MS approach refinement

According to Eichelbaum and colleagues, a high content of cysteine residues in albumin-derived peptides is responsible for non-specific covalent bonds with the alkyne groups of the resin. Cysteine alkylation of the supernatants before the cyclo-addition reaction can reduce the contamination by blocking free-reactive cysteine residues (Eichelbaum and colleagues, personal communication).

In parallel with the addition of the alkylation step in the protocol, as second option, we tried to lower the albumin content from the collected mPrOs supernatants before the cyclo-addition step through an albumin deprivation kit (Pierce™ Albumin Depletion kit, 85160, Life Tech.). However, since albumin deprivation kits are highly efficient for human albumin but very low for bovine albumin, we modified the receipt of the methionine-free medium by replacing AlbuMAX™ with human albumin.

As shown by the results of the CLICK-MS analysis described in **Fig. 4.10A**, albumin deprivation was totally unsuccessful by leading to a lower protein identification power than without the deprivation step.

On the other hand, the addition of the alkylation step reduced albumin peptides (measured as fraction of albumin detected in the analysis, **Fig. 4.10A**, right histogram) thus increasing the protein identification power of MS analysis. Finally, we noted that human albumin compared to AlbuMAX™ led to a higher number of identified proteins with also an improved quality of the MS data (*data not shown*).

Taking into account all these observations, the inclusion of the alkylation step in the CLICK-MS protocol and the replacement of AlbuMAX™ with human albumin in the methionine-free mPrOs medium have substantially improved the CLICK-MS approach for the analysis of mPrOs protein secretome.

##### 4.3.2.1. Robustness of CLICK-MS approach and pathway analysis

Once refined the CLICK-MS protocol, the second milestone to achieve was “*reproducibility*”. In order to evaluate the robustness of CLICK-MS approach to profiling mPrOs protein secretome, we performed CLICK-MS analysis from wild type mPrOs derived from inbred C57B6/J mouse prostate. The decision to shift to organoids derived from inbred C57B6/J mice was dependent by the profound characterization of C57B6/J organoids, compared to the CD1, conducted in our laboratory in the past years (Cambuli *et al.*, *in preparation*). Four independent

biological replicates were analyzed over six months and more than 200 proteins *per* replicate were unequivocally identified by at least two unique peptides. The number of identified peptides uniquely associated to a specific protein was used as a proxy for the presence of that protein in the sample and it allows to measure the degree of overlap among the 4 replicas. With 172 proteins recurrently identified in all the 4 biological replicates

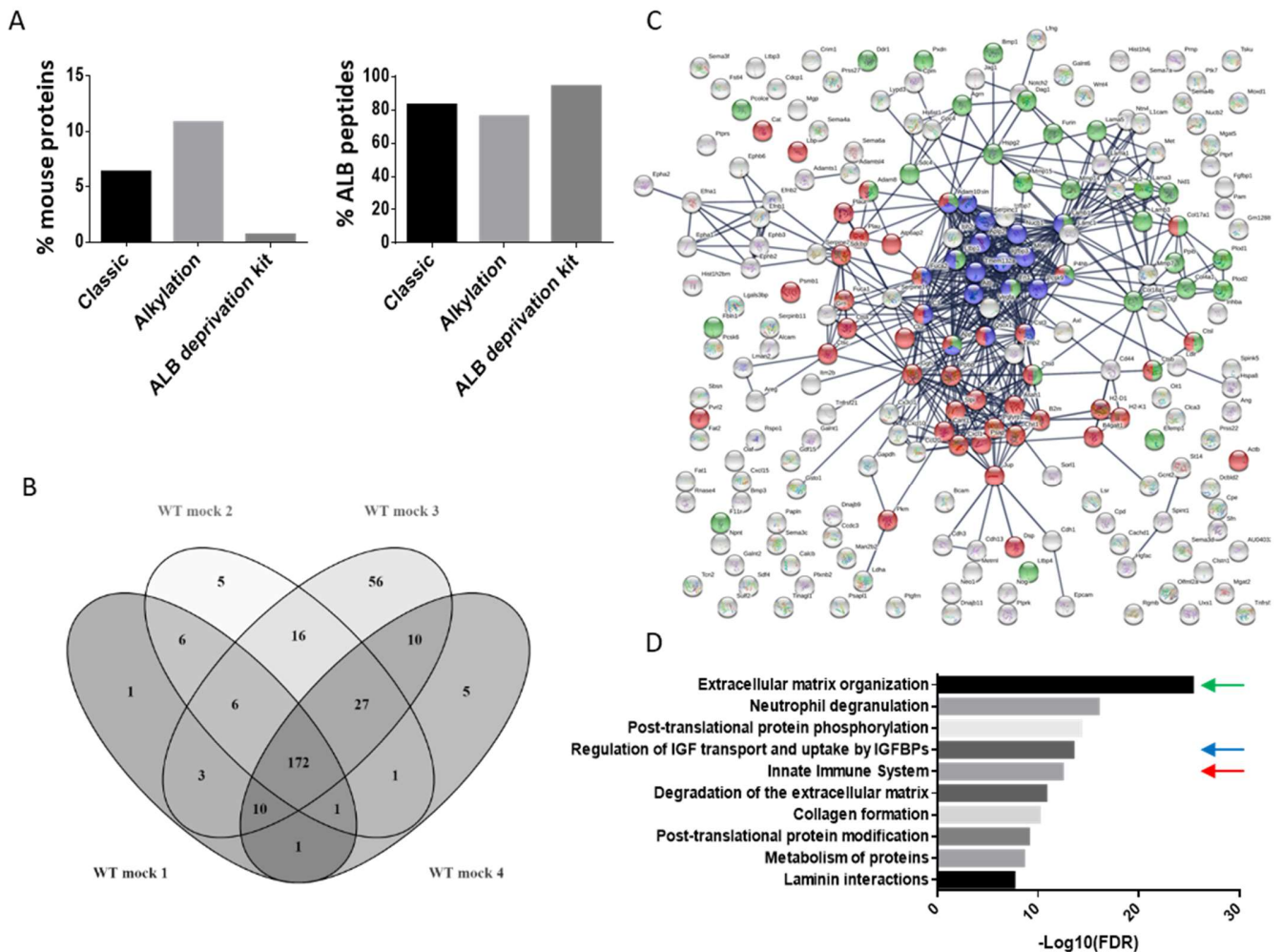


**Fig. 4.10:** CLICK-MS approach refinement. A) Results obtained after applying different methods for albumin deprivation. Left histogram shows the percentage of mouse identified proteins from the total number of identified proteins during MS analysis, right graph shows the percentage of identified peptides associated to albumin during the MS analysis. B) Venn diagram showing the number of proteins identified from the analysis of 4 biological replicates of wild type mPROs. The diagram shows how many proteins are present in one or more-than-one replica, a protein is considered present in a specific sample if identified with at least 2 “Unique peptides”. C) Network analysis of proteins obtained from the analysis of wild type mPROs considering only proteins identified with at least 2 “Unique peptides” in at least 3 different biological replicates. Network generated with STRING v11.0 (confidence score  $\geq 0.9$ ), colored spots highlight proteins associated with a particular Reactome pathway: green  $\rightarrow$  Extracellular matrix organization (MMU-1474244); blue  $\rightarrow$  Regulation of IGF transport and uptake by IGFBPs (MMU-381426); red  $\rightarrow$  Innate immune system (MMU-168249). D) Histogram showing the top 10 enriched pathways identified with STRING analysis within the network present in C. Entries are sorted based on False Discovery Rate (FDR), colored arrows indicate the pathways highlighted in C maintaining the same color code.

(Fig. 4.10B), CLICK-MS showed robustness beyond the expectation and further proved the remarkable stability of wild type mPROs cultures over time (Karthaus *et al.*, 2014; Drost *et al.*, 2016; Cambuli *et al.*, *in preparation*).

To our knowledge, an unbiased profile of wild type prostate organoids protein secretome has not yet been described. Characterization of proteins actively released by wild type prostate organoids in the extracellular milieu can contribute to the better understanding of this novel biological model and, in turn, to open new windows of opportunity to decipher physiology and disease of prostate tissue. Accordingly, different types of pathways analysis were performed on the list of secreted proteins described in Table-S2. Only those proteins identified in at least 3 out of 4 replicates by at least two unique peptides were included in the analyses. STRING software (V 11.0; Mering *et al.*, 2003; Szklarczyk *et al.*, 2019) was used to investigate protein networks. Data generated from this analysis includes a total number of 216 proteins and shows 3 highly connected cores of elements (Fig. 4.10C-D). As a consequence of the high level of confidence (interaction score  $\geq 0.9$ ) imposed to the analysis, almost 40% of proteins are not connected with any other element meaning that other interesting networks could potentially emerge by lowering stringency. From this analysis, the three most represented pathways are highlighted with colored nodes: Extracellular matrix (ECM) organization (MMU-1474244) in green; Regulation of IGF transport and uptake by IGF-BPs (MMU-381426) in blue, and Innate immune system (MMU-168249) in red. The fact that these 3 processes include most of the highly connected nodes emphasizes a possible functional crosstalk between prostate organoid cells and the surrounding environment that can pave the way for future studies aimed at enriching our knowledge about the epithelial-to-epithelial and epithelial-to-stroma cells interactions in normal and pathological conditions.

In addition to the network analysis, ontology classification was performed on the protein list by using DAVID V. 6.8 online tool (Huang, Sherman and Lempicki, 2008, 2009). As expected, the most significant enriched GO-terms in the analysis were related to the *extracellular region* (115 hits,  $9.4E-48$ ), *extracellular space* (106 hits,  $8.0E-45$ ), *extracellular exosomes* (130 hits,  $1.1E-41$ ), *extracellular matrix* (44 hits,  $4.2E-20$ ), and *basement membrane* (26 hits,  $9.9E-13$ ) (Table-S3). Importantly, a literature-based study of the identified proteins defined more than 20% (Pavlou and Diamandis, 2010; Eichelbaum *et al.*, 2012; Principe *et al.*, 2012; Nurdin *et al.*, 2016; Shi *et al.*, 2017) as already known prostate secreted factors, thus further reinforcing the thesis that mPROs can be an interesting new biological system to model and study prostate tissue.

## 4.4. Studying ERG role(s) in precursor prostate lesions from an extracellular perspective.

### 4.4.1. Profiling the secreted protein signature of ERG expressing mPrOs

Based on the encouraging results obtained from the analysis of the supernatants of wild type mPrOs, we run the CLICK-MS studies of the supernatants collected from the remaining three experimental conditions (wild type mPrOs doxy, mPrOs-ERG<sub>M40</sub> mock, mPrOs-ERG<sub>M40</sub> doxy). Doxycycline treated wild type mPrOs were included in the study to evaluate the potential influence of doxycycline administration on mPrOs protein secretome.

Organoids were treated for 96 hours either with or without doxycycline (1µg/ml) before methionine depletion and labeled over night with AHA (see Material and Methods section 8.8.2 of the thesis for details). Phenotypic analysis of organoids cultures before and after the labeling did not show relevant differences in mPrOs cultures or signs of toxicity due to the procedure (**Fig. 4.11A**).

As for the wild type mock condition, 4 biological independent replicates were analyzed for each one of the three conditions. Approximately 200 proteins per sample were identified (by at least two unique peptides), of which 150, 154 and 142 were recurrently found in all the 4 replicates of wild type mPrOs doxycycline, mPrOs-ERG<sub>M40</sub> mock, and mPrOs-ERG<sub>M40</sub> doxycycline, respectively (**Fig. 4.11B-D** and Table-S2). Following the evaluation of the consistency of our analysis across the 4 biological independent replicates for each condition, the number of shared proteins among the 4 different conditions was analyzed (**Fig. 4.11E**). In order to increase the coverage of our study, we included in this analysis proteins identified by minimum 2 unique peptides in at least 3 replicates out of 4. As shown by the Venn diagram in **Fig. 4.11E**, the largest fraction of proteins (n=147) were identified in all the 4 different conditions, a small number (n=17) characterized exclusively the supernatant of doxycycline-induced ERG<sub>M40</sub> expressing organoid, while n=24 were present in all the other three conditions but mPrOs-ERG<sub>M40</sub> doxycycline (**Fig. 4.11E** and Table-S2).

Based on the minor but reproducible ERG<sub>M40</sub> dependent qualitative alteration of the mPrOs secretome summarized in the Venn diagrams of **Fig. 4.11**, we applied MaxQuant label-free quantification, based on LFQ algorithm, exploiting the MaxQuant/Perseus software suite (Cox *et al.*, 2014; Tyanova *et al.*, 2016) to estimate significant differences in the amount of the secreted proteins between ERG<sub>M40</sub> positive and ERG<sub>M40</sub> negative mPrOs.

The heatmap in **Fig. 4.12A**, obtained by plotting the intensity values calculated for every single identified protein in the 4 replicates of the 4 conditions, suggested a possible ERG-driven signature associated with differences in the relative amount of secreted proteins. Accordingly, the Volcano plot in **Fig. 4.12B** highlighted 37 candidates



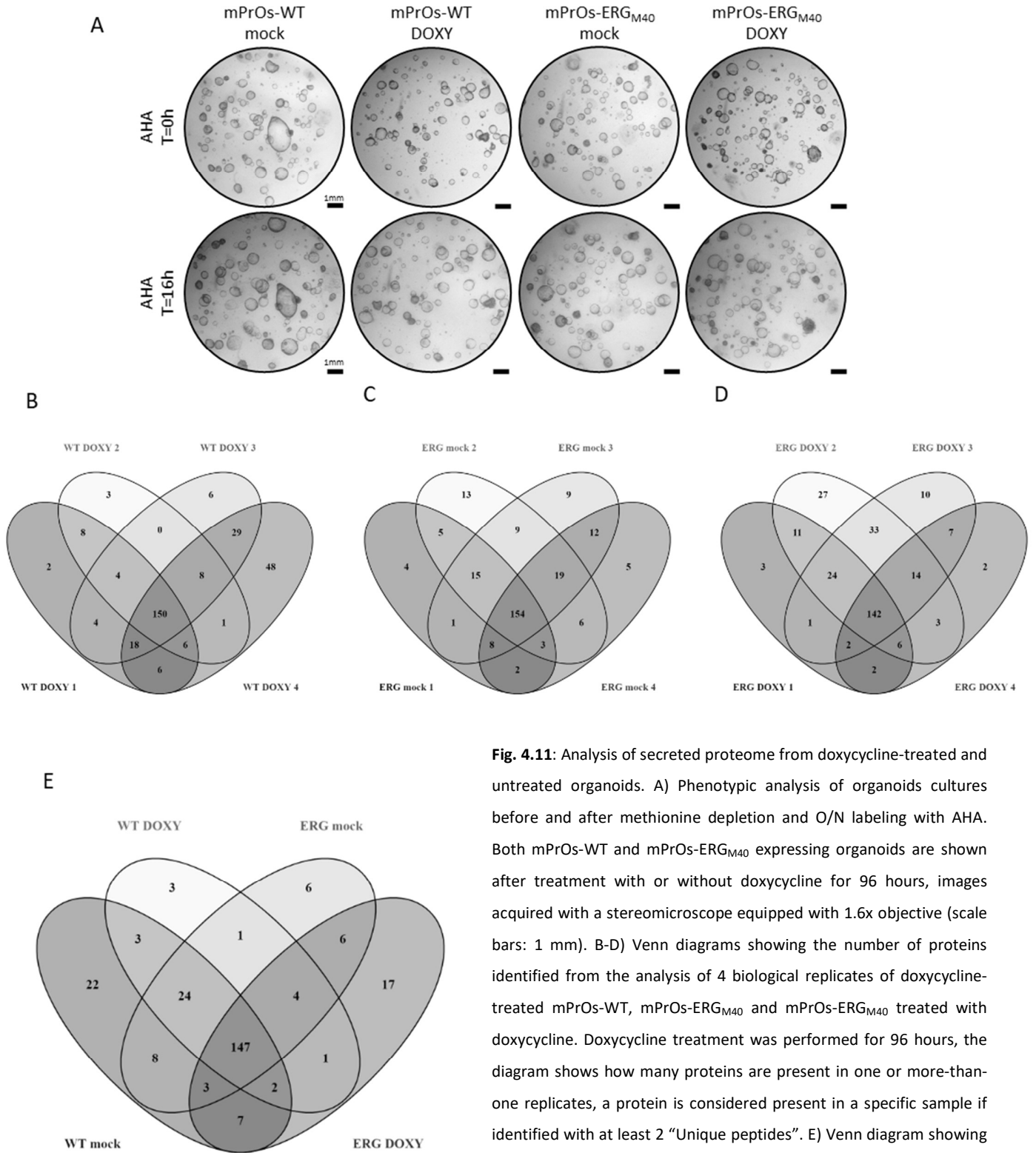


**Fig. 4.11:** Analysis of secreted proteome from doxycycline-treated and untreated organoids. A) Phenotypic analysis of organoids cultures before and after methionine depletion and O/N labeling with AHA. Both mPrOs-WT and mPrOs-ERG<sub>M40</sub> expressing organoids are shown after treatment with or without doxycycline for 96 hours, images acquired with a stereomicroscope equipped with 1.6x objective (scale bars: 1 mm). B-D) Venn diagrams showing the number of proteins identified from the analysis of 4 biological replicates of doxycycline-treated mPrOs-WT, mPrOs-ERG<sub>M40</sub> and mPrOs-ERG<sub>M40</sub> treated with doxycycline. Doxycycline treatment was performed for 96 hours, the diagram shows how many proteins are present in one or more-than-one replicates, a protein is considered present in a specific sample if identified with at least 2 “Unique peptides”. E) Venn diagram showing the degree of shared proteins comparing the 4 analyzed conditions. Identified proteins were associated to a specific condition if identified with at least 2 “Unique peptides” in at least 3 biological replicates.

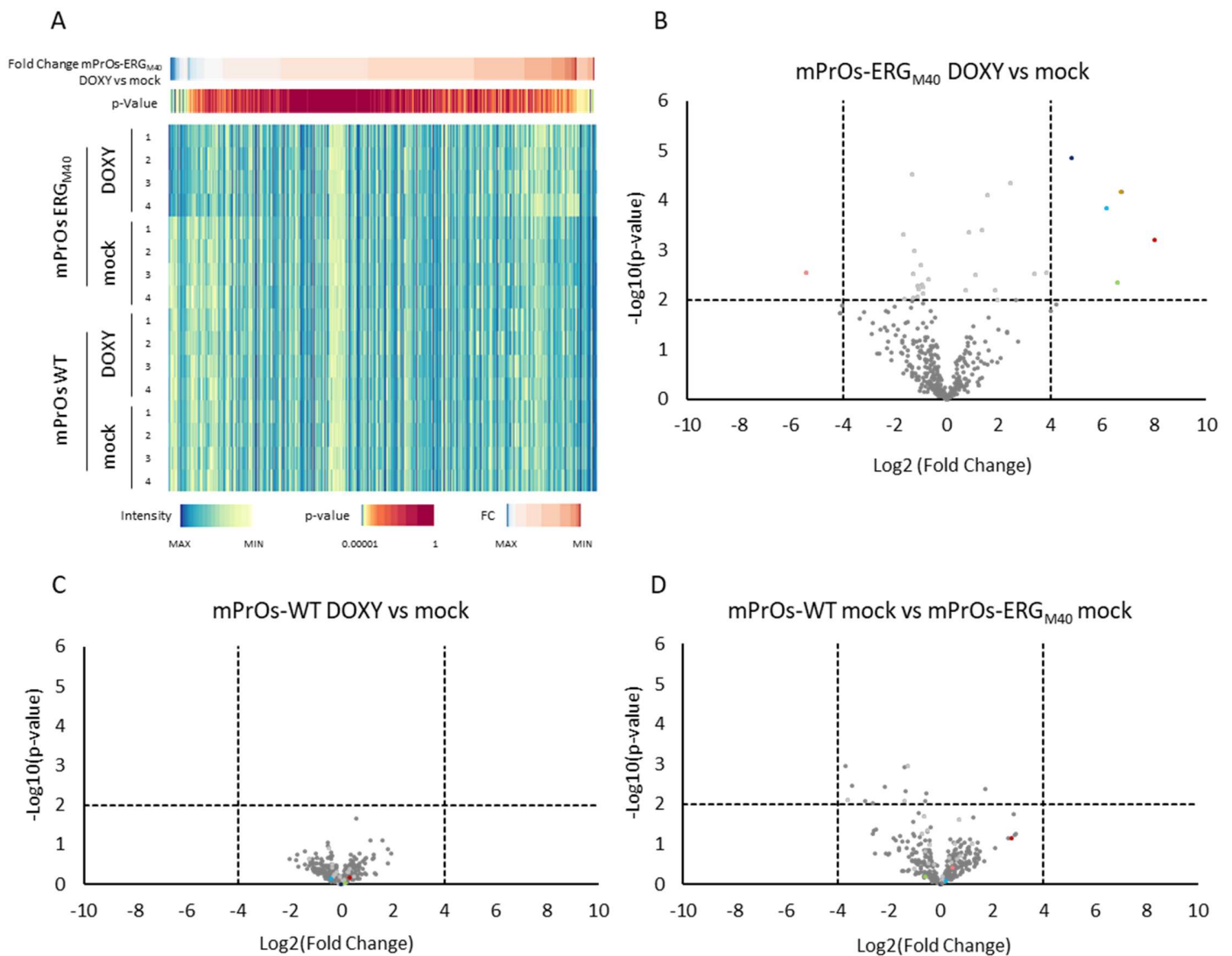


**Fig. 4.12:** Analysis of ERG-induced alterations in secreted proteome. A) Heatmap showing LFQ intensity values for each proteins within each analyzed sample. Proteins are sorted based on Fold Change and p-values calculated comparing mPrOs-ERG<sub>M40</sub> treated with or without doxycycline, each column identifies a different protein. B) Volcano plot showing differential secretion of proteins comparing mPrOs-ERG<sub>M40</sub> treated with and without doxycycline. X-axis shows the degree of variation between the two samples, Y-axis shows the significance of the observed variation. Dark grey spots indicate proteins that fail to meet the parameters specified in section 4.4.1 of the Results chapter, light grey spots indicate proteins that are above the significance threshold but with low FC value, colored spots are associated to the proteins (reported in Table 1) that were selected using the parameters specified before. C-D) Volcano plots showing differential secretion of proteins comparing mPrOs-WT treated with and without doxycycline and mPrOs-WT mock versus mPrOs-ERG<sub>M40</sub> mock, respectively. X-axis shows the degree of variation between the two analyzed conditions, Y-axis shows the significance of the observed variation, light grey and colored spots identify the same protein as indicated in B.

whose differential secretion in doxycycline induced versus mock mPrOs-ERG<sub>M40</sub> was higher than 2 folds (either Fold Change (FC) > 2 or FC < 0.5) and associated with a significant p-value (Benjamini-Hochberg correction, 20% FDR). Comparisons of wild type mPrOs mock versus doxycycline (Fig. 4.12C) and wild type mPrOs mock versus mPrOs-ERG<sub>M40</sub> mock (Fig. 4.12D) did not show significant changes on the composition of organoids secretome,

thus supporting the thesis of a direct involvement of ERG<sub>M40</sub> expression in the secretome alteration described in **Fig. 4.12B**.

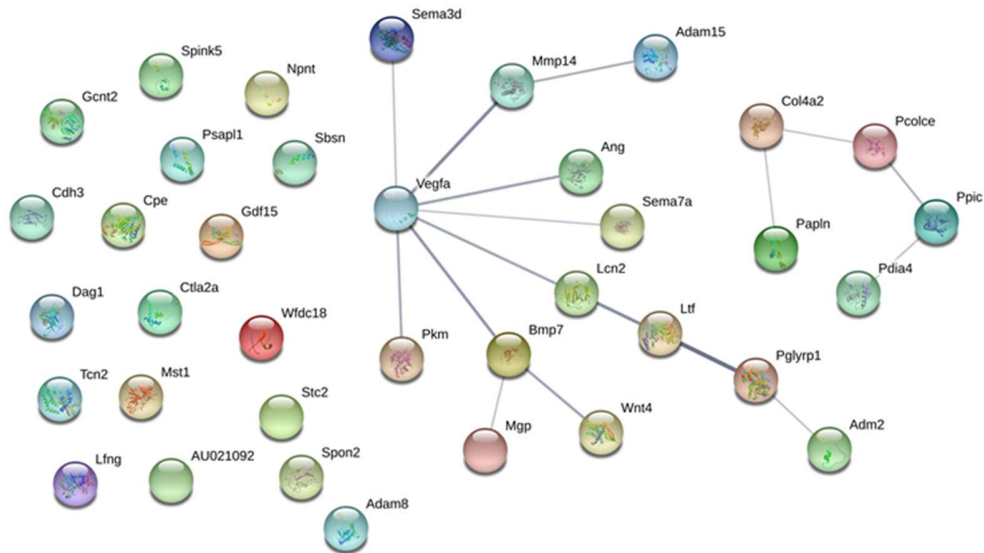


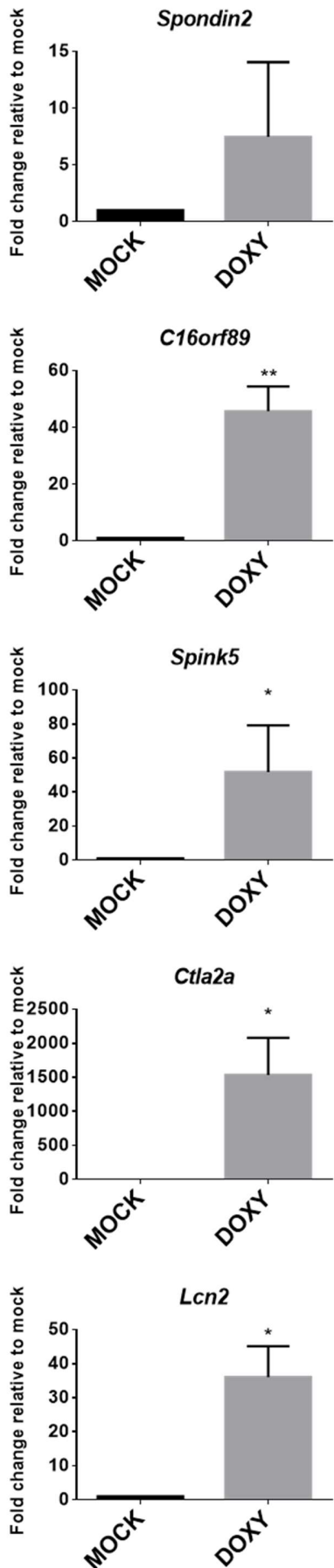
**Fig. 4.13:** Protein-protein interactions analysis in secreted proteome under ERG influence. Protein network analysis of the 37 candidate proteins identified as differentially secreted in mPrOs-ERG<sub>M40</sub> comparing treatments with and without doxycycline, network generated with STRING v11.0 (confidence score  $\geq 0.4$ ).

#### 4.4.2. Data mining from ERG-driven secretome

The analysis showed in the previous paragraph highlighted the differences in secreted proteins among the different conditions, especially the fact that ERG overexpression induces detectable changes in the protein secretome of mPrOs. In order to understand possible consequences of this alteration, the 37 candidates were subjected to further analysis starting with the network enrichment study done before for secreted proteins of wild type mPrOs. The list of 37 proteins was submitted to STRING and the resulting network is shown in **Fig. 4.13**. The limited number of medium-high confidence connections (interaction score  $\geq 0.4$ ) between the 37 candidates could suggest a multi-levels action associated with ERG<sub>M40</sub> modulation of protein secretome in mPrOs.

In a last attempt to unveil possible consequences associated with ERG<sub>M40</sub> expression in precursor lesion of human prostate, we selected only the top hits ( $\log_2(FC) > 4$  or  $\log_2(FC) < -4$ ) and corrected  $p$ -value  $< 0.01$  ( $-\log_{10}(\text{Benjamini} - \text{Hochberg } P \text{ value}) > 2$ ) and studied the functions of these 6 proteins (highlighted by colored spots in the volcano plots in **Fig. 4.12B-D**) looking at the literature. Interestingly, this analysis pointed out the involvement of several of them with the immune system and the immune response regulation (Table 1).

<b>Table 1 – Hand curated analysis of selected proteins</b>		
<b>Protein name</b>	<b>Function</b>	<b>References</b>
SPINK5	Th2 regulation of B-cells activation; Control of pro-inflammatory cascade in absence of external or immune stimulation	Briot <i>et al.</i> , 2009; Furio and Hovnanian, 2011, 2014
CTLA2 $\alpha$	Secreted inhibitor of Cathepsin L protein; Inflammation-induced release in mouse tissues enhances CD4 <sup>+</sup> T cell differentiation in T <sub>Reg</sub>	Kurata <i>et al.</i> 2003; Sugita <i>et al.</i> 2008; Sugita <i>et al.</i> 2009
LCN2	Induction of M2 macrophage polarization; Iron trafficking and bacteriostatic activity; Cellular and context dependent survival factor	Devireddy <i>et al.</i> , 2001; Flo <i>et al.</i> , 2004; Berger <i>et al.</i> , 2006; Iannetti <i>et al.</i> , 2008; Li and Chan, 2011; Warszawska <i>et al.</i> , 2013
SPON2	Potentially involved in pathogen recognition; Recruitment of M1 macrophages; Upregulated in cancer, may promote aggressiveness	Li <i>et al.</i> 2009; Zhang <i>et al.</i> , 2015, 2018; Schmid <i>et al.</i> , 2016; Jin <i>et al.</i> , 2017
C16ORF89	Unknown function; May be linked to thyroid development	Afink <i>et al.</i> 2010
SBSN	Overexpression associated with tumor proliferation and metastasis; Upregulation in tumor-associated epithelium leads to increased angiogenesis	Shao <i>et al.</i> , 2012; Alam <i>et al.</i> , 2014; Zhu <i>et al.</i> , 2016



#### 4.4.3. RNA expression analysis of oversecreted proteins

Being ERG<sub>M40</sub> a transcription factor, we analyzed the expression of the top 5 oversecreted proteins via RT-qPCR to determine a possible transcriptional control of ERG<sub>M40</sub> on the 5 genes in the mPrOs context. Although we noticed a high variability among different biological replicates, potentially dependent by different levels of ERG<sub>M40</sub> expression in the different rounds of induction (Fig. 4.4C), data presented in Fig. 4.14 showed a significant increase in the relative amount of the transcript of all 5 genes upon doxycycline induced ERG<sub>M40</sub> expression compared to controls. This finding demonstrated that over secretion of *Spink5*, *Lcn2*, *Spon2*, *Ctla2a* and *C16orf89* is, at least in part, consequence of an ERG<sub>M40</sub>-dependent sustained gene expression.

The identification of a signature of secreted proteins associated with ERG<sub>M40</sub> expression in prostate organoids could open new window of opportunities to better understand the role(s) of ERG<sub>M40</sub> during the very early steps of prostate tumorigenesis and show how CLICK-MS approach can represent a valuable and innovative approach for the study of tissue physiology, homeostasis and disease.

**Fig. 4.14:** RNA expression analysis of oversecreted proteins. The histograms show the results of RT-qPCR analysis for the 5 oversecreted proteins identified in section 4.4.2 of the result chapter. RNA was extracted and retrotranscribed from mPrOs-ERG<sub>M40</sub> after mock or doxycycline treatment for 96 hours; mock sample used as reference; N=3. Statistical analyses performed with GraphPad PRISM V. 6.01; \*= p value <0,05; \*\*= p-value <0,01

## 5. DISCUSSION

### 5.1. Biotechnology driven PCa research

PCa is one of the most common cancer in men with a global incidence of more than 1 million new cases each year (Ferlay *et al.*, 2015). Over the past 10 years significant progress has been done in terms of genomic, genetic and molecular characterization of PCa; despite that, both tumor diagnosis and treatments of PCa are still poorly influenced by this gained knowledge.

One possible cause of this delay can be the fact that functional studies aimed at modeling and studying novel molecular signatures identified through deep genomic and transcriptomic analysis of human PCa are massively based on commercially available 2D PCa cell lines and, just in part, on different types of mouse models. Although the importance of both approaches is unquestionable, they show relevant limitations that make more complicate, if not impossible, to further improve our knowledge on mechanisms leading to tumor initiation, progression and resistance to therapy. Among others, commercially available PCa cell lines are relatively few and exclusively derived from metastatic lesions, none from primary tumor. Even if they can be used to study the androgen pathway and mechanisms of resistance to androgen deprivation therapy, rarely they can be informative to decipher mechanisms and pathways involved in prostate tumor onset or in the metastatic progression of the disease. Furthermore, the genomic instability which characterizes both immortalized and tumor cell lines is responsible for the presence of sub-clones into the same culture showing very heterogeneous genomic contents with diffused aneuploidy. Last but not least, 2D growing systems based on single cell adhesion on plasticware, minimally recapitulate the cellular organization of both normal and neoplastic prostate epithelium which is characterized by functional clusters of cell-to-cell and cell-to-extracellular matrix interactions and specific gradients of hormones, oxygen, metabolites, and drugs permeability. 2D culture on plasticware is considered one of the possible causes of the turning-off of the androgen pathway in almost all the commercially available immortalized prostate cell lines.

PCa field experienced a generational change in 2014 with the development of 3D organoid cultures from both mouse and human normal adult prostate (Chua *et al.*, 2014; Karthaus *et al.*, 2014; Drost *et al.*, 2016). Prostate organoids are becoming a very important model for the study of PCa owing several advantages respect to prostate cell lines. Even if revolutionary, prostate organoids remain a model for *in vitro* and *in vivo* studies and as such they present a set of “limitations”.

The main improvement of the organoid model is the presence of a 3D cytoarchitecture very similar to the tissue of origin with both luminal and basal epithelial cells juxtapose to correctly recapitulate the internal (luminal) and the external (basal) layers of prostate tissue. However, neuroendocrine cells are missing and, even

though they possess a fully functional androgen pathway, luminal differentiation markers analysis characterizes these cells as progenitors more than terminally differentiated cells. This is also in line with the high proliferation rate of the cells inside organoids, which is a further misalignment respect to the very quiescent epithelium of adult mouse and human prostate. However, by preserving intact all the major onco-suppressive cellular pathways (e.g. TP53, RB, and PTEN), wild type organoid have a tight control on their genome stability, which remains unperturbed even after 12 months of continuous culture (Cambuli *et al.*, *in preparation*; Chua *et al.*, 2014; Karthaus *et al.*, 2014; Lancaster and Knoblich, 2014; Drost *et al.*, 2016).

Further it should be mentioned the possibility to manipulate organoids through genetic engineering approaches such as lentiviral or retroviral transduction of CRISPR/Cas9 machinery, or vectors for the constitutive or inducible expression of exogenous cDNAs and/or shRNAs against endogenous transcripts. The fact that organoids behavior and alterations can be tracked and followed through many different cellular and molecular approaches at the desired time points, it makes them useful also for drug screens (Drost and Clevers, 2018). Importantly, wild type and (genetically or pharmacologically) manipulated organoids can then be implanted under the kidney capsule or, orthotopically, into the prostate of adult male mice with minimally invasive surgical procedures in order to generate *in vivo* models of prostate disease. Notably, in case of mouse prostate organoids derived from mice with a pure genetic background (in bred colonies), the use of syngeneic mice as recipients will allow researchers to study the interactions of wild type and manipulated organoids with a fully competent immune system (Cambuli *et al.*, *in preparation*).

Many things, however, deserve to be better investigated and understood. Prostate organoids can be efficiently obtained from mouse and human healthy adult prostate tissue and at lower efficiency from human advanced metastatic prostate cancers. As for PCa cell lines, published protocols do not support the growth of organoids (tumoroids) from primary prostate cancer (Gao *et al.*, 2014; Drost and Clevers, 2018; Puca *et al.*, 2018). If tumoroids derived from metastatic lesions of PCa patients pave the way to a refined personalized approach, better treatments and more effective decision in a reduced time window, the inability to grow tumoroid from human primary lesions remains a road block to overcome.

In this scenario, genetic and pharmacologic manipulation of wild type mouse and human prostate organoids can push our understanding of the molecular mechanisms supporting the precursor-to-malignant transition of PIN and HGPIN prostate lesions, and, concomitantly, help us to define the right growth conditions to establish tumoroid lines from primary PCa lesions.

## 5.2. Identification of ERG-induced alterations in mPrOs

Being the most prevalent alteration in prostate cancer, ERG rearrangement was heavily studied in the past years from many different groups. *ERG* genomic rearrangement and expression is considered a very early event in the history of PCa being identified in a significant fraction of PIN and HGPIN precursor human prostate lesions (Mosquera *et al.*, 2008; He *et al.*, 2012; Teng *et al.*, 2013; Park *et al.*, 2014; Lee *et al.*, 2015; Morais *et al.*, 2016).

However, *in vitro* and *in vivo* experiments show that ERG expression *per se* is insufficient to induce full prostate cell transformation (Klezovitch *et al.*, 2008; Tomlins *et al.*, 2008; Carver *et al.*, 2009; King *et al.*, 2009; Chen *et al.*, 2013) while it has been robustly associated to increased migratory and invasive potential of immortalized and malignant prostate cells (Alaimo *et al.*, *in preparation*; Demichelis *et al.*, 2007; Perner *et al.*, 2007; Carver *et al.*, 2009). The very early expression of ERG in precursor prostate lesions hardly explains its involvement in PCa progression towards more advanced stages of the disease.

Thinking about the possible hurdles that a precursor prostate lesion (PIN or HGPIN) must overcome to potentially develop a frank prostatic carcinoma, cell growth and proliferation in the absence of stimuli and immune surveillance should be on the priority list.

The first phenotype associated to ERG<sub>M40</sub> expression in the mPrOs was the increased in cytokeratin 8 and a reduction of both cytokeratin 5 and Ki67 staining (**Fig. 4.5, 4.6A-C**). This condition could be interpreted as an increased commitment of mPrOs cells towards the luminal lineage combined with the reduction of the proliferative potential and the acquisition of a more quiescent state. While the influence on cellular differentiation may explain the increase of the luminal compartment observed in human PIN/HGPIN, the induction of a quiescent state is counterintuitive since an increase in proliferation is expected.

However, a very interesting feature of ERG<sub>M40</sub> expressing mPrOs is their ability to grow without EGF (**Fig. 4.8**). Based on our findings, ERG<sub>M40</sub> supports mPrOs survival and growth in medium deprived of EGF, a condition that is not permissive for the growth of both wild type and ERG<sub>M40</sub> negative organoids (Cambuli *et al.*, *in preparation*; Chua *et al.*, 2014; Karthaus *et al.*, 2014; Drost *et al.*, 2016).

The ability to “*sustain proliferative signaling*” is one of the original cancer hallmarks defined by Hanahan and Weinberg in their milestone papers (Hanahan and Weinberg, 2000, 2011). This result suggests that ERG<sub>M40</sub> expression in normal prostate cells could uncouple them from the growth-promoting signals tightly controlling tissue homeostasis, thus making PIN and HGPIN cells “*master of their own destiny*” (Hanahan and Weinberg, 2000, 2011).

Even though the ability to sustain proliferation is an important pre-requisite for cellular transformation, it may be not sufficient in the complex environment represented by the human tissue where pre-malignant cells are surrounded by the stromal compartment and, in particular, by immune cells. It is well-known that inflammation



and activated cells are present already at the very early stage of tumorigenic transformation (Mantovani *et al.*, 2008) meaning that, to develop a tumor, pre-cancerous cells need to influence and hijack immune response to hide themselves, a second hallmark in the tumorigenic process defined by Hanahan and Weinberg as “*avoiding immune destruction*” (Hanahan and Weinberg, 2011).

By profiling ERG<sub>M40</sub> protein secretome in mPrOs, we identified several proteins (*Lcn2*, *Spink5*, *Spon2*, *Ctla2a*) differentially involved in the crosstalk with the immune system (Table 1). These findings may suggest a novel pro-tumorigenic role of ERG<sub>M40</sub> in precursor PIN/HGPIN lesions aimed at shaping the stroma microenvironment stimulating the formation of an immunosuppressive shield that can reduce the negative pressure of the innate and adaptive immune system thus favoring PIN/HGPIN establishment and progression towards PCa through the acquisition of additional molecular alterations.

### 5.2.1. Lipocalin2 (*Lcn2*)

Also known as Neutrophil Gelatinase-Associated Lipocalin2, this protein is released from innate immune cells and exerts a bacteriostatic effect by binding with very high affinity iron siderophores released by bacteria to internalize extracellular Fe(III). By reducing availability of Fe(III) in the microenvironment, LCN2 impairs bacterial growth and helps the inflammatory response (Flo *et al.*, 2004; Berger *et al.*, 2006). Independently by its role as Fe(III) scavenger, recently Warszawska and colleagues in a paper published on Journal of Clinical Investigation have described LCN2 promoting the M2 polarization of M1 macrophages (Warszawska *et al.*, 2013).

Moving apart from the immune system, LCN2 is involved in iron trafficking and intracellular storage, a critical element for cancer cells that can favor many different processes including proliferation and resistance to stress. Accordingly, LCN2 is upregulated in many types of tumors where it may act as a survival factor with a context dependent activation and regulation (Devireddy *et al.*, 2001; Iannetti *et al.*, 2008; Li and Chan, 2011). However, eukaryotic siderophores and membrane receptors for LCN2 are minimally characterized.

Finally, LCN2 interact and stabilize MMP9 preventing its self-degradation and, in turn, sustaining its activity. This LCN2 function has been associated with increased tumor aggressiveness, angiogenesis and invasiveness (Jung *et al.*, 2017).

### 5.2.2. Spondin2 (*Spon2*)

This protein is known to be involved in pathogen recognition, recruitment of M1 macrophages (Zhang *et al.*, 2018) and activation of the immune response (Li *et al.*, 2009). *Spon2* is found upregulated in several types of cancer where it is generally associated with cell migration and invasion (Zhang *et al.*, 2015; Schmid *et al.*, 2016; Jin *et al.*, 2017).

This protein is particularly interesting for PCa (Qian *et al.*, 2012; Lucarelli *et al.*, 2013). In these two independent publications, authors describe higher levels of secreted Spondin2 in the serum and urine of PCa patients. They hypothesize that combination of PSA and SPON2 biochemical quantification can improve the diagnostic power of the test. Despite being very encouraging and promising, the results that they present show a very high variability among SPON2 levels measured in PCa patients therefore reducing the potential clinical impact of this new biomarker. Since distinct alterations may have different effects on SPON2 levels, this may explain the variability observed in these two works. A better characterization of this condition and the regulation of this protein may allow the development of an improved test that is more precisely focused on a specific condition.

### 5.2.3. Serine Protease Inhibitor Kazal-type 5 (*Spink5*)

SPINK5 is a multiple domains protein with an inhibitory function against many serine proteases (e.g. KLK5, KLK7 and KLK14). Dysfunctions of this molecule are involved in so called Netherton syndrome, a pathology that causes defects in the formation and development of the skin (Chavanas *et al.*, 2000) together with other symptoms. A characteristic SPINK5 function is the negative control of a Th2 pro-inflammatory environment that leads to the accumulation and activation of pro-allergenic immune B-cells (Briot *et al.*, 2009; Furio and Hovnanian, 2014).

### 5.2.4. Cytotoxic T Lymphocyte-Associated protein 2 alpha (*Ctla2α*)

Mouse CTLA2α protein interacts and inhibits the activity of cathepsin enzymes, mainly L and H family members (Yamamoto *et al.*, 2002; Kurata *et al.*, 2003) which are involved in lysosomal protein degradation and antigen processing therefore playing an important role in the immune response (Conus and Simon, 2010). It was also observed that secreted CTLA2α can interact with T lymphocytes and influence their differentiation toward T-regulatory cells (Sugita *et al.*, 2008, 2009). These findings underline the robust association between this molecule and immune system, and, in particular, the involvement of CTLA2α in the establishment of an immune-suppressive condition.

CTLA2α is a quite interesting protein, however, there are not orthologous molecules in the human proteome. Intriguingly, protein sequence homology analysis showed that murine CTLA2α is identical to the “I-29” inhibitor domain present at the N-terminus of specific pro-cathepsin proteins (both murine and human). This inhibitor domain prevents enzyme activity by blocking its active site. Following the N-terminal domain cut and release, the mature form of cathepsins become enzymatically active. While the role of mature cathepsins in lysosomal protein degradation is very well characterized, possible roles of the “I-29” inhibitory domain released after the proteolytic cut is completely underestimated.

In order to evaluate a potential transcriptional control of human *Cathepsin-L* gene by ERG, we analyzed both mouse and human *Cathepsin-L* gene promoters taking into account a region spanning 5 kilobases upstream the transcriptional start site and the first intron. We started with the analysis of predicted transcription factor binding sites and we observed the presence of a conserved cluster of ETS responsive elements in the proximity of the transcription start site of *Ctla2a* and mouse and human *Cathepsin-L* genes (Fig. 5.1). This result supports the hypothesis of a connection between ERG<sub>M40</sub> and I-29 level in human prostate through the transcriptional regulation of *Cathepsin* genes.

Possible extracellular functions of human “I-29” domain in the control of the immune response similar to that played by mouse CTLA2 $\alpha$  cannot be excluded and should deserve attention.

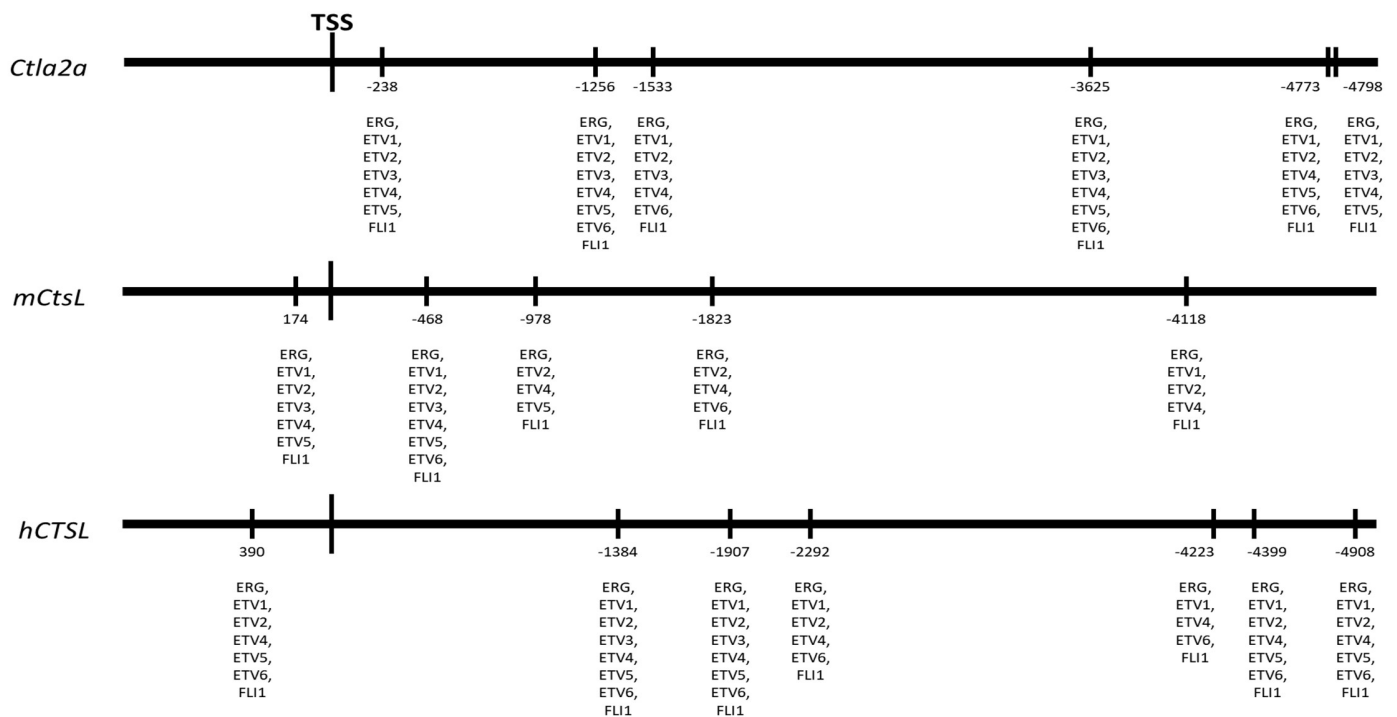


**Fig. 5.1:** Analysis of predicted ETS-binding sites at *Ctla2a*, mouse *CtsL* and human *CTSL* promoters. The scheme shows the predicted binding sites for ETS transcription factors (ERG, ETV1-6 and FLI1) within a region starting 5 kilobases upstream up to 1 kilobase downstream the transcription start site. The figure highlights the presence of a cluster of ETS responsive elements immediately upstream the transcription start site of the *Ctla2a* gene. Analysis of mouse and human *cathepsin L* genes (*mCtsL* and *hCTSL*, respectively) shows the presence, in both cases, of binding sites for ETS transcription factors. Data obtained from Eukaryotic Promoter Database (Dreos R. et al., 2014, 2017).

## 6. FUTURE PERSPECTIVES

### 6.1. Understanding the effects of mPrOs secreted factors

We are now setting the experimental conditions to investigate the possible role of ERG<sub>M40</sub> on surrounding microenvironment focusing in particular on macrophages, naïve T lymphocytes (CD4<sup>+</sup>) and stromal fibroblasts that seem to be highly affected by the secreted proteins identified.

In details, undifferentiated macrophages will be derived from the bone marrow of wild type mice and then treated with the mPrOs conditioned medium derived from both wild type and ERG<sub>M40</sub> engineered organoids induced or not with doxycycline. Macrophages will then be analyzed looking at variations in the polarization status, in particular we hypothesize that ERG-related factors may favor M2-regulatory population respect to M1-active macrophages.

On the other hand, we will also analyze CD4<sup>+</sup> T lymphocytes derived from mouse spleen. CD4<sup>+</sup> T cells will be treated as described for macrophages and the induction of T-regulatory cell (Tregs) differentiation will be analyzed by gene expression analysis of FoxP3, known as the master regulator of Tregs differentiation, and other downstream targets of this transcription factor. From this experiment we expect to observe an increase of T-regulatory cells induced by factors released upon expression of ERG<sub>M40</sub> in mPrOs.

In addition to the analysis on selected immune populations, we are also setting up a collaboration with the laboratory of Prof. Valeria Poli at the University of Turin to analyze the influence of mPrOs-secreted factors on fibroblasts. Concretely, these cells will be treated with organoids-conditioned medium as described above and then they will be analyzed looking at the expression of specific genes associated with the transition from normal to cancer-associated fibroblast (CAF). We expect to observe an increase in the CAF population due to ERG-driven secretion of specific factors from mPrOs.

Another possible approach for the analysis of ERG<sub>M40</sub> engineered organoids focuses on orthotopic transplantation into immune competent mice. In fact, it will be possible to inject mPrOs in syngeneic animals and analyze their ability to engraft and/or evolve in presence or absence of doxycycline induction. The results presented in this thesis suggest that induced engineered mPrOs are potentially less affected by restrictive growth conditions and can create a supportive environment meaning that ERG<sub>M40</sub>-expressing organoids may have a higher possibility to survive and originate a precancerous-like lesion in the prostate tissue.

The identification of one or more of these interactions may further verify our hypothesis of a key function of ERG in precancerous lesion acting as a tumor supportive factor at both intra- and extra-cellular levels.

## 6.2. Potential clinical application of ERG-driven secreted factors

Looking from a clinical perspective, the results obtained in this work have the potential to improve clinician's toolkit in the PCa field leading to improved knowledge and diagnosis. However, they need to be analyzed and confirmed on a more complex setting that closely resemble those specific conditions.

To address this point, the first step will be to move from *in-vitro* to *in-vivo*, analyzing biofluids from mouse models, bearing ERG overexpression in the prostate, to understand if it is possible to recapitulate our previous results. The model developed by Sawyers' laboratory few years ago (Chen *et al.*, 2013) will be of great help thanks to its constitutive expression of ERG in the prostate epithelium, specific analysis on urine and/or serum, and comparison with wild type animals, will allow to determine which proteins can be identified and those that can be more informative.

Once some of these proteins will be confirmed via ELISA assay, they may compose a more specific ERG-related secreted proteins signature that can be used to stratify men with elevated PSA levels and the presence of an ERG<sup>+</sup> lesion, adding another level of information to current approaches.

The identification of an ERG precancerous lesion at a very early stage may increase our ability to determine those patients that are more at risk of developing PCa and that may significantly benefit more frequent analyses. The aim is to look more closely to the potential lesion and switch to an active intervention (e.g. surgical removal or radiotherapy) as soon as it is needed to avoid future progression and evolution of the tumor while minimizing the potential harm and drawbacks for the patient.

In addition to the use of ERG-related secreted protein signature as a prevention-like tool to improve available information on patient's status, those same molecules may also represent a target for potential treatments. If the hypothesized influence of ERG-driven secreted factors on the surrounding microenvironment will be confirmed, we can focus our efforts on trying to identify the molecular mechanisms responsible for that process. Once determined the factors involved, it will be possible to suggest a treatment to patients characterized by ERG<sup>+</sup> PIN/HGPIN in order to prevent or block the formation of a supportive environment and so inhibiting future tumor development.

Overall, the results showed in this work represent a promising starting point for a better understanding of prostate tumorigenesis and evolution, since this methodology can also be applied to study other known PCa alterations it can highlight, and potentially explain, differences or similarities among prostate tumors. Moreover, the possibility to correlate these data with clinically relevant information may foster the development of diagnostic tools or approaches for patient's stratification and achieve something that researchers in PCa field are pursuing since many years.

## 7. CONCLUSIONS

In conclusion, the results obtained in this project show how the combination of innovative biological models with advanced methodological approaches can help to deepen our understanding on organ physiology and disease by addressing questions that were previously impossible to address.

By studying ERG<sub>M40</sub> in mPrOs, this project has shed light on possible important functions of ERG<sub>M40</sub> in precursor prostate lesions, such as the luminal commitment, the limitation of the proliferative potential in favor of a more quiescent cellular status, and the ability to sustain cell proliferation in the presence of limited growth stimuli. Moreover, by coupling mPrOs biological system with CLICK chemistry enrichment and Mass Spectrometry, we analyzed the secreted proteome of wild-type prostate organoids and identified the alterations induced by ectopic ERG expression, which suggest a possible strategy to hijack immune system surveillance.

Taken together these findings characterize a precursor condition that is prone to the malignant transformation and that may prime and sustain the development of prostate cancer.

In addition to the main goal of this work, the project demonstrates that the engineering of prostate organoids is a valuable strategy for the creation of new models for the study of molecular alterations commonly identified in human PCa and the mechanisms involved in cellular transformation and tumor evolution.

## 8. MATERIALS AND METHODS

### 8.1. Mouse Prostate Organoids (mPrOs)

#### 8.1.1. Reagents and solutions used for mPrOs culture

##### Small molecule stock solutions

EGF: 50 µg/ml recombinant EGF (PeproTech, 315-09) in 0.1% PBS-BSA

Noggin: 100 µg/ml recombinant Noggin (PeproTech, 120-10C) in 0.1% PBS-BSA

R-Spondin1 recombinant: 500 µg/ml recombinant R-Spondin1 (PeproTech, 120-38) in 0.1% PBS-BSA

A83-01: 5 mM A83-01 (Tocris, 2393) in DMSO

DHT: 100 µM DHT (Merck, 10300) in 100% Ethanol

Y-27632: 10 mM Y-27632 (Merck, Y0503) in PBS

adDMEM 2+: Advanced DMEM/F12 (Thermo Fisher Scientific, 12634010), 0.01 M HEPES (Thermo Fisher Scientific, 15630049), 2 mM GlutaMAX™ Supplement (Thermo Fisher Scientific, 35050061)

adDMEM 4+: adDMEM 2+, 1x B-27™ Supplement (50X) (Thermo Fisher Scientific, 17504001), 1.25 mM N-Acetyl-L-cysteine (Merck, A9165)

ENRAD c.m.: adDMEM 4+, 10% R-spondin1 conditioned medium, EGF 50 ng/ml, Noggin 100 ng/ml, A83-01 0.2 µM, DHT 10 nM

-NRAD c.m.: adDMEM 4+, 10% R-spondin1 conditioned medium, Noggin 100 ng/ml, A83-01 0.2 µM, DHT 10 nM

ENRAD rec: adDMEM 4+, R-spondin1 recombinant 500 ng/ml, EGF 50 ng/ml, Noggin 100 ng/ml, A83-01 0.2 µM, DHT 10 nM

Dispasell 10x: 10 mg/ml Dispasell (Thermo Fisher Scientific, 17105041) in adDMEM 2+

Dispasell 1x: dilute 1:10 Dispasell 10x in adDMEM 2+

PBS-BSA 0.1%: 0.1% Bovine Serum Albumin (BSA, Merck, A3059) diluted in PBS, filtered with 0.22 µm filter before use

Collagen solution: 8 mg/ml Collagen type 1 (Corning, 354249), 10% PBS 10x, 20 mM filtered NaOH, adDMEM 4+ up to final volume

Depletion medium (Human Albumin): It is prepared starting from DMEM without Methionine and Cysteine (Thermo Fischer Scientific, 21013024) supplemented with all the molecules present in Table 2

Depletion Medium (Albumax™): this formulation differs from Depletion medium (Human Albumin) since it contains ALBUMAX™ II Lipid Rich BSA (Thermo Fischer Scientific, 11021029) at a final concentration of 400 mg/L, as a substitute for Human Albumin. All the other supplements are the same displayed in Table 2

AHA medium: 0.1 mM AHA (Jena Bioscience, CLK-AA005) in Depletion medium

Methionine medium: 17.24 mg/L of Methionine (Merck, M5308) in Depletion medium

<b>Table 2 – Components of DEPLETION medium (Human Albumin)</b>		
<b>Medium Supplement</b>	<b>Final concentration</b>	<b>Company (#Catalogue)</b>
Human Albumin	400 mg/L	Merck (A9731)
Non-Essential Amino acids Solution	1x	Thermo Fischer Scientific (11140035)
L-Cysteine	2.4 mg/L	Merck (C7352)
Ascorbic acid	2.5 mg/L	Cayman Chemicals (16457)
Human Holo-Transferrin	7.5 mg/L	Merck (T0665)
Bovine Insulin	10 mg/L	Merck (I1882)
Ethanolamine	19.5 µM	Merck (E0135)
L-Glutathione reduced	1 mg/L	Merck (G4251)
Sodium pyruvate	1 mM	Thermo Fischer Scientific (11360039)
HEPES	0.01 M	Thermo Fischer Scientific (15630049)
GLUTAMAX	2 mM	Thermo Fischer Scientific (35050038)
B27	1x	Thermo Fischer Scientific (17504044)
N-Acetyl-L-Cysteine	1.25 mM	Merck (A9165)
EGF	50 ng/ml	PeptoTech (315-09)
A83-01	0.2 µM	Tocris (2393)
Noggin	100 ng/ml	PeptoTech (120-10C)
Recombinant R-Spondin1	500 ng/ml	PeptoTech (120-38)
DHT	10 nM	Merck (10300)

### 8.1.2. mPrOs culture

Establishment of 3D primary prostate cultures from WT mice, either C57B6/J or CD1 strains, was done according to the protocol published by Drost and colleagues (Drost *et al.*, 2016). Mouse prostate organoids (mPrOs) culture is based on the same protocol and further improvements developed in our laboratories. Detailed protocol will be provided in the work of Cambuli and colleagues (Cambuli *et al.*, *in preparation*).

The following protocol is intended for 12 well plates containing 3 domes/well. When changing plate format, the volumes must be modified accordingly. The mPrOs are cultured exploiting ECM-like domes composed by 80% Matrigel® (Corning® Matrigel® Growth Factor Reduced Basement Membrane Matrix, #356231, Corning) and incubated at 37 °C. Defined medium (ENRAD c.m.) is refreshed every 2-to-3 days until organoids reach a proper dimension for passing or Matrigel® starts to loosen, which usually happens every 6-8 days.



Matrigel® domes are first detached and mechanically disaggregated using DispaseII 1X, then collected into a 1.5 ml Eppendorf tube and incubated at 37 °C for 5 min to complete Matrigel® disaggregation. After incubation, TrypLE/Y-27632 (10 µM) is added to the solution and the tube is placed back at 37 °C for other 5 min to deactivate DispaseII enzyme. The sample is centrifuged (300 g, 5 min) to pellet the organoids, washed once with 1 ml of 0.1% PBS-BSA, centrifuged again (300 g, 5 min) and the supernatant is discarded up to 100 µl. Subsequently, 400 µl of addMEM 4+/Y-27632(10 µM) are added and the mPrOs are mechanically disaggregated by pipetting them. After pipetting, the single cells/clumps are counted and the desired number of Organoids-forming Units (UFO) are transferred in a new tube adding addMEM 4+ up to 20% of the final volume and maintained in ice. The remaining volume is composed by Matrigel® that is added to the cells immediately before seeding the culture in the well (usually 3 domes of 40 µl per well) and the plate is then incubated at 37 °C for 15 min in order to allow hydrogel domes to polymerize. Finally, when the domes are completely solid, 1 ml of ENRAD c.m. + Y-27632 (10 µM) is added to each well and the culture is incubated at 37 °C in the presence of 5% CO<sub>2</sub>. Note that Y-27632 is used only for the initial 24-72 hours of culture.

### 8.1.3. Sample preparation for IF and IHC

Organoids are cultured in Matrigel® and treated as needed until the day before the end of the experiment, at this point they must be passed into collagen-based matrix to allow proper downstream processing. The mPrOs are collected into a 1.5 ml Eppendorf tube with a spatula and 300-400 µl of DispaseII 10x are added to the sample. To dissolve the Matrigel® without stressing the cells, mPrOs are then incubated for 30 min at 37 °C with gentle shaking. An equal amount of TrypLE is added to the tube, incubated at 37 °C for additional 3 min to block Dispase activity and then washed twice with 0.1% PBS-BSA allowing the organoids to sink by gravity. The washing solution is removed as much as possible and the organoids are resuspended in collagen solution before seeding them in the same way as for passing them. Finally, they are incubated for 15 min at 37 °C, to polymerize the collagen, before adding the medium with the proper treatment and placing them back in the incubator.

### 8.1.4. EGF deprivation experiment

Two days before seeding the organoids for the experiment, 50% of the samples are treated with doxycycline as indicated in the section 4.2.2 of the Results chapter. This experiment is performed in 24 well plates with a single dome for each plate. The culture is processed as for organoids passaging (section 8.1.2) and 1200 UFO are seeded for each dome adding the medium -NRAD c.m. (without EGF) + Y-27632. After O/N incubation, doxycycline (1 µg/ml, Merck, D9891) is added to already treated samples; medium is refreshed every 2-3 days. At day 8, the

organoids are passed again to continue the experiment up to 2 weeks, thus, the sample is entirely seeded in a new well and doxycycline is added 24 hours after seeding.

Every day the samples are observed at the stereomicroscope (Leica MZ16 F) and photos are taken from each condition. At day 14, samples are incubated with 5  $\mu$ M Calcein viability dye (Prodotti Gianni, BMS65-0853-78) for 1 hour and then analyzed via fluorescence imaging.

#### 8.1.5. EdU labeling and FACS analysis

To perform this experiment, 1500 organoids units are seeded for each dome and 3 domes per condition are analyzed. Organoids are labeled with 10  $\mu$ M EdU for 3 hours before harvesting them, mPrOs are detached adding Dispase II 1x and incubated for 5 min at 37 °C; after that TrypLE is added to the sample and incubated for additional 5 min at 37 °C. The samples are centrifuged (5 min, 300 g) and washed twice with 1% PBS-BSA. Subsequently, they are mechanically dissociated into single cells and filtered through a 30  $\mu$ m cup strainer (Falcon 30  $\mu$ m sterile cup, BD Biosciences, 340626). Cells are pelleted and then processed following the manufacturer protocol (Click-iT™ Plus EdU Alexa Fluor™ 488 Flow Cytometry Assay Kit, Thermo Fisher Scientific, C10632). After the incorporation of the fluorescent probe (Alexa Fluor™ 488), cells were also incubated with ToPro to stain DNA content and then analyzed with FACS CANTO present in the Cell Analysis & Separation Facility (BD Biosciences). Data are analyzed with the FlowJo V10 software and GraphPad PRISM (V. 6.01).

#### 8.1.6. Engineering mPrOs

In order to transduce organoids, cultures are detached and dissociated into single cells, counted and a total amount of 50,000 cells/reaction are used. Usually, more than one reaction is prepared to increase the efficiency of the process. In the meantime, the following solution is prepared: viral vectors (0.3 RTU/reaction), polybrene (4  $\mu$ g/ml) and complete medium up to final volume (150  $\mu$ l). The transduction starts mixing equal amounts of cells and viral vectors containing solution that are plated into 96 well low-adhesion plates for spinoculation. This step, which increases the interaction between viral-like particles and cells, is achieved centrifuging the plate for 1 hour at 600 g. Cells are then gently resuspended, collected into an Eppendorf tube and incubated for 3-4 hours at 37 °C to allow the permeation of the vector inside the cells. After the incubation, the sample is pelleted and plated as usual in 80% Matrigel® where domes are allowed to polymerize before adding complete medium and incubate the culture at 37 °C. Usually, a step of antibiotic selection is needed to maintain in culture only the transduced cells, adding the antibiotic at least 48 hours after transduction. In particular, mPrOs transduced with

the pTGMP-ERG are selected with puromycin 1 $\mu$ g/ml (InvivoGen, ANT-PR-1). Usually, about 6-10 days of puromycin selection are needed to appreciate the formation of resistant organoids.

#### 8.1.7. RNA extraction from mPrOs

RNA extraction is performed with the RNeasy Plus Micro kit (Qiagen, 74034). To collect RNA from mPrOs, 3 domes (1200-1500 UFO/dome) are processed for each analyzed condition. At the end of the treatment, the sample is mechanically dissociated with Dispasell 1x, collected in an Eppendorf and incubated at 37 °C for 5 min. After incubation, it is washed with 0.1% PBS-BSA and centrifuged (300 g, 5 min) for 2-3 times before resuspending the cell pellet in the provided lysis buffer. Cells are then additionally lysed with a syringe before proceeding with the protocol indicated by the manufacturer. The RNA is eluted with 33  $\mu$ l of RNase-free water and quantified with the nanodrop device (Thermo Scientific™ NanoDrop™ 2000c Spectrophotometer, Thermo Fisher Scientific, 11840461).

#### 8.1.8. Protein extraction from mPrOs

Protein are usually collected from 6 domes (1200-1500 UFO/dome) of mPrOs for each analyzed condition. At the end of the treatment the sample is mechanically dissociated with Dispasell 1x, collected in an Eppendorf tube and incubated at 37 °C for 5 min. After this step, TrypLE is added and incubated for other 5 min at 37 °C. Samples are then centrifuged (300 g, 5 min), washed 2-3 times with ice-cold PBS and the obtained pellet is lysed resuspending it in RIPA buffer (50 mM Tris-HCl, pH 7.5, 150 mM NaCl, 1% Triton X-100, 1% sodium deoxycholate, 1% NP-40 ), supplemented with the appropriate amount of protease and phosphatase inhibitors. Samples are then kept at 4 °C for 30 min with gentle shaking to allow complete cell lysis. To collect the soluble protein fraction, samples are centrifuged (18000 g, 20 min, 4 °C) and transferred to a new Eppendorf tube before quantifying protein concentration via BSA assay (Pierce™ BCA Protein Assay kit, Thermo Fisher Scientific, 23225).

### 8.2. RNA Reverse Transcription

RNA is retrotranscribed into cDNA for PCR and qPCR analysis using the iScript™ cDNA synthesis kit (BioRad; 1708891). After RNA quantification, 1000 ng of RNA are retrotranscribed following the protocol indicated by the manufacturer. At the end of the reaction samples are stored at -20 °C until further use.

### 8.3. Quantitative Real Time PCR (RT-qPCR)

Quantitative gene expression analysis is achieved through RT-qPCR exploiting the qPCRBIO SyGreen Mix (PCRBiosystems, PB20.14-05). Reaction mix is prepared following manufacturer instructions for a final volume of 10  $\mu$ l, including 10 ng of cDNA input for each reaction and gene-specific primers used at a final concentration of 0.2  $\mu$ M. The complete list of primers used in this dissertation is reported in Table 3. The experiments are performed in three or more technical duplicates using the CFX96 Real Time PCR machine from BioRad following the subsequent protocol:

1. Initial denaturation                    95 °C, 4 min
2. Step specific denaturation        95 °C, 15 s
3. Annealing                                60 °C, 20 s
4. Elongation                                72 °C, 30 s
5. Return to step 2                        x45
6. melting curve analysis            60-95 °C,  $\Delta$  temp 0.5 °C, 5 s/cycle

Results are then processed using BioRad CFX Manager software (V3.1) while gene expression and statistical analysis is performed through GraphPad PRISM (V. 6.01).

<b>Table 3 – List of primers used for qRT-PCR analysis</b>		
<b>GENE</b>	<b>PRIMER NAME</b>	<b>SEQUENCE</b>
<i>mTbp</i>	mTBP_Fw	CGGTCGCGTCATTTTCTCCGC
	mTBP_Rv	GTGGGGAGGCCAAGCCCTGA
<i>hERG</i>	hERG_Fw2	AGACTTCCAAGATGAGCCCAC
	hERG_Rv2	CCCATCGATGTTCTGGAATAAC
<i>mErg</i>	mERG-Fw1	CTAGTCAGGTGAATGGTTCCAG
	mERG-Rv1	TTGTGGTCATATTGGGAGGC
<i>mPlau</i>	mPLAU_Fw1	CATCCATCCAGTCCTTGCGT
	mPLAU_Rv1	GTGTTGGCCTTCTCCTCGGTA
<i>mFam25c</i>	mFam25c_Fw1	AGTTCACGCAGTGGAAAGAGG
	mFam25c_Rv1	GGTGTGGGTGACCTTCTCAG
<i>mSmim6</i>	mSMIM6_Fw1	GAAGGACAGCCTGACTTGC
	mSMIM6_Rv1	CACATACCCAAACACAACAGC
<i>mMmp3</i>	mMMP3_Fw2	TTGGCGCAAATCTCTCAGGA
	mMMP3_Rv2	TCCACCCTTGAGTCAACACC
<i>mCk5</i>	mCK5_Fw	GTGGGGGCAGCCGCTCTTTC
	mCK5_Rv	TCCAGGAACCGCACCTTGTCG
<i>mCk8</i>	mCK8_Fw	AGCTCGCTCTCGAACCTCCGT
	mCK8_Rv	GCTCCAGGAAGCGCACCTTGTC
<i>mLcn2</i>	mLCN2_Fw2	CCGAAAGACTTCTGAAAACAAGC
	mLCN2_Rv2	AAAGATGGAGTGGCAGACAG
<i>mSpink5</i>	mSPINK5_Fw1	AAAGTGGGGCTGGTTTCAGACC
	mSPINK5_Rv1	TTCCCGATACTGAGCACATTC
<i>mC16orf89</i>	mC16orf89_Fw1	CTTCTACCTCAAGCAGAGTGAC
	mC16orf89_Rv1	GCAACTTCCAAAACCCAGG
<i>mCtla2a</i>	mCTLA2a_Fw2	CTATCTGTGAACAGAAGCTGC
	mCTLA2a_Rv2	CTTCTGGAGTCAAGTCAC
<i>mSpondin2</i>	mSPONDIN2_Fw1	GCAACTATCCCACAAGACACAG
	mSPONDIN2_Rv1	AAACCTCACAGTCCAGCG
<i>mPscA</i>	mPSCA_Fw1	GCTCACTGCAACCATGAAGA
	mPSCA_Rv1	GCTAAGTAGGTGGCCAGCAG
<i>mFkbp5</i>	mFKBP5_Fw1	AGCCGGGAAGCCTAAGTTTG
	mFKBP5_Rv1	ACTTGCCTCCCTGAAGTACA

#### 8.4. Immunofluorescence (IF) of Formalin-fixed Paraffin-embedded sections

Organoids embedded in collagen domes are washed 2 times with PBS and fixed incubating them for 5 hours with 4% paraformaldehyde (PFA) at room temperature (RT) with gentle shaking. Samples are then washed 3 times with PBS, collected in a histological cassette and subjected to ethanol dehydration and paraffin embedding. After solidification, paraffin blocks are cut with a microtome (5 µm sections), collected on microscope slides and allowed to dry O/N at 37 °C. Slides then undergo deparaffinization and antigen unmasking with sodium citrate (Vector Laboratories, H3300), before proceeding with IF protocol. Slides are treated with Blocking solution

(5% PBS, 0.1% Triton-X in PBS) for 1hour at RT and then incubated O/N at 4 °C with the primary antibody diluted in blocking solution at the appropriate degree (Table 4).

After incubation with primary antibodies, slides are washed 3 times with PBS and then incubated for 2 hours at RT, preventing light exposure, with the secondary fluorescent antibody diluted in blocking solution. Subsequently, they are washed 3 times with PBS and nuclei are stained with DAPI incubating the slides at RT for 15-20 min. The samples are then washed 3 more times in PBS and finally mounted with proper IF mountant. The slides are maintained O/N at RT preventing light exposure to allow them to dry and, finally, stored at 4 °C.

The samples are observed and imaged with the Zeiss Axio Imager M2 present at the Advanced Imaging Cell Facility. In the case of Ki67 staining and quantification, images are visualized using ImageJ software (V. 1.50i) and positive cells are counted based on single channel pictures. The statistical analysis is performed through GraphPad PRISM (V. 6.01).

**Table 4 – List of primary antibodies used for immunofluorescence**

Company	Catalogue #	Protein	Host	Dilution
Biolegend	905901	Cytokeratin5	Chicken	1:500
Merck	MABT329	Cytokeratin 8 (clone TROMA-1)	Rat	1:200
AbCam	AB92513	ERG (clone EPR3864)	Rabbit	1:250
eBioscience	BMS14-5698-82	Ki67 (clone SolA15)	Rat	1:500

**List of secondary antibodies used for immunofluorescence**

Company	Catalogue #	Protein	Host	Dilution
Life Technologies	A21208	$\alpha$ -rabbit Alexa Fluor 488	Donkey	1:500
Life Technologies	A21209	$\alpha$ -rat Alexa Fluor 594	Donkey	1:500
Life Technologies	A21094	$\alpha$ -chicken Alexa Fluor 633	Goat	1:500

## 8.5. Hematoxylin & Eosin staining of Fomalin-fixed Paraffin-embedded sections

Organoids are fixed with 4% PFA, embedded into paraffin blocks and sectioned as indicated in the previous section (8.4) of this chapter. The slides are deparaffinized, incubated with Gill Haematoxylin (Merck, GHS232) and then washed with water. Subsequently, samples are washed with ethanol and then incubated with Eosin Y

(Merck, HT110132); after staining with eosin, samples are washed two times with ethanol and finally with xylene before mounting the coverslip. Images are obtained with the Zeiss Axio Imager M2 present at the Advanced Imaging Cell Facility.

## 8.6. AR Immunohistochemistry staining of Formalin-fixed Paraffin-embedded sections

Organoids are fixed with 4% PFA, embedded into paraffin blocks, sectioned and deparaffinized as indicated in the section 8.4 of this chapter; after that samples are washed with PBS and incubated with peroxidase inhibitor solution (80% methanol, 1% Hydrogen Peroxyde (H<sub>2</sub>O<sub>2</sub>) in PBS) to block endogenous peroxidases. They are then blocked with blocking solution for 1 hour at RT and subsequently incubated O/N at 4 °C with the AR-primary antibody (AR-N20, Santa Cruz Biotechnology, sc-816) diluted 1:500 in blocking solution. After incubation with the primary antibody, slides are washed with PBS and then incubated for 1 hour at RT with the biotin-conjugated secondary antibody (Jackson ImmunoResearch, 711-065-152, diluted 1:250 in blocking solution); subsequently samples are washed again in PBS and incubated for 1 hour at RT with the Avidin-Biotin complex (Vectastain® Elite ABC Peroxidase kit, Vector Labs, PK-6100). After this step section are washed with PBS and incubated with DAB revelation solution (2-10 min; Vectastain® Elite ABC Peroxidase kit, Vector Labs, SK-4100); reaction is stopped with washing slides with water and then coverslip is applied to the slide. Samples are observed and imaged with the Zeiss Axio Imager M2 present at the Advanced Imaging Cell Facility

## 8.7. Immunoblot analysis

Proteins, previously extracted and quantified with BCA assay, are then analyzed via Poly-acrylamide Gel Electrophoresis (SDS-PAGE) and western blot approach. Usually 20 µg of protein from each sample are used for the experiments, mixing them with Loading Buffer 5x and water up to final volume. The samples are boiled for 10 min at 95 °C. Proteins are separated by 12% SDS-PAGE and transferred on Polyvinylidene fluoride (PVDF) membrane (Merck, GE10600023) using a wet electroblotting system. Membrane is then blocked for 1 hour at RT in either 5% non-fat dry milk or 5% BSA in TBS-T buffer (50 mM Tris-HCl, pH 7.5, 150 mM NaCl, 0.1% Tween 20), and incubated O/N at 4 °C with gentle shaking with the primary antibody at the appropriate dilution in either non-fat dry milk- or BSA-TBS-T (the antibodies used are reported in Table 5). After 3 washes with TBS-T the membrane is incubated with an HRP-conjugated secondary antibody (either anti-rabbit or anti-mouse depending

on the host species of the primary antibody, GE Healthcare: GEHNA934-GEHNA311) diluted 1:2000-1:5000 in blocking buffer for 1 hour at RT.

Subsequently, the membrane is washed with TBST and the signal is detected using ECL Select detection kit (Euroclone, GEHRPN2235) with an Alliance LD2 device (UVITEC). Protein levels were quantified by densitometry using ImageJ software (ImageJ 1.50i) and statistical analysis is performed through GraphPad PRISM (V. 6.1).

<b>Company</b>	<b>Catalogue #</b>	<b>Protein</b>	<b>Host</b>	<b>Dilution</b>
Biolegend	905501	Cytokeratin 5	Rabbit	1:1000
AbCam	AB53280	Cytokeratin 8 (clone EP1628Y)	Rabbit	1:1000
AbCam	AB133264	ERG (clone EPR3864[2])	Rabbit	1:1000
Thermo Fischer Scientific	MA515738	GAPDH (clone GA1R)	Mouse	1:4000
Santa Cruz	SC-816	AR N-20	Rabbit	1:1000
Merck	A2228	β-actin (clone AC-74)	Mouse	1:1000

## 8.8. CLICK-IT enrichment of secreted proteins

### 8.8.1. AHA and Methionine labeling of newly synthesized proteins from CD1-derived mPros

Organoids are seeded in 6-well plate, 7 domes/well and 2000 UFO/dome. For the analysis of secreted proteins, the medium from 3 wells was pulled together and treated as a single sample. When mPrOs are fully grown, a step of Methionine starvation is performed incubating the samples for 2 hours with Depletion medium (Albumax™) before O/N labeling at 37 °C with either AHA medium or Methionine medium (both are prepared with Albumax™-containing Depletion medium). Subsequently, conditioned medium from either AHA-labeled or Met-labeled cultures is collected and centrifuged (1000 g, 5 min) to pellet cells and debris, then transferred to a new tube, supplemented with protease inhibitors and stored at -80 °C until further processing. The organoids remaining after labeling and conditioned medium collection are used for either RNA or protein extraction.



### 8.8.2. AHA labeling of newly synthesized proteins from C57B6/J-derived mPrOs

Organoids are seeded in 6-well plate, 7 domes/well and 2000 UFO/dome. For the analysis of secreted proteins, the medium from 3 wells was pulled together and treated as a single sample. After treating samples with or without doxycycline (1 µg/ml) for 96 hours, cultures undergo Methionine depletion incubating the samples for 2 hours with Depletion medium (Human Albumin) before O/N labeling at 37 °C with AHA medium (prepared with human albumin-containing Depletion medium). Subsequently, conditioned medium from labeled cultures is collected and centrifuged (1000 g, 5 min) to pellet cells and debris, then transferred to a new tube, supplemented with protease inhibitors and stored at -80 °C until further processing. The organoids remaining after labeling and conditioned medium collection are used for either RNA or protein extraction.

### 8.8.3. CLICK-IT enrichment of secreted proteins from conditioned medium of CD1-derived mPrOs

The protocol for CLICK-IT enrichment of AHA-labeled secreted proteins is based on Click-iT™ protein enrichment kit (Thermo Fisher Scientific, C10416) with further modifications derived from the work of Eichelbaum and colleagues (Eichelbaum *et al.*, 2012; Eichelbaum and Krijgsveld, 2014; and personal communications). The medium containing AHA-labeled proteins, or Met-labeled proteins used as control, is concentrated through centrifugation (4500 g, 4 °C) up to a final volume of ~250 µl exploiting protein concentrator (Pierce™ Protein Concentrator PES, 3K MWCO, Thermo Fisher Scientific, 88515). The concentrated medium is then mixed with equal volume of UREA lysis Buffer (8 M Urea; 200 mM Tris-HCl, pH 8; 4% CHAPS; 1 M NaCl). The sample is then added to the alkyl resin, previously washed with milliQ water, and mixed with an equal volume of 2x Catalyst solution (1:8 reaction additive 1, 2 mM CuSO<sub>4</sub>, 1:50 reaction additive 2, in milliQ water). The reaction mix for cyclo-addition reaction is incubated O/N at RT with continuous rotation.

After incubation, the sample is centrifuged (1200 g, 1 min) and washed once with milliQ water before incubating with 10 mM DTT in SDS washing buffer (100 mM Tris-HCl, pH 8; 1% SDS; 250 mM NaCl; 5 mM EDTA) for 15 min at 70 °C plus another 15 min at RT. The samples are centrifuged to discard DTT-containing solution and incubated for 30 min with 40 mM Iodoacetamide solution (Iodoacetamide salt diluted in SDS washing buffer) with gentle shaking (preventing light exposure). The resin is resuspended and then transferred into a spin column for subsequent washes with: SDS washing buffer; Washing buffer #2 (8 M Urea; 100 mM Tris-HCl, pH 8); 20% Isopropanol buffer and 20% Acetonitrile buffer. At the end of this steps, the resin is resuspended in Digestion buffer (100 mM Tris-HCl, pH 8; 2 mM CaCl<sub>2</sub>; 10% acetonitrile) and centrifuged before incubating the sample with

2.5 ng/ $\mu$ l of MS-grade Trypsin (Pierce™ Trypsin protease, MS grade, Thermo Fished Scientific, 90057) diluted in Digestion buffer. The sample are vortexed and incubated O/N at 37 °C with continuous rotation.

After tryptic digestion, the resin is centrifuged and the supernatant transferred in a new collection tube, the resin is then washed with milliQ water and centrifuged again to recover as much peptide as possible. The resulting peptide mix is then acidified with trifluoroacetic acid (0.2%, final volume 1 ml in milliQ water) and stored at -80°C until MS analysis.

#### 8.8.4. MS analysis and identification of enriched proteins

##### 8.8.4.1. Stage tip purification

Before LC-MS/MS analysis, tryptic peptides are purified by reversed-phase (C18) stage-tip purification (Rappsilber, Mann and Ishihama, 2007). Stage tips are first conditioned with 50  $\mu$ l of 0.1% trifluoroacetic acid containing 50% acetonitrile and then equilibrated with 50  $\mu$ l of 0.1% trifluoroacetic acid. Tryptic peptides (400  $\mu$ l of peptide solution) were loaded onto the stage-tips. After a 50  $\mu$ l wash by 0.1% trifluoroacetic acid and a 50  $\mu$ l wash by 0.1% formic acid, peptides are eluted from the stage tips by adding 10  $\mu$ l of 80% acetonitrile/ 0.1% formic acid. Eluted peptides are then evaporated to dryness in a vacuum centrifuge and subsequently resuspended in 20  $\mu$ l of 0.1% formic acid/2% acetonitrile.

##### 8.8.4.2. LC-MS/MS analysis

LC-MS/MS analysis is performed by an EASY-LC 1000 coupled to a Q-Exactive mass spectrometer (Thermo Fisher Scientific). The analytical nanoLC column is a pulled fused silica capillary, 75  $\mu$ m i.d., in-house packed to a length of 12 cm with 3  $\mu$ m C18 silica particles (Dr. Maisch GmbH). Peptide mixtures are loaded directly onto the analytical column. A binary gradient is used for peptide elution. Mobile phase A is composed by 0.1% formic acid, 2% acetonitrile, whereas mobile phase B is 0.1% formic acid, 80% acetonitrile. Gradient elution is achieved at 300 nl/min flow rate, and ramped from 6% B to 40% B in 90 min, and from 40% B to 100% B in additional 18 min; after 10 min at 100% B, mobile phase composition is finally brought to 0% B in 2 min. MS detection is performed on a quadrupole-orbitrap mass spectrometer Q-Exactive (Thermo Fisher Scientific) operating in positive ion mode, with nanoelectrospray (nESI) potential at 1800 V applied on the column front-end via a tee piece. Data-dependent acquisition is performed using a top-12 method with resolution (FWHM), AGC target and maximum injection time (ms) for full MS and MS/MS of, respectively, 70,000/35,000, 1e6/1e5, 50/120. Mass window for precursor ion isolation is 1.6 m/z, and normalized collision energy is 25. Dynamic exclusion is 25 s. Injected amounts of samples vary from 4 to 8  $\mu$ l, depending on peptide amount estimated from a preliminary injection.

#### 8.8.4.3. Data analysis

LC-MS/MS data analysis is conducted using the MaxQuant/Perseus software suite. Label-free quantification is activated in MaxQuant, using default parameters except for the following: **i)** minimum peak length = 4; **ii)** mass accuracy = 3 ppm; **iii)** retention time window for match-between-runs options = 0.5 min (match-between-runs was set to “ON”, with an alignment time window of 20 min). Data are searched on the *Mus musculus* reference proteome, downloaded on August 11, 2018 (53,345 sequences). Label free quantification of proteins is based on the LFQ algorithm (Cox *et al.*, 2014) and requires a minimum of one unique/razor peptide associated to a specific identified protein.

The protein summary output table is loaded in Perseus for statistical and bioinformatics analysis. After removing hits from reverse and contaminants database and transforming LFQ intensity data in logarithmic space, proteins are filtered based on valid values (measurement present in at least 2 biological replicates of at least one sample group). Missing values are imputed using default parameters. Finally, significantly different proteins are searched by applying a two-sided t-test with correction for multiple hypothesis testing according to Benjamini-Hochberg (FDR < 0.2).

#### 8.8.5. Albumin Deprivation

Conditioned medium obtained using Depletion medium (Human albumin) and AHA-medium (derived from human albumin-containing Depletion medium), see section 8.8.2 in this chapter, was concentrated using Pierce protein concentrator, it was then processed with the Pierce™ Albumin Depletion kit (Thermo Fischer Scientific, 85160) following manufacturer instructions. After several washes, eluted proteins are then used for CLICK enrichment starting directly from cyclo-addition reaction (see section 8.8.3 in this chapter).

#### 8.8.6. Refined CLICK-iT protocol for enrichment of secreted proteins from conditioned medium of C57B6/J-derived mPrOs

The refined protocol for enrichment of AHA-labeled secreted proteins is almost entirely equal to the one present in section 8.8.3 of this chapter. The difference is due to the presence of an additional alkylation step that is intended to reduce the a-specific binding of albumin proteins to the resin and so the presence non-mPrOs derived peptides in the final mix. The additional alkylation step is performed after conditioned medium concentration and mixing with UREA lysis buffer; it is obtained adding to the samples 1 mM Iodoacetamide

solution (Iodoacetamide salt diluted in SDS washing buffer) and incubating them for 30 min at 20 °C with mild centrifugation (3000-4000 g). After the additional alkylation step the protocol continues as indicated before with cyclo-addition reaction, reduction-alkylation, washes and final tryptic digestion.

## 8.9. Shared protein analysis

Identified proteins were analyzed using the Unique peptides parameter as a proxy for protein presence in that biological replica. To understand the degree of shared proteins within each condition, a molecule was marked as present in a specific replica if it is present with at least 2 unique peptides. Venn diagrams were obtained using Venny 2.1.0 (<http://bioinfogp.cnb.csic.es/tools/venny/>) using the ID of associated proteins as input. For the analysis of common proteins among the different conditions, a protein was marked as associated to a specific condition if present with at least 2 unique peptides in at least 3 out of 4 biological replicas and the resulting list of proteins ID was used as input for the design of Venn diagram.

Hand curated analysis of top protein hits (Chapter 0) was performed searching in Pubmed with the complete protein name as input parameter, giving priority to articles discussing about this protein in the context of PCa research.

## 8.10. Protein network and gene ontology analysis

The analysis of protein network and enriched pathways identified from untreated WT secreted proteome was performed exploiting the list derived from the analysis of shared proteins regarding that condition. The list of proteins ID was then analyzed for protein-protein association using STRING V11.0 (Mering *et al.*, 2003; Szklarczyk *et al.*, 2019) ([https://string-db.org/cgi/input.pl?sessionId=jvug55270PPS&input\\_page\\_show\\_search=on](https://string-db.org/cgi/input.pl?sessionId=jvug55270PPS&input_page_show_search=on)). The same tools are also used to analyze the list of differentially secreted proteins identified comparing doxycycline-treated mPrOs-ERG with untreated engineered organoids. The last were selected as having FDR lower than 20% and a variation higher than 100% ( $FC < 0.5$  or  $FC > 2$ ).

Gene ontology analysis is performed with DAVID Functional annotation (Database for Annotation, Visualization and Integrated Discovery; <https://david.ncifcrf.gov/summary.jsp>; Huang, Sherman and Lempicki, 2008, 2009). The list of proteins identified in C57B6/J-derived mPrOs-WT (see chapter 4.3.2.1 and Table-S2) is given as input to the online tool, selecting “*Mus Musculus*” as background list. The analysis is then performed with default parameters except for the Functional Annotation Clustering, where we selected Classification stringency “Highest”, and resulting tables from enriched ontologies are analyzed and reported in Table-S3.

## 8.11. Statistical Analysis

In all graphs, data are expressed as mean  $\pm$  SD of at least three independent biological replicates except when otherwise indicated. Differences were analyzed by Student's t test using PRISM 6 (GraphPad V. 6.01). P-values  $< 0.05$  were considered significant.

\*= p-value  $< 0,05$ ; \*\*=  $0,05 < p$ -value  $< 0,001$ ; \*\*\*= p-value  $< 0,001$

## 9. ACKNOWLEDGMENTS

The work presented here is the result of an interesting and challenging 4-years-long PhD project, however, this would not have been possible without the help of many colleagues and collaborators.

In particular, I want to thank my PI, prof. Andrea Lunardi, whose mentorship and dedication guided me through the entire doctoral program.

A special thanks goes also to all the present and former members of the Armenise-Harvard Laboratory of Cancer Biology & Genetics. In particular I want to acknowledge: Dr. Alessandro Alaimo for his continuous support and active contribution to this project; Dr. Francesco Cambuli for his crucial contribution to the establishment in our laboratory of the mPrOs technology; Drs Veronica Foletto and Dario De Felice that share with me the everyday PhD life and that help me with the mPrOs model; Dr. Sacha Genovesi for his help with immunofluorescence experiments, image acquisition and analysis; Dr. Arianna Bertossi that helped me with flow cytometry analysis and that will contribute in the future experiments on macrophage and CD4<sup>+</sup> T lymphocytes differentiation; Dr. Josep Rubert for his effort in the characterization of the mPrOs metabolomic profile and, finally, to all the past and present students that joined our laboratory.

I want to acknowledge Dr. Marianna Kruithof-de Julio who hosted me in her laboratory at the University of Bern during my visiting period. Thanks to this experience I had the possibility to learn innovative in vitro and in vivo experimental approaches, meet many valuable scientists, and set up a fruitful scientific collaboration.

A very special thanks goes to Prof. Marco Gaspari from the Magna Graecia University of Catanzaro who performed all the mass spectrometry analysis presented in this work. The long-lasting experience of prof. Gaspari in the field of proteomic together with his profound interest and enthusiasm in applying his expertise and knowledge to the 3D organoid system has been an invaluable factor for the successful development of this project.

Finally, I am very grateful to the Giovanni Armenise Harvard foundation, which funded my PhD fellowship and supported my research activity, and to all CIBIO people for the amazing scientific environment in which I had the opportunity to work in the past four years.

## 10. ACKNOWLEDGMENTS (part Two)

During this very long period I spent so much time at CIBIO struggling with experiments, techniques and cells; probably I wouldn't be here without the help and presence of all the many people that I met during past years.

I will start thanking my PI Andrea that welcomed me in his laboratory back in 2015 when I was looking for a PhD, he had faith in my potential and helped me working and developing it during the time we spent together. I must admit that we had some ups and downs during this adventure, but in the end, he helped me become a more independent scientist and a better person.

A big thank to all the members of the **LunardiLab**.

To Alessandro for being the mentor I needed and a continuous help during the many lab-hours we spent together, for all the fun we had during the past four years and for laughing at bad/stressing moments.

To Sacha, the greatest lab-manager that everyone needs, without your help I wouldn't have done everything that is written in this thesis (or probably I would have taken 4 more years...), thanks for your patience and I wish you good luck for your future.

To Veronica for sharing with me the pros and cons of being PhDs in LunardiLab and for being the friendly colleague you are, you helped me focus on the most important aspects of my PhD and you are always helpful when I forget something, we had also funny moments during the past years but remember to be always strong!

To Dario, the youngest PhD in LunardiLab, we may be different but you helped me focus on what I had to do and stimulated me to improve every time, I hope you will enjoy this time more than I did.

To Francesco, I hope this may reach you some day in NY, for your effort in this laboratory from the very beginning and for teaching me the basics of working with mPROs, we had our conflict once but that also helped me to grow up and understand who I want to become.

To Arianna, may you read this someday, I have to thank you for your suggestions and your help, you brought a different perspective in this prostate-focused laboratory and your help was and is important to finish this work.

To Josep, the true Spanish member of LunardiLab, your different perspective and your positiveness were very important for me and also for all of us, thank you for your help and our discussions, unfortunately we couldn't do what we had in mind but probably someday... good luck for your next step.

To all our past and present students that decided to join LunardiLab and be part of this strange family (Simone, Michela, Stefania, Alice, Maria Dilia, Enrico, Eleonora, Emiliana, Rubens, Martina, Josè), every one of you gave something to me that I will never forget and I hope you will realize your dreams someday, thank you.

Thanks to CIBIO (that changed from Centre to Department) for being my home since 2009 when I first started as a freshman and to the PhD school for accepting me and giving me this opportunity, to all the professors that helped me in those years and all the students that shared good and bad things with me.

Thanks to all the **CIBIOPEOPLE** that I met during this adventure, it will be almost impossible to write down all your names here, but you will always have my gratitude. Thank you for everything: from lending me an aliquot of your reagent to teaching me how to use an instrument, from sharing with me your “100%-functioning” protocol to cheering me whenever I needed. I know I may have been boring or inappropriate sometime but thank you for the patience, I will try to improve that.

Thanks to 31<sup>st</sup> PhD students, you are the best (Dario, Laura, Michela, Isabelle, Alice, Blerta, Duhan, Ilaria, Eloina, Serena, Paolo). I don't know what I can say to you, I will always remember my friends, you, that supported me during these years. Thank you for the help, the fun and all the moments we had together, it was a beautiful adventure especially thanks to you.

Thanks to my lunch-mates (and dinner, aperitivo, kaffè, funny moments, etc.) for the moments we shared and the bond we created, you helped me a lot in both “ups and downs” and I will thank you forever for all the fun and adventures we had together.

Thanks to: Dario, we met long time ago but despite all our differences we are and will be good friends; Laura, I'm glad I met the strong and always supportive person that you are and that helped me a lot; Fruits, it doesn't mind what is and will be happening all your traits shape the person you are so never change them; Kalina, I can say that I have a friend from Poland that is one of the kindest person I ever met; Erna, I can also say I have a friend from Lithuania that is always enthusiast and open minded; Arnold, it doesn't mind if you are often late since you are always a good and positive person; Simone, those few times you are here in Italy it's a pleasure to meet with a nice person like you; Valeria, your sunny-warm attitude is your best quality and never give up. Thanks also to all the people that enjoyed it with us during their time spent in CIBIO.

A special thanks to my second family in Trento, the group of good/old friends that live with me at Salesiani. We shared a lot of good moments and events that I will always remember; I have to remember in particular Luca, Matteo, Emanuele, Daniele, all the members of the volley team and all those that contributed to create this special world. Last, but not least, big thanks to our directors, don Carlo and don Eugenio.

Thanks to all my old friends that are always present when I'm home in Zevio: Andrea, Celine, Mattia, Serena, Fede, Teba, Matteo, Giulia, Silvia, Filippo, Sabri, Jacopo, Michela, Lorenzo, Cecilia, Silvia, Elena and Fabio. Some are closer while some are far away, some are busier while some are always there; I like to spend time with you and share moments, discussions, happy events and everything else together. I wish to all of you



all the best and I hope you will realize your dreams, wherever they will bring you. I am very very lucky I met all of you!

Finally, thanks to my family. I don't know how to say it since there are so much things that you did and are doing for me, I hope you understand that I couldn't have done everything I did without you and that I appreciate and I'm glad for everything you are doing for me. **THANK YOU!**

Enjoy what you are doing and what you will do in your future.

Follow your dreams, wherever they will take you.

Live your life at the best you can and remember always to smile, it will make you feel better even in your hard times and it will make others feel better too.

*This final chapter was not edited, so please excuse me for the errors you found.*

## 11. REFERENCES

- Abate-Shen, C. and Shen, M. M. (2000) 'Molecular genetics of prostate cancer.', *Genes & Development*, pp. 2410–2434. doi: 10.1101/gad.819500.2410.
- Abeshouse, A. *et al.* (2015) 'The Molecular Taxonomy of Primary Prostate Cancer', *Cell*, 163(4), pp. 1011–1025. doi: 10.1016/j.cell.2015.10.025.
- Afink, G. B. *et al.* (2010) 'Initial Characterization of C16orf89 , A Novel Thyroid-Specific Gene', *Thyroid*, 20(7), pp. 811–821. doi: 10.1089/thy.2009.0366.
- Alaimo, A. *et al.* (no date) 'Pharmacological activation of TRPM8 channel overcomes innate resistance to standard-of-care therapies in prostate cancer', *in preparation*.
- Alam, M. T. *et al.* (2014) 'Suprabasin as a novel tumor endothelial cell marker', *Cancer Science*, 105(12), pp. 1533–1540. doi: 10.1111/cas.12549.
- Antonica, F. *et al.* (2012) 'Generation of functional thyroid from embryonic stem cells', *Nature*. Nature Publishing Group, 491(7422), pp. 66–71. doi: 10.1038/nature11525.
- Armenia, J. *et al.* (2018) 'The long tail of oncogenic drivers in prostate cancer', *Nature Genetics*, 50(5), pp. 645–651. doi: 10.1038/s41588-018-0078-z.
- Arvand, A. and Denny, C. T. (2001) 'Biology of EWS/ETS fusions in Ewing's family tumors', *Oncogene*, 20(40 REV. ISS. 4), pp. 5747–5754. doi: 10.1038/sj.onc.1204598.
- Attard, G. *et al.* (2016) 'Prostate cancer', *The Lancet*, 387(10013), pp. 70–82. doi: 10.1016/S0140-6736(14)61947-4.
- Bagert, J. D. *et al.* (2014) 'Quantitative, Time-Resolved Proteomic Analysis by Combining Bioorthogonal Noncanonical Amino Acid Tagging and Pulsed Stable Isotope Labeling by Amino Acids in Cell Culture', *Molecular & Cellular Proteomics*, 13(5), pp. 1352–1358. doi: 10.1074/mcp.M113.031914.
- Barbosa, G. O. *et al.* (2019) 'Heparanase-1 activity and the early postnatal prostate development', *Developmental Dynamics*, 248(3), pp. 211–220. doi: 10.1002/dvdy.12.
- Barros-Silva, J. D. *et al.* (2018) 'Single-Cell Analysis Identifies LY6D as a Marker Linking Castration-Resistant Prostate Luminal Cells to Prostate Progenitors and Cancer', *Cell Reports*, 25(12), pp. 3504-3518.e6. doi: 10.1016/j.celrep.2018.11.069.
- Beer, T. M. *et al.* (2014) 'Enzalutamide in metastatic prostate cancer before chemotherapy.', *The New England journal of medicine*, 371(5), pp. 424–33. doi: 10.1056/NEJMoa1405095.
- Berger, T. *et al.* (2006) 'Lipocalin 2-deficient mice exhibit increased sensitivity to Escherichia coli infection but not to ischemia-reperfusion injury', *Proceedings of the National Academy of Sciences*, 103(6), pp. 1834–1839. doi:

10.1073/pnas.0510847103.

- Bielski, C. M. *et al.* (2018) 'Genome doubling shapes the evolution and prognosis of advanced cancers', *Nature Genetics*. Springer US, 50(8), pp. 1189–1195. doi: 10.1038/s41588-018-0165-1.
- Blee, A. M. *et al.* (2018) 'TMPRSS2-ERG Controls Luminal Epithelial Lineage and Antiandrogen Sensitivity in PTEN and TP53 -Mutated Prostate Cancer', *Clinical Cancer Research*, 24(18), pp. 4551–4565. doi: 10.1158/1078-0432.CCR-18-0653.
- Boj, S. F. *et al.* (2015) 'Organoid Models of Human and Mouse Ductal Pancreatic Cancer', *Cell*, 160(1–2), pp. 324–338. doi: 10.1016/j.cell.2014.12.021.
- Bostwick, D. G. and Qian, J. (2004) 'High-Grade prostatic intraepithelial neoplasia', *Modern Pathology*, 17, pp. 360–379. doi: 10.4111/kju.2012.53.5.297.
- Briot, A. *et al.* (2009) 'Kallikrein 5 induces atopic dermatitis-like lesions through PAR2-mediated thymic stromal lymphopoietin expression in Netherton syndrome', *The Journal of Experimental Medicine*, 206(5), pp. 1135–1147. doi: 10.1084/jem.20082242.
- Cambuli, F. *et al.* (no date) '3D organoids unravel critical insights into prostate tissue homeostasis and tumorigenesis', *in preparation*.
- Carreira, S. *et al.* (2014) 'Tumor clone dynamics in lethal prostate cancer.', *Science translational medicine*, 6(254), p. 254ra125. doi: 10.1126/scitranslmed.3009448.
- Carver, B. S. *et al.* (2009) 'Aberrant ERG expression cooperates with loss of PTEN to promote cancer progression in the prostate.', *Nature genetics*, 41(5), pp. 619–24. doi: 10.1038/ng.370.
- Chavanas, S. *et al.* (2000) 'Mutations in SPINK5, encoding a serine protease inhibitor, cause Netherton syndrome', *Nature Genetics*, 25(2), pp. 141–142. doi: 10.1038/75977.
- Chen, Y., Chi, P., Rockowitz, S., laquinta, Phillip J, *et al.* (2013) 'ETS factors reprogram the androgen receptor cistrome and prime prostate tumorigenesis in response to PTEN loss', *Nature Medicine*. Nature Publishing Group, 19(8), pp. 1023–1029. doi: 10.1038/nm.3216.
- Chua, C. W. *et al.* (2014) 'Single luminal epithelial progenitors can generate prostate organoids in culture', *Nature Cell Biology*, 16(10), pp. 951–961. doi: 10.1038/ncb3047.
- Chua, C. W. *et al.* (2018) 'Differential requirements of androgen receptor in luminal progenitors during prostate regeneration and tumor initiation', *eLife*, 7, pp. 1–26. doi: 10.7554/elife.28768.
- Clevers, H. (2016) 'Modeling Development and Disease with Organoids', *Cell*. Elsevier Inc., 165(7), pp. 1586–1597. doi: 10.1016/j.cell.2016.05.082.
- Conus, S. and Simon, H. U. (2010) 'Cathepsins and their involvement in immune responses', *Swiss Medical Weekly*, 140(JULY). doi: 10.4414/smw.2010.13042.
- Cox, J. *et al.* (2014) 'Accurate proteome-wide label-free quantification by delayed normalization and maximal

- peptide ratio extraction, termed MaxLFQ.', *Molecular & cellular proteomics : MCP*, 13(9), pp. 2513–26. doi: 10.1074/mcp.M113.031591.
- Demichelis, F. *et al.* (2007) 'TMPRSS2:ERG gene fusion associated with lethal prostate cancer in a watchful waiting cohort', *Oncogene*, 26(31), pp. 4596–4599. doi: 10.1038/sj.onc.1210237.
- Devireddy, L. R. *et al.* (2001) 'Induction of apoptosis by a secreted lipocalin that is transcriptionally regulated by IL-3 deprivation', *Science*, 293(5531), pp. 829–834. doi: 10.1126/science.1061075.
- Dieterich, D. C. *et al.* (2006) 'Selective identification of newly synthesized proteins in mammalian cells using bioorthogonal noncanonical amino acid tagging (BONCAT)', *Proceedings of the National Academy of Sciences*, 103(25), pp. 9482–9487. doi: 10.1073/pnas.0601637103.
- Ding, Z. *et al.* (2011) 'SMAD4-dependent barrier constrains prostate cancer growth and metastatic progression', *Nature*. Nature Publishing Group, 470(7333), pp. 269–273. doi: 10.1038/nature09677.
- Drost, J. *et al.* (2016) 'Organoid culture systems for prostate epithelial and cancer tissue', *Nat Protoc*. Nature Publishing Group, 11(2), pp. 347–358. doi: 10.1038/nprot.2016.006.
- Drost, J. and Clevers, H. (2018) 'Organoids in cancer research', *Nature Reviews Cancer*. Springer US, pp. 1–12. doi: 10.1038/s41568-018-0007-6.
- Eichelbaum, K. *et al.* (2012) 'Selective enrichment of newly synthesized proteins for quantitative secretome analysis', *Nature Biotechnology*. Nature Publishing Group, 30(10), pp. 984–990. doi: 10.1038/nbt.2356.
- Eichelbaum, K. and Krijgsveld, J. (2014) 'Combining Pulsed SILAC labeling and Click-Chemistry for Quantitative Secretome Analysis', *Methods in Molecular Biology*. doi: 10.1017/CBO9781107415324.004.
- Eiraku, M. *et al.* (2008) 'Self-Organized Formation of Polarized Cortical Tissues from ESCs and Its Active Manipulation by Extrinsic Signals', *Cell Stem Cell*. Elsevier Inc., 3(5), pp. 519–532. doi: 10.1016/j.stem.2008.09.002.
- Eiraku, M. *et al.* (2011) 'Self-organizing optic-cup morphogenesis in three-dimensional culture', *Nature*. Nature Publishing Group, 472, pp. 51–56. doi: 10.1038/nature09941.
- Ferlay, J. *et al.* (2015) 'Cancer incidence and mortality worldwide: Sources, methods and major patterns in GLOBOCAN 2012', *International Journal of Cancer*, 136(5), pp. E359–E386. doi: 10.1002/ijc.29210.
- Fessler, E. *et al.* (2016) 'TGF $\beta$  signaling directs serrated adenomas to the mesenchymal colorectal cancer subtype', *EMBO Molecular Medicine*, 8(7), pp. 745–760. doi: 10.15252/emmm.201606184.
- Flo, T. H. *et al.* (2004) 'Lipocalin 2 mediates an innate immune response to bacterial infection by sequestering iron', *Nature*, 432(7019), pp. 917–921. doi: 10.1038/nature03104.
- Furio, L. and Hovnanian, A. (2011) 'When Activity Requires Breaking Up: LEKTI Proteolytic Activation Cascade for Specific Proteinase Inhibition', *Journal of Investigative Dermatology*. Elsevier Masson SAS, 131(11), pp. 2169–2173. doi: 10.1038/jid.2011.295.

- Furio, L. and Hovnanian, A. (2014) 'Netherton syndrome: Defective kallikrein inhibition in the skin leads to skin inflammation and allergy', *Biological Chemistry*, 395(9), pp. 945–958. doi: 10.1515/hsz-2014-0137.
- Gao, D. *et al.* (2014) 'Organoid cultures derived from patients with advanced prostate cancer', *Cell*. Elsevier Inc., 159(1), pp. 176–187. doi: 10.1016/j.cell.2014.08.016.
- Gorthi, A. and Bishop, A. J. R. (2018) 'Ewing sarcoma fusion oncogene: At the crossroads of transcription and DNA damage response', *Molecular & Cellular Oncology*, 5(4), p. e1465014. doi: 10.1080/23723556.2018.1465014.
- Grünewald, T. G. P. *et al.* (2018) 'Ewing sarcoma', *Nature Reviews Disease Primers*, 4(1), p. 5. doi: 10.1038/s41572-018-0003-x.
- Hanahan, D. and Weinberg, R. A. (2000) 'The Hallmarks of Cancer', *Cell*, 100(1), pp. 57–70. doi: 10.1016/S0092-8674(00)81683-9.
- Hanahan, D. and Weinberg, R. A. (2011) 'Hallmarks of Cancer: The Next Generation', *Cell*. Elsevier Inc., 144(5), pp. 646–674. doi: 10.1016/j.cell.2011.02.013.
- He, H. *et al.* (2012) 'Expression of ERG protein, a prostate cancer specific marker, in high grade prostatic intraepithelial neoplasia (HGPIN): Lack of utility to stratify cancer risks associated with HGPIN', *BJU International*, 110(11 B), pp. 751–755. doi: 10.1111/j.1464-410X.2012.11557.x.
- Hodson, R. (2015) 'Small organ, big reach.', *Nature*, 528(7582), pp. S118-9. doi: 10.1038/528S118a.
- Huang, D. W., Sherman, B. T. and Lempicki, R. A. (2008) 'Systematic and integrative analysis of large gene lists using DAVID bioinformatics resources', *Nature Protocols*. Nature Publishing Group, 4, p. 44. Available at: <https://doi.org/10.1038/nprot.2008.211>.
- Huang, D. W., Sherman, B. T. and Lempicki, R. A. (2009) 'Bioinformatics enrichment tools: Paths toward the comprehensive functional analysis of large gene lists', *Nucleic Acids Research*, 37(1), pp. 1–13. doi: 10.1093/nar/gkn923.
- Huch, M. *et al.* (2015) 'Long-Term Culture of Genome-Stable Bipotent Stem Cells from Adult Human Liver', *Cell*. The Authors, 160(1–2), pp. 299–312. doi: 10.1016/j.cell.2014.11.050.
- Iannetti, A. *et al.* (2008) 'The neutrophil gelatinase-associated lipocalin (NGAL), a NF- $\kappa$ B-regulated gene, is a survival factor for thyroid neoplastic cells', *Proceedings of the National Academy of Sciences*, 105(37), pp. 14058–14063. doi: 10.1073/pnas.0710846105.
- Ichikawa, H. *et al.* (1994) 'An RNA-binding Protein Gene, TLS/FUS, Is Fused to ERG in Human Myeloid Leukemia with t(16;21) Chromosomal Translocation', *Cancer Research*, 54, pp. 2865–2868.
- Jain, R. *et al.* (2015) 'Plasticity of Hopx+ type I alveolar cells to regenerate type II cells in the lung', *Nature Communications*, 6(1), p. 6727. doi: 10.1038/ncomms7727.
- Jin, C. *et al.* (2017) 'Elevated spondin-2 expression correlates with progression and prognosis in gastric cancer', *Oncotarget*, 8(6), pp. 10416–10424. doi: 10.18632/oncotarget.14423.

- Jung, M. *et al.* (2017) 'Lipocalin-2 and iron trafficking in the tumor microenvironment', *Pharmacological Research*. Elsevier Ltd, 120, pp. 146–156. doi: 10.1016/j.phrs.2017.03.018.
- Karthaus, W. R. *et al.* (2014) 'Identification of multipotent luminal progenitor cells in human prostate organoid cultures', *Cell*. Elsevier Inc., 159(1), pp. 163–175. doi: 10.1016/j.cell.2014.08.017.
- King, J. C. *et al.* (2009) 'Cooperativity of TMPRSS2-ERG with PI3-kinase pathway activation in prostate oncogenesis.', *Nature genetics*, 41(5), pp. 524–6. doi: 10.1038/ng.371.
- Klezovitch, O. *et al.* (2008) 'A causal role for ERG in neoplastic transformation of prostate epithelium', *Proceedings of the National Academy of Sciences*, 105(6), pp. 2105–2110. doi: 10.1073/pnas.0711711105.
- Kolb, H. C., Finn, M. G. and Sharpless, K. B. (2001) 'Click Chemistry: Diverse Chemical Function from a Few Good Reactions', *Angewandte Chemie International Edition*, 40(11), pp. 2004–2021. doi: 10.1002/1521-3773(20010601)40:11<2004::AID-ANIE2004>3.0.CO;2-5.
- Kumar-Sinha, C., Tomlins, S. a and Chinnaiyan, A. M. (2008) 'Recurrent gene fusions in prostate cancer', *Nature Reviews Cancer*, 8(7), pp. 497–511. doi: 10.1038/nrc2402.
- Kurata, M. *et al.* (2003) 'Expression, purification, and inhibitory activities of mouse cytotoxic T-lymphocyte antigen-2 $\alpha$ ', *Protein Expression and Purification*, 32(1), pp. 119–125. doi: 10.1016/S1046-5928(03)00222-5.
- Lancaster, M. A. and Knoblich, J. A. (2014) 'Organogenesis in a dish: Modeling development and disease using organoid technologies', *Science*, 345(6194), pp. 1247125–1247125. doi: 10.1126/science.1247125.
- Lee, S. L. *et al.* (2015) 'ERG expression in prostate needle biopsy: Potential diagnostic and prognostic implications', *Applied Immunohistochemistry and Molecular Morphology*, 23(7), pp. 499–505. doi: 10.1097/PAI.0000000000000119.
- Li, C. and Chan, Y. R. (2011) 'Lipocalin 2 regulation and its complex role in inflammation and cancer', *Cytokine*. Elsevier Ltd, 56(2), pp. 435–441. doi: 10.1016/j.cyto.2011.07.021.
- Li, Y. *et al.* (2009) 'Structure of the F-spondin domain of mindin, an integrin ligand and pattern recognition molecule', *The EMBO Journal*, 28(3), pp. 286–297. doi: 10.1038/emboj.2008.288.
- Lin, B. *et al.* (1999) 'Prostate-localized and androgen-regulated expression of the membrane-bound serine protease TMPRSS2.', *Cancer research*, 59(17), pp. 4180–4. Available at: <http://www.ncbi.nlm.nih.gov/pubmed/10485450>.
- Loughran, S. J. *et al.* (2008) 'The transcription factor Erg is essential for definitive hematopoiesis and the function of adult hematopoietic stem cells', *Nature Immunology*, 9(7), pp. 810–819. doi: 10.1038/ni.1617.
- Lucarelli, G. *et al.* (2013) 'Spondin-2, a secreted extracellular matrix protein, is a novel diagnostic biomarker for prostate cancer', *Journal of Urology*. Elsevier Ltd, 190(6), pp. 2271–2277. doi: 10.1016/j.juro.2013.05.004.
- Maher, S., Jjunju, F. P. M. and Taylor, S. (2015) 'Colloquium : 100 years of mass spectrometry: Perspectives and future trends', *Reviews of Modern Physics*, 87(1), pp. 113–135. doi: 10.1103/RevModPhys.87.113.

- Mantovani, A. *et al.* (2008) 'Cancer-related inflammation', *Nature*, 454(7203), pp. 436–444. doi: 10.1038/nature07205.
- Massagué, J. (2012) 'TGF $\beta$  signalling in context', *Nature Reviews Molecular Cell Biology*. Nature Publishing Group, 13(10), pp. 616–630. doi: 10.1038/nrm3434.
- McCracken, K. W. *et al.* (2014) 'Modelling human development and disease in pluripotent stem-cell-derived gastric organoids', *Nature*, 516(7531), pp. 400–404. doi: 10.1038/nature13863.
- Mering, C. v. *et al.* (2003) 'STRING: a database of predicted functional associations between proteins', *Nucleic Acids Research*, 31(1), pp. 258–261. doi: 10.1093/nar/gkg034.
- Montironi, R. *et al.* (2007) 'Mechanisms of Disease: High-grade prostatic intraepithelial neoplasia and other proposed preneoplastic lesions in the prostate', *Nature Clinical Practice Urology*, 4(6), pp. 321–332. doi: 10.1038/ncpuro0815.
- Morais, C. L. *et al.* (2016) 'ERG and PTEN status of isolated high-grade PIN occurring in cystoprostatectomy specimens without invasive prostatic adenocarcinoma', *Human Pathology*. Elsevier Inc., 55, pp. 117–125. doi: 10.1016/j.humpath.2016.04.017.
- Mosquera, J.-M. *et al.* (2008) 'Characterization of TMPRSS2-ERG Fusion High-Grade Prostatic Intraepithelial Neoplasia and Potential Clinical Implications', *Clinical Cancer Research*, 14(11), pp. 3380–3385. doi: 10.1158/1078-0432.CCR-07-5194.
- Muguruma, K. *et al.* (2015) 'Self-Organization of Polarized Cerebellar Tissue in 3D Culture of Human Pluripotent Stem Cells', *Cell Reports*, 10(4), pp. 537–550. doi: 10.1016/j.celrep.2014.12.051.
- Myers, R. P. (2000) 'Structure of the adult prostate from a clinician's standpoint', *Clinical Anatomy*, 13(3), pp. 214–215. doi: 10.1002/(SICI)1098-2353(2000)13:3<214::AID-CA10>3.0.CO;2-N.
- Njoroge, R. N., Vatapalli, R. J. and Abdulkadir, S. A. (2019) 'Organoids Increase the Predictive Value of in vitro Cancer Chemoprevention Studies for in vivo Outcome', *Frontiers in Oncology*, 9(February), pp. 1–10. doi: 10.3389/fonc.2019.00077.
- Nuridin, A. *et al.* (2016) 'Global and Targeted Proteomics of Prostate Cancer Cell Secretome: Combination of 2-Dimensional Image-Converted Analysis of Liquid Chromatography and Mass Spectrometry and In Silico Selection Selected Reaction Monitoring Analysis', *Journal of Pharmaceutical Sciences*. Elsevier Ltd, 105(11), pp. 3440–3452. doi: 10.1016/j.xphs.2016.08.013.
- Paoloni-Giacobino, A. *et al.* (1997) 'Cloning of the TMPRSS2 Gene, Which Encodes a Novel Serine Protease with Transmembrane, LDLRA, and SRCR Domains and Maps to 21q22.3', *Genomics*, 44(3), pp. 309–320. doi: 10.1006/geno.1997.4845.
- Park, J. W. *et al.* (2016) 'Prostate epithelial cell of origin determines cancer differentiation state in an organoid transformation assay', *Proceedings of the National Academy of Sciences*, 113(16), pp. 4482–4487. doi:

10.1073/pnas.1603645113.

- Park, K. *et al.* (2014) 'TMPRSS2:ERG Gene Fusion Predicts Subsequent Detection of Prostate Cancer in Patients With High-Grade Prostatic Intraepithelial Neoplasia', *Journal of Clinical Oncology*, 32(3), pp. 206–211. doi: 10.1200/JCO.2013.49.8386.
- Pavlou, M. P. and Diamandis, E. P. (2010) 'The cancer cell secretome: A good source for discovering biomarkers?', *Journal of Proteomics*. Elsevier B.V., 73(10), pp. 1896–1906. doi: 10.1016/j.jprot.2010.04.003.
- Perner, S. *et al.* (2007) 'TMPRSS2-ERG Fusion Prostate Cancer: An Early Molecular Event Associated With Invasion', *The American Journal of Surgical Pathology*, 31(6), pp. 882–888. doi: 10.1097/01.pas.0000213424.38503.aa.
- Prescher, J. A. and Bertozzi, C. R. (2005) 'Chemistry in living systems', *Nature Chemical Biology*, 1(1), pp. 13–21. doi: 10.1038/nchembio0605-13.
- Principe, S. *et al.* (2012) 'Identification of Prostate-Enriched Proteins by In-depth Proteomic Analyses of Expressed Prostatic Secretions in Urine', *Journal of Proteome Research*, 11(4), pp. 2386–2396. doi: 10.1021/pr2011236.
- Prins, G. S. and Putz, O. (2008) 'Molecular signaling pathways that regulate prostate gland development', *Differentiation*. International Society of Differentiation, 76(6), pp. 641–659. doi: 10.1111/j.1432-0436.2008.00277.x.
- Puca, L. *et al.* (2018) 'Patient derived organoids to model rare prostate cancer phenotypes', *Nature Communications*. Springer US, pp. 1–10. doi: 10.1038/s41467-018-04495-z.
- Qian, X. *et al.* (2012) 'Spondin-2 (SPON2), a more prostate-cancer-specific diagnostic biomarker.', *PLoS one*, 7(5), pp. 1–10. doi: 10.1371/journal.pone.0037225.
- Rappsilber, J., Mann, M. and Ishihama, Y. (2007) 'Protocol for micro-purification, enrichment, pre-fractionation and storage of peptides for proteomics using StageTips', *Nature Protocols*, 2(8), pp. 1896–1906. doi: 10.1038/nprot.2007.261.
- Robinson, D. *et al.* (2015) 'Integrative Clinical Genomics of Advanced Prostate Cancer', *Cell*, 161(5), pp. 1215–1228. doi: 10.1016/j.cell.2015.05.001.
- Ryan, C. J. *et al.* (2013) 'Abiraterone in Metastatic Prostate Cancer without Previous Chemotherapy', *New England Journal of Medicine*, 368(2), pp. 138–148. doi: 10.1056/NEJMoa1209096.
- Sato, T. *et al.* (2009) 'Single Lgr5 stem cells build crypt-villus structures in vitro without a mesenchymal niche', *Nature*. Nature Publishing Group, 459(7244), pp. 262–265. doi: 10.1038/nature07935.
- Schmid, F. *et al.* (2016) 'SPON2, a newly identified target gene of MACC1, drives colorectal cancer metastasis in mice and is prognostic for colorectal cancer patient survival', *Oncogene*. Nature Publishing Group, 35(46), pp. 5942–5952. doi: 10.1038/onc.2015.451.



- Shao, C. *et al.* (2012) 'Suprabasin Is Hypomethylated and Associated with Metastasis in Salivary Adenoid Cystic Carcinoma', *PLoS ONE*. Edited by M.-T. Teh, 7(11), p. e48582. doi: 10.1371/journal.pone.0048582.
- Shen, M. and Abate-Shen, C. (2010) 'Molecular genetics of prostate cancer: new prospects for old challenges', *Genes & development*, (212), pp. 1967–2000. doi: 10.1101/gad.1965810.GENES.
- Shi, T. *et al.* (2017) 'Multiplexed targeted mass spectrometry assays for prostate cancer-associated urinary proteins', *Oncotarget*, 8(60), pp. 101887–101898. doi: 10.18632/oncotarget.21710.
- Shoag, J. *et al.* (2018) 'SPOP mutation drives prostate neoplasia without stabilizing oncogenic transcription factor ERG', *Journal of Clinical Investigation*, 128(1), pp. 381–386. doi: 10.1172/JCI96551.
- Sletten, E. M. and Bertozzi, C. R. (2011) 'From Mechanism to Mouse: A Tale of Two Bioorthogonal Reactions', *Accounts of Chemical Research*, 44(9), pp. 666–676. doi: 10.1021/ar200148z.
- Sohn, E. (2015) 'Diagnostic dilemma', *Nature*, 528, pp. 120–122. doi: 10.1038/528S120a.
- Sorensen, P. H. B. *et al.* (1994) 'A second Ewing's sarcoma translocation, t(21 ;22), fuses the EWS gene to another ETS-family transcription factor, ERG', *Nature genetics*, 6, pp. 146–151.
- Sugita, S. *et al.* (2008) 'Retinal Pigment Epithelium-Derived CTLA-2 Induces TGF-Producing T Regulatory Cells', *The Journal of Immunology*, 181(11), pp. 7525–7536. doi: 10.4049/jimmunol.181.11.7525.
- Sugita, S. *et al.* (2009) 'Acquisition of T Regulatory Function in Cathepsin L-Inhibited T Cells by Eye-Derived CTLA-2 during Inflammatory Conditions', *The Journal of Immunology*, 183(8), pp. 5013–5022. doi: 10.4049/jimmunol.0901623.
- Szklarczyk, D. *et al.* (2019) 'STRING v11: protein–protein association networks with increased coverage, supporting functional discovery in genome-wide experimental datasets', *Nucleic Acids Research*. Oxford University Press, 47(D1), pp. D607–D613. doi: 10.1093/nar/gky1131.
- Taoudi, S. *et al.* (2011) 'ERG dependence distinguishes developmental control of hematopoietic stem cell maintenance from hematopoietic specification', *Genes & Development*, 25(3), pp. 251–262. doi: 10.1101/gad.2009211.
- Taylor, B. S. *et al.* (2010) 'Integrative Genomic Profiling of Human Prostate Cancer', *Cancer Cell*. Elsevier Ltd, 18(1), pp. 11–22. doi: 10.1016/j.ccr.2010.05.026.
- Teng, L. H. *et al.* (2013) 'ERG Protein Expression Is of Limited Prognostic Value in Men with Localized Prostate Cancer', *ISRN Urology*, 2013, pp. 1–6. doi: 10.1155/2013/786545.
- Thompson, I. M. *et al.* (2004) 'Prevalence of Prostate Cancer among Men with a Prostate-Specific Antigen Level  $\leq 4.0$  ng per Milliliter', *The New England journal of medicine*, 350(22), pp. 2239–2246. doi: 10.1056/NEJMoa1604221.
- Toivanen, R. and Shen, M. M. (2017) 'Prostate organogenesis: tissue induction, hormonal regulation and cell type specification', *Development*, 144(8), pp. 1382–1398. doi: 10.1242/dev.148270.

- Tomlins, S. A. *et al.* (2005) 'Recurrent Fusion of *TMPRSS2* and ETS Transcription Factor Genes in Prostate Cancer', *Science*, 310(5748), pp. 644–648. doi: 10.1126/science.1117679.
- Tomlins, S. a *et al.* (2008) 'Role of the *TMPRSS2*-*ERG* gene fusion in prostate cancer.', *Neoplasia*, 10(2), pp. 177–188. doi: 10.1593/neo.07822.
- Tran, C. *et al.* (2009) 'Development of a Second-Generation Antiandrogen for Treatment of Advanced Prostate Cancer', *Science*, 324(5928), pp. 787–790. doi: 10.1126/science.1168175.
- Tyanova, S. *et al.* (2016) 'The Perseus computational platform for comprehensive analysis of (prote)omics data', *Nature Methods*, 13(9), pp. 731–740. doi: 10.1038/nmeth.3901.
- Wadman, M. (2015) 'When Less is More', *Nature*, 528, pp. S126–S127.
- Wang, Yuzhuo *et al.* (2001) 'Cell differentiation lineage in the prostate', *Differentiation*, 68, pp. 270–279. doi: 10.1046/j.1432-0436.2001.680414.x.
- Warszawska, J. M. *et al.* (2013) 'Lipocalin 2 deactivates macrophages and worsens pneumococcal pneumonia outcomes', *Journal of Clinical Investigation*, 123(8), pp. 3363–3372. doi: 10.1172/JCI67911.
- Watson, P. A., Arora, V. K. and Sawyers, C. L. (2015) 'Emerging mechanisms of resistance to androgen receptor inhibitors in prostate cancer', *Nature Reviews Cancer*. Nature Publishing Group, 15(12), pp. 701–711. doi: 10.1038/nrc4016.
- Wei, X. *et al.* (2019) 'Spatially Restricted Stromal Wnt Signaling Restrains Prostate Epithelial Progenitor Growth through Direct and Indirect Mechanisms', *Cell Stem Cell*. Elsevier Inc., 24(5), pp. 753-768.e6. doi: 10.1016/j.stem.2019.03.010.
- Wuidart, A. *et al.* (2016) 'Quantitative lineage tracing strategies to resolve multipotency in tissue-specific stem cells', *Genes & Development*, 30, pp. 1261–1277. doi: 10.1101/gad.280057.116.
- Yamamoto, Y. *et al.* (2002) 'Novel cysteine proteinase inhibitors homologous to the proregions of cysteine proteinases', *Curr. Protein Pept. Sci.*, 3(1389–2037), pp. 231–238. doi: 10.2174/1389203024605331.
- Yi, H. *et al.* (1997) 'Inhibition of apoptosis by normal and aberrant Fli-1 and erg proteins involved in human solid tumors and leukemias', *Oncogene*, 14(11), pp. 1259–1268. doi: 10.1038/sj.onc.1201099.
- Yu, Jindan *et al.* (2010) 'An Integrated Network of Androgen Receptor, Polycomb, and *TMPRSS2*-*ERG* Gene Fusions in Prostate Cancer Progression', *Cancer Cell*. Elsevier Ltd, 17(5), pp. 443–454. doi: 10.1016/j.ccr.2010.03.018.
- Zhang, Q. *et al.* (2015) 'Upregulation of spondin-2 predicts poor survival of colorectal carcinoma patients', *Oncotarget*, 6(17). doi: 10.18632/oncotarget.3822.
- Zhang, Y.-L. *et al.* (2018) 'SPON2 Promotes M1-like Macrophage Recruitment and Inhibits Hepatocellular Carcinoma Metastasis by Distinct Integrin–Rho GTPase–Hippo Pathways', *Cancer Research*, 78(9), pp. 2305–2317. doi: 10.1158/0008-5472.CAN-17-2867.

Zhu, J. *et al.* (2016) 'Overexpression of Suprabasin is Associated with Proliferation and Tumorigenicity of Esophageal Squamous Cell Carcinoma', *Scientific Reports*. Nature Publishing Group, 6(1), p. 21549. doi: 10.1038/srep21549.

# 3D organoids unravel critical insights into prostate tissue homeostasis and tumorigenesis

Francesco Cambuli<sup>1,\*,§</sup>, Veronica Foletto<sup>1,§</sup>, Dario De Felice<sup>1</sup>, Alessandro Alaimo<sup>1</sup>, Sacha Genovesi<sup>1</sup>, Arianna Bertossi<sup>1</sup>, Marco Lorenzoni<sup>1</sup>, Maria Dilia Palumbieri<sup>1</sup>, Michela Zaffagni<sup>1</sup>, Emiliana Bertossio<sup>1</sup>, Martina Celotti<sup>1</sup>, Francesco Berardinelli<sup>2</sup>, Antonio Antocchia<sup>2</sup>, Francesco Gandolfi<sup>3</sup>, Alessandro Romanel<sup>3</sup> and Andrea Lunardi<sup>1,§</sup>

<sup>1</sup>The Armenise-Harvard Laboratory of Cancer Biology & Genetics, Department of Cellular and Computational Integrative Biology, University of Trento, Italy

<sup>2</sup>Department of Science, University of Roma Tre, Italy

<sup>3</sup>Laboratory of Bioinformatics and Computational Genomics, Department of Cellular and Computational Integrative Biology, University of Trento, Italy

#Present Address: Herbert Irving Comprehensive Cancer Center, Columbia University Medical Center, NY, USA

§Equally contributed

§Corresponding Author: Francesco Cambuli [fc2597@cumc.columbia.edu](mailto:fc2597@cumc.columbia.edu); Andrea Lunardi [andrea.lunardi@unitn.it](mailto:andrea.lunardi@unitn.it)

The recent development of prostate organoid cultures has opened new opportunities for the study of tissue homeostasis, aging and tumorigenesis. However, our understanding of the precise cellular identities and signaling pathways governing prostate organoids is still limited, thus lessening our ability to recapitulate in vitro key aspects of normal prostate and cancer biology.

Here, based on an in-depth characterization of a newly generated mouse biobank, we propose cycling basal and luminal prostate progenitor cells as the main organoid-forming cell types, and identify a previously unrecognized arm of the Tgf- $\beta$  pathway as a major repressor of cell proliferation in highly quiescent adult prostate cells. Importantly, we report the isolation and characterization of prostate organoid lines capable to spontaneously adapt to Tgf- $\beta$  signaling and overcome this proliferative barrier.

Our findings shed light on novel mechanisms through which prostate cells can acquire the life-threatening potential for cell-autonomous unlimited growth.

# Pharmacological activation of TRPM8 channel overcomes innate resistance to standard-of-care therapies in prostate cancer

Alessandro Alaimo<sup>1</sup>, Marco Lorenzoni<sup>1</sup>, Paolo Ambrosino<sup>2</sup>, Arianna Bertossi<sup>1</sup>, Alessandra Bisio<sup>1</sup>, Alice Macchia<sup>1,3</sup>, Eugenio Zoni<sup>4</sup>, Sacha Genovesi<sup>1</sup>, Francesco Cambuli<sup>1</sup>, Veronica Foletto<sup>1</sup>, Dario De Felice<sup>1</sup>, Maria Virginia Soldovieri<sup>2</sup>, Francesco Gandolfi<sup>1</sup>, Gianluca Petris<sup>1</sup>, Anna Cereseto<sup>1</sup>, Maria Caterina Mione<sup>1</sup>, Marco Durante<sup>5</sup>, Alvaro Villarroel<sup>6</sup>, Mattia Barbareschi<sup>7</sup>, Arkaitz Carracedo<sup>3</sup>, George Thalmann<sup>4</sup>, Alessandro Romanel<sup>1</sup>, Maurizio Tagliatela<sup>2,8</sup>, Marianna Kruithof-de Julio<sup>4,9</sup> and Andrea Lunardi<sup>1</sup>

<sup>1</sup>Department of Cellular and Computational Integrative Biology (CIBIO), University of Trento, Trento, Italy.

<sup>2</sup>Department of Health Sciences, University of Molise, Campobasso, Italy.

<sup>3</sup>CIC bioGUNE, Bizkaia Technology Park, Derio, Spain.

<sup>4</sup>Urology Research Laboratory, Department of Urology and Department of Clinical Research, University of Bern, Bern, Switzerland.

<sup>5</sup>Trento Institute for Fundamental Physics and Applications (TIFPA), INFN, University of Trento, Trento, Italy.

<sup>6</sup>Instituto Biofisika, University of the Basque Country (CSIC-UPV/EHU), Leioa, Spain.

<sup>7</sup>Unit of Surgical Pathology, Santa Chiara Hospital, Trento, Italy.

<sup>8</sup>Department of Neuroscience, University of Naples "Federico II", Naples, Italy.

<sup>9</sup>Department of Urology, Leiden University Medical Centre, Leiden, The Netherlands.

## Corresponding Author

Andrea Lunardi, Armenise-Harvard Laboratory of Cancer Biology & Genetics, Centre for Integrative Biology (CIBIO), University of Trento, Via Sommarive 9 Povo Trento, 38123, Italy. Phone: 39-0461-285288; E-mail: [andrea.lunardi@unitn.it](mailto:andrea.lunardi@unitn.it)

Discovery of novel ‘*druggable*’ targets is a primary goal in cancer translational research. Transient Receptor Potential subfamily M member 8 (TRPM8) is a cation channel almost exclusively expressed by the luminal compartment of the prostate epithelium in the human body. Primarily associated with calcium homeostasis, TRPM8 levels rise in primary and metastatic prostate cancer (PCa), which makes it a possible oncogenic factor and a suitable target of potential clinical interest.

Herein, we show that increased TRPM8 levels in prostate cells favor calcium uptake and activation of pro-survival calcium/calmodulin-dependent kinase II (CaMKII). Nevertheless, by combining a multidisciplinary approach to an *in vitro* genetic platform modelling prostate tumorigenesis, we demonstrate that potent TRPM8 agonists synergize with X-ray treatments to induce massive apoptotic response in radioresistant pre-malignant and malignant preclinical prototypes of primary prostate lesions. As well, TRPM8 activation enhances docetaxel and enzalutamide efficacy in eradicating hormone naïve metastatic PCa cells.

Overall, our findings identify TRPM8 as a valuable target for the treatment of PCa and provide a solid rationale to pursue the clinical testing of TRPM8 agonists in combination with standard-of-care therapies in PCa patients.